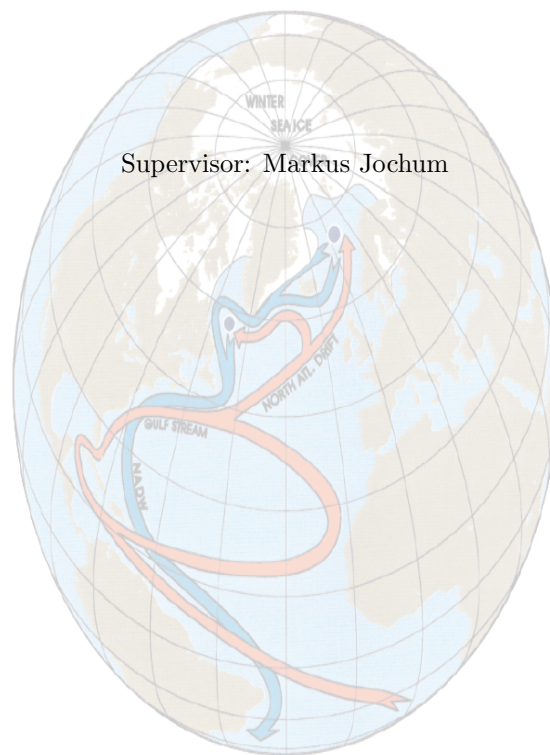


Determining the driving processes of the Atlantic Meridional Overturning Circulation from CCSM data

Thomas Eriksen

January 31, 2017



Abstract

This study contains analysis of data obtained from the Climate Community System Model (CCSM) 3.5 with the objective of determining the driver of the Atlantic Meridional Overturning Circulation (AMOC). The model was run with initial conditions resembling a Pliocene climate. The main hypothesized drivers were the meridional density difference, the strength of the winds over the Southern Ocean, the deep water formation in the north Atlantic, and the transport of the subpolar gyre. The analysis consisted of a quantitative and a qualitative part. In the quantitative part the focus was on finding the correlation coefficient between the AMOC and the hypothesized drives, and in the qualitative the purpose was to find a causal relation. Furthermore, the quantitative analysis provided a basis on which to perform the qualitative part. Because of distinctly different behavior of the AMOC in the early and latter part of the simulation both analyses were performed in two separate temporal regimes. In both regimes the overall analysis of the data supported the claim that it is the deep water formation in the Denmark Strait and the Labrador Sea which should be considered the most important driver, although with a large influence of the subpolar gyre in transporting high salinity waters to these regions. Two feedback mechanisms in the behavior of the AMOC, deep water formation and subpolar gyre transport must be highlighted in this regard. First, the so-called salt-advection feedback; an increase in upper ocean northward salinity flux towards the subpolar Atlantic increases the density here. This enables deep water formation which again increases the overturning. Second, the convective feedback; when convection takes place the vertical density difference is being lowered due to mixing. This process decreases the energy input required for deep convection, which is thereby sustained. Since the deep water formation occurs in a region with a fresh water flux from the atmosphere to the ocean (since precipitation is higher than evaporation) a continuous freshening of the upper ocean take place. If convection does not occur for consecutive years, the fresh water accumulates and therefore lightens the upper ocean further inhibiting deep water formation. The analyzed data support the conclusion that both these feedback processes can have a very large influence on the deep water formation and therefore on the AMOC strength.

Contents

1	Introduction	1
2	Description of the model	2
3	Theory	3
3.1	Thermohaline driven flow	3
3.2	Sverdrup balance	6
3.3	Ekman pumping in the Southern Ocean	9
3.4	Gyre circulation	11
4	Hypotheses	13
4.1	Hypothesis 1: The AMOC is controlled by the meridional density difference .	13
4.2	Hypothesis 2: The AMOC is controlled by the Southern Ocean winds	14
4.3	Hypothesis 3: The AMOC is controlled the strength of the deep water formation in the north Atlantic	15
4.4	Hypothesis 4: The AMOC is controlled by the strength of the subpolar gyre .	16
4.5	Overview and a note on the subpolar gyre	16
5	Preliminary Analysis	17
5.1	AMOC behavior	17
5.2	The correlation between the AMOC and the meridional density difference . .	19
5.3	The correlation between the AMOC and the Southern Ocean winds	23
5.4	The correlation between the AMOC and the deep water formation	26
5.5	The correlation between the AMOC and the subpolar gyre	31
5.6	Summary of the preliminary analysis	32
6	Qualitative analysis	38
6.1	First regime behavior and regime transition	38
6.2	Oscillatory behavior in the second regime	49
6.3	Summary of the analysis	53

7	Discussion	54
7.1	Discussion of the quantitative and qualitative analysis	54
7.2	Discussion of the hypothesized drivers and the AMOC	55
7.2.1	Discussion of the deep water formation	56
7.2.2	Discussion of the meridional density difference	57
7.2.3	Discussion of the role and representation of the subpolar gyre	58
7.2.4	Evaluation of the AMOC	62
7.3	Secondary variables, factors and mechanisms	63
7.3.1	Sea Ice	63
7.3.2	The Denmark Strait Overflow Water	66
7.3.3	Heat fluxes between ocean and atmosphere	69
7.3.4	Overall assessment of the influence of secondary variables	70
7.4	Suggestions for further analysis and research	70
7.5	Summary of the discussion	71
8	Conclusion	72

1 Introduction

Due to the immense amount of heat stored in the Atlantic Ocean the circulation in this is a major component of the worlds climate system. While low latitudes receive far more electromagnetic energy from the Sun than they emit, the opposite is true of the high latitudes. Here the outgoing radiation exceeds that from the incoming Sun. This means that in order for the planet to hold a regional steady temperature, energy has to be transported from low to high latitudes via the atmosphere and the oceans. In the Atlantic ocean the north/south transport of water is dubbed the Atlantic Meridional Overturning Circulation (AMOC), and this is a huge contributor of energy transport from low to high latitudes with as much as 1.3 PW (1 PW = 10^{15} W) reported across $\sim 25^\circ$ N (Ganachaud and Wunsch, 2000). Often erroneously used synonymous with the thermohaline circulation, the AMOC is thus geographically defined as the zonally integrated net circulation in the meridional-vertical plane.

Therefore it is intuitive to consider the AMOC to consist of four branches: first, a northward flowing branch. This lies in the upper part of the ocean. Second, a sinking branch where the formation of the deepwater occurs due to an increase in surface and near surface density. This takes place in the northernmost Atlantic. Third, a southward flowing branch, that transport the dense water away from the high latitudes. This is located at around $\sim 1000 - 2500m$ depth (Kuhlbrodt et al., 2007). At last, an upwelling branch is needed to complete the circulation. This part has traditionally been under debate, but the two most prominent theories have been a uniform (global or basin scale) upwelling (Stommel and Arons, 1959; Munk, 1966), and a wind driven upwelling taking place south of the Drake Passage (Toggweiler and Samuels, 1995).

Because of its heat capacity and this circulation the Atlantic Ocean has the ability to both store and redistribute heat, and this is exactly why it is regarded as such a indispensable climate component.

The correlation between changes in the AMOC and previous climate change is also thoroughly documentet. In a review article Rahmstorf (2002) referred to the ocean as a highly non-linear amplifier of climate change owing the non-linearity to a salinity feedback that enables two equilibrium states. The idea of the ocean as a non-linear system with two equilibrium states was first presented by Stommel (1961) in a simple two box model, but later also by Manabe and Stouffer (1988) in a coupled ocean-atmosphere model. In this study the two equilibria differs distinctly in terms of the Atlantic thermohaline circulation. A breakthrough in linking the AMOC with previous climate change came with McManus et al. (2004). On the basis of $^{231}Pa/^{230}Th$ - a so-called kinematic proxy for the meridional overturning - measurements from subtropical North Atlantic sediment cores, he linked the AMOC to both abrupt cooling around 17.500yr ago and 12.500yr ago and subsequent deglaciations. Rapid changes in these measurements coincide with regional warming, exemplifying the importance of the the meridional overturning for rapid climate change.

All in all it is safe to say, that the AMOC is a significant part of the global climate system, that the non-linearity in its behavior, and its ability to redistribute heat, all make it a possible source of large and rapid climatic change, and that the correlation between previous rapid climate change and variations in the meridional overturning circulation have been well documented.

To give an overview of the projections of the strength of the AMOC, the IPCC's fifth

assessment report states that the AMOC will *likely* undergo a weakening in the near term - that is until 2050, and that there is *low confidence* in these projections. However, over the entire course of the 21st century all models in the IPCC ensemble show a weakening of the AMOC to formalize the conclusion that it is *very likely* that the AMOC will weaken over the entire 21st century. In the four different RCP's the best estimates of the reduction in AMOC strength ranges from 11% to 34% (Kirtman et al., 2014; Collins et al., 2014)

Perhaps this formulation depicts pretty well our current understanding of the AMOC: the overall picture is relatively clear, but the large differences and uncertainties in and across climate models reveal that the underlying details in terms of driving mechanisms, internal feedbacks, responses to perturbations, and so forth are not adequately understood. Are we to give a more precise projection of how the AMOC responds to future climate change and vice versa in climate models, the knowledge of several distinct processes influential on the AMOC needs to be improved.

Despite the tremendous amount of work on both the influence on and impact of the AMOC, a coherent theory of how the AMOC functions in terms of causality and driving mechanisms is still missing in the literature, however, and the topic of this thesis will be a hypotheses-testing and an analysis of the possible physical mechanisms that drives the AMOC.

The report of the thesis will be structured as follows: section 2 will contain a brief description of the model, from which data has been analyzed, and the initial conditions from which it was run; section 3 will explain the necessary and relevant theoretical concepts, which has formed the foundation on which the analysis have been performed; section 4 formulates the hypotheses which have been tested in the thesis on the background of the theory and other relevant recent research, section 5 contains a preliminary analysis focusing on quantitative measures, which will be elucidated in due course, and results of this analysis; section 6 provides an in-depth qualitative analysis of the correlation found in section 5, with an objective of finding causal relation and direction, and accompanying results; section 7 will give an elaborating perspective, critical stand on the way in which the entire study has been carried out, and suggestions for further research ; in the end section 8 gives an overall conclusion of the results and discussion.

2 Description of the model

The model from which the data has been obtained is the Community Climate System Model (CCSM) version 3.5. This is a fully coupled general circulation model with a land, ocean, sea ice, and atmospheric component. The atmospheric component uses the *T31* spectral truncation with a horizontal grid of a 3.75° resolution in the zonal direction and a meridional resolution which varies from 3.68° to 3.71° from the pole to the equator. The sea ice component is also defined on this grid.

The ocean component is defined on a non-uniform grid with 100 grid points in the zonal direction and 116 grid points in the meridional direction, 25 layers in the vertical and the north pole placed over Greenland. Because of the non-uniform grid the zonal resolution varies from 40 km around the grid north pole to 400 km along the equator, and the meridional resolution varies from 40 km close to the north pole and 380 km in the subtropical Atlantic. This varying resolution allows for a better representation of the physical processes occurring near the polar regions, while still obtaining relatively low simulation time. The vertical

resolution varies from $8m$ in the top layer and $497m$ in the bottom layer.

The model was run for 1000 year simulation with the special initial conditions of very high ocean temperature and very uniform ocean salinity. The initial sea surface temperature ranges from 30°C in the tropical Atlantic to 24°C and 27°C at the boundary between the Atlantic and the Southern Ocean, while in the deep ocean temperatures are $11 - 12^{\circ}\text{C}$. The initial sea surface salinity ranges from 35 g/kg in the subtropical Atlantic to 32 g/kg at the estuary of the Amazon River and hold a close to uniform value of around 34 g/kg in most of the upper Atlantic. In the deep ocean salinity differs slightly on the fourth decimal. These initial conditions were applied to represent the climate of the Pliocene.

3 Theory

This section should explain a brief theoretical background and contain a deduction of the key concepts, that are needed in order to understand why the respective hypotheses are the ones tested.

3.1 Thermohaline driven flow

The idea of how oceanic flow is essentially driven by density differences was greatly illuminated by Stommel (1961). The fact that the ocean is both cooled and heated at the surface has, in combination with the opposite effects on density by salinity and temperature, large implications on how the ocean behaves. Results from Stommel's theory will be highlighted in this section with a focus on feedbacks and the conditions for stability.

The results presented in Stommel (1961) is based on an imagined two vessel experiment where two containers of water are connected in the top via an overflow and in the bottom via a capillary tube (as depicted in figure 1). In this way advection between them can freely take place. Both containers are well mixed, so that their respective density (and temperature and salinity) is uniform. Futhermore, they are both in contact with a resevoir with a fixed temperature, \mathcal{T} , and salinity, \mathcal{S} , and with which temperature and salinity can be exchanged. The tube connecting the two containers in the bottom has a resistance k , which is defined such that the flow here is directed from high pressure to low by the relation $kq = \rho_1 - \rho_2$, where q is the flow in the capillary tube and the overflow.

If we are now concerned with symmetric solutions, we can define a sinlge temperature, $T = T_1 = -T_2$ and correspondingly salinity, where the subscript would otherwise indicate which container is being described. This means that for each container the of change of temperature and salinity will depend on the transfer from the reservoir and on the flow between them in the following way:

$$\frac{\partial T}{\partial t} = c(\mathcal{T} - T) - |2q|T$$

$$\frac{\partial S}{\partial t} = d(\mathcal{S} - S) - |2q|S$$

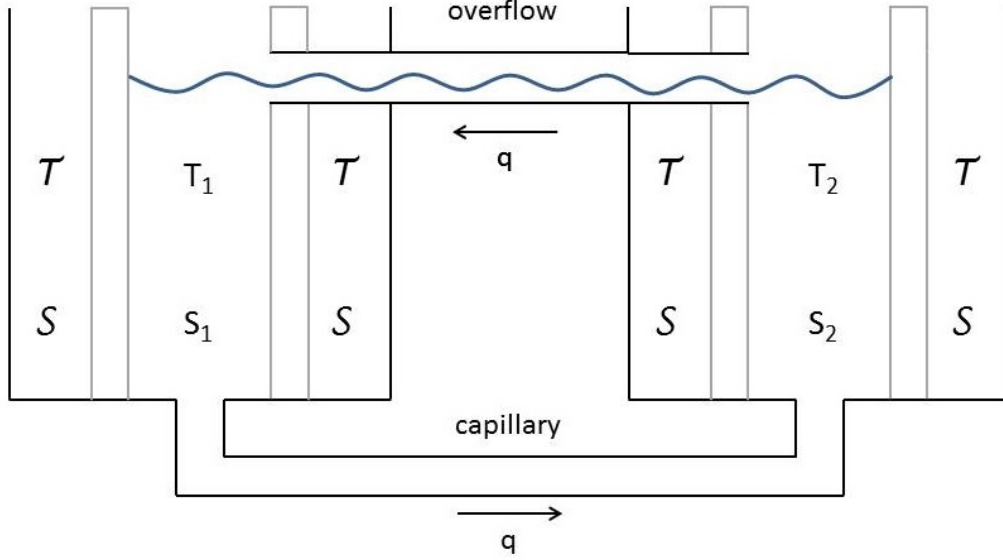


Figure 1: Setup used by Stommel (1961)

where c and d are transfer coefficient of temperature and salinity respectively. If the density is described by the equation of state given by

$$\rho = \rho_0 \cdot (1 - \alpha T + \beta S)$$

the rates of change can be made dimensionless by introducing certain quantities. First of all

$$f = \frac{2q}{c}$$

$$\lambda = k \cdot \frac{c}{4\rho_0\alpha T}$$

are introduced, so that the directional flow in the capillary tube given as $kq = \rho_1 - \rho_2$ is made dimensionless as

$$\lambda \cdot f = \frac{2q}{c} \cdot k \cdot \frac{c}{4\rho_0\alpha T} = \frac{1}{2} \cdot \frac{kq}{\rho_0\alpha T} \quad (1)$$

which is the original flow scaled by a characteristic change in density by temperature. Furthermore, the temperature and salinity is scaled with those of the reservoirs \mathcal{T} and \mathcal{S} in order to obtain the dimensionless rates of change as

$$\frac{\partial y}{\partial \tau} = 1 - y - |f|y \quad (2)$$

$$\frac{\partial x}{\partial \tau} = \delta(1 - x) - |f|x \quad (3)$$

where $y = \frac{T}{\mathcal{T}}$, $x = \frac{S}{\mathcal{S}}$ is the dimensionless temperature and salinity respectively, $\delta = \frac{d}{c}$ is the ratio of transfer coefficients, and $\tau = ct$ is a characteristic time scale associated with the transfer of temperature. In truth at this point all variables, except the salinity, have been scaled with the characteristic values associated with the change in temperature.

From the symmetric definition of temperature and salinity and the equation of state, the original flow gives

$$kq = \rho_1 - \rho_2 = \rho_o[(1 - \alpha T_1 + \beta S_1) - (1 - \alpha T_2 + \beta S_2)]$$

$$kq = 2\rho_0(-\alpha T + \beta S)$$

which is substituted into equation 1

$$\lambda \cdot f = \frac{-\alpha T + \beta S}{\alpha \mathcal{T}}$$

$$\lambda \cdot f = -y + \frac{\beta \mathcal{S}}{\alpha \mathcal{T}} x$$

$$\lambda \cdot f = -y + Rx \quad (4)$$

where $R = \frac{\beta \mathcal{S}}{\alpha \mathcal{T}}$ is the ratio of the effect of salinity and temperature on the density in an equilibrium state. The equations 2, 3 and 1 thus constitute the governing equations for the dimensionless flow of the system. The fact that the flow is dependent on the (dimensionless) quantities of temperature and salinity itself reveal the nonlinearity of the system, i.e. the flow is dependent on temperature and salinity, and the temperature and salinity is dependent on the flow. Solving the equilibrium case of equations 2 and 3 (by setting the left hand side equal to zero) in terms of y and x yields

$$x = \frac{1}{1 + |f|/d}$$

$$y = \frac{1}{1 + |f|}$$

which, when substituted into equation 4, leaves a function ϕ for the flow in the equilibrium state

$$\phi(f, R, d) \equiv \lambda f = -\frac{1}{1 + |f|} + R \frac{1}{1 + |f|/d} \quad (5)$$

Since the flow is dependent on the salinity and temperatures themselves, equation 5 represents a balance between the flow and these in equilibrium states. The number of solutions will depend on the choice of parameters λ , R and d . For instance Stommel (1961) chose the values $\lambda = 1/5$, $R = 2$, and $d = 1/6$ and found three possible equilibrium states - a, b, and c - with $f = -1.1$, $f = -0.30$ and $f = 0.23$ respectively.

These three equilibrium states represent three different ways in which the flow takes place between the containers without changing. Since the sign of f determines the direction of the flow, it was shown in a phase diagram that in the first two cases the flow is dominated by temperature - from cold to warm - and in the last case it was dominated by salinity - from saline to fresh. Furthermore, it was shown that the first case, a, was a stable node, and the third case, c, was a stable spiral, while the last case, b, was a saddle point.

The results by Stommel (1961) highlighted the possible ways in which thermohaline forcing can sustain a flow, and the stability of the flow to perturbations. The fact that the number of equilibrium states depends on the choice of parameters imply that slight changes in the inherent physical properties of the system, i.e. the values of transfer coefficients and the effects of temperature and salinity on temperature, can induce large changes in the flow. This has later been addressed by Rahmstorf (1996) who argued that the AMOC was driven by a density gradient on the basis of results from a conceptual model study much inspired by that of Stommel (1961). Furthermore, Rahmstorf (1996) performed perturbations experiments in order to address the stability of the flow. The conceptual model was perturbed by freshwater fluxes and transitions between equilibrium states - as predicted by Stommel - was found.

3.2 Sverdrup balance

The fact, however, that the mathematical experiment by Stommel (1961) was not based on the fundamental equations of motion, makes the effects of density differences incomparable with those other possible forces. In physical oceanography it has become traditional - as an approximation - to think of the mass transport in the ocean as consisting of a part driven by pressure differences and a part driven by surface wind stress. The former is termed the geostrophic transport, the latter the Ekman transport. Despite the fact that wind induced stresses are only acting as a direct force on the surface of the ocean, a remarkable result can be obtained by considering the motion of the ocean in a single vertical interval and applying a couple of assumptions. Furthermore, this result has large consequences when accompanied by certain topographic features, as the divergence and convergence of its associated transport can induce vertical velocities at the base of the so-called Ekman layer as a compensation for the addition or removal of water as illustrated schematically in figure 2. This process is known as Ekman pumping.

The starting point of the theoretical paragraph will be the horizontal momentum equation, and the first objective will be to deduce a simple expression for the vertically integrated meridional transport. This deduction follows Pedlosky (1998)

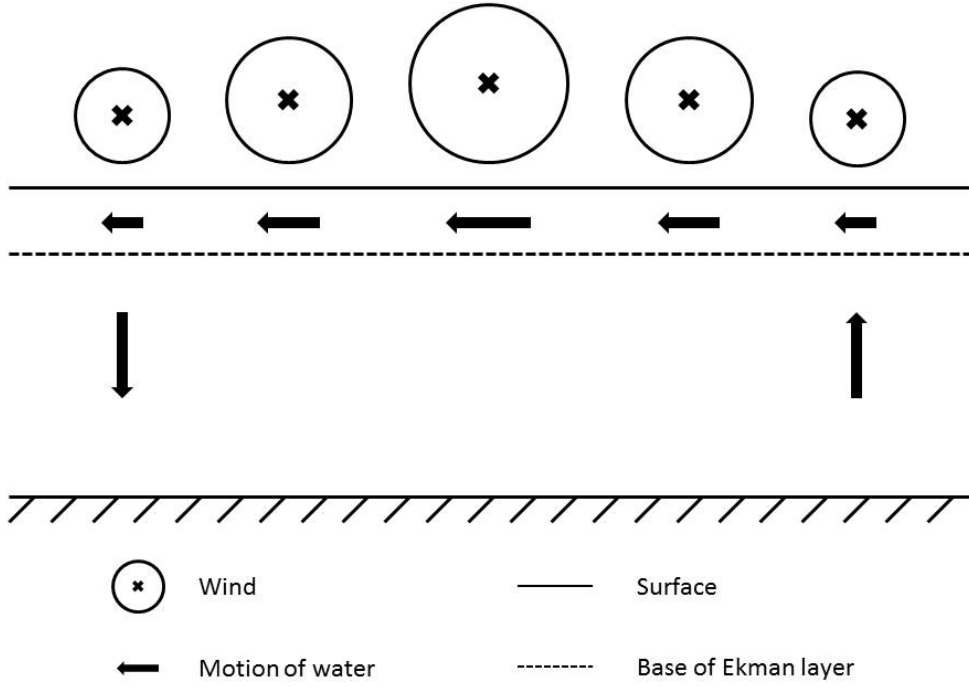


Figure 2: Schematic illustration of how divergence and convergence of Ekman transport induce a vertical velocity below the Ekman layer

$$\frac{D\vec{u}}{Dt} + 2f\hat{k} \times \vec{u} = -\frac{\nabla p}{\rho} + \frac{1}{\rho} \frac{\partial \vec{\tau}}{\partial z} + \vec{F}$$

Here the terms from left to right are as follows; the horizontal Lagrangian acceleration, the coriolis force, the pressure gradient force, the vertical divergence of the horizontal wind stress and the horizontal stress associated with molecular friction.

The ratio of the relative acceleration to the coriolis force is

$$\frac{UU/L}{fU} = \frac{U}{fL} \equiv R_0$$

where U is a characteristic velocity, f is the coriolis parameter, L is a characteristic length scale, and R_0 is the Rossby number. For large scale flows values for U, L and f of 1 cm/s, 1000 km and 10^{-4} s^{-1} are realistic and give a Rossby number $R_0 = 10^{-4}$, i.e. an acceleration negligible as compared to the coriolis force. If we, furthermore, assume that molecular friction is small we are left with

$$\rho f \hat{k} \times \vec{u} = -\nabla p + \frac{\partial \vec{\tau}}{\partial z} \quad (6)$$

by multiplying with the density. This is the aforementioned approximation, where the flow is driven by the wind stress and pressure gradients. At this point the equation will be split into a zonal and a meridional part for simplicity.

$$\begin{aligned} -\rho f v &= -\frac{\partial p}{\partial x} + \frac{\partial \tau}{\partial z} \\ \rho f u &= -\frac{\partial p}{\partial y} + \frac{\partial \tau}{\partial z} \end{aligned}$$

To eliminate the pressure gradient the meridional derivative of the first will be subtracted from the zonal derivative of the second

$$\frac{\partial}{\partial x}(\rho f u) + \frac{\partial}{\partial y}(\rho f v) = \frac{\partial^2 \tau}{\partial x \partial z} - \frac{\partial^2 \tau}{\partial y \partial z}$$

By ignoring the order of differentiation on the right hand side and assuming a constant density on the left we obtain

$$\rho_0 f \frac{\partial u}{\partial x} + \rho_0 \left(f \frac{\partial v}{\partial y} + v \frac{\partial f}{\partial y} \right) = \frac{\partial}{\partial z} \left(\frac{\partial \tau}{\partial x} - \frac{\partial \tau}{\partial y} \right) = \frac{\partial}{\partial z} \left(\hat{k} \cdot \nabla \times \tau \right)$$

Since the meridional derivative of f is β this reduces to

$$\rho_0 f \left(\frac{\partial u}{\partial x} + \frac{\partial v}{\partial y} \right) + \rho_0 \beta v = \frac{\partial}{\partial z} \left(\hat{k} \cdot \nabla \times \tau \right)$$

which, by using the continuity equation $\nabla \cdot \vec{u} = 0$ and assuming incompressibility relates the meridional and vertical velocity to the wind stress

$$\rho_0 \beta v = \rho_0 f \frac{\partial w}{\partial z} + \frac{\partial}{\partial z} \left(\hat{k} \cdot \nabla \times \tau \right)$$

If this is vertically integrated from the bottom to the top of a water column the left hand side will give the meridional transport of the entire water column, whereas the right hand side will evaluate the vertical velocity and the wind stress at the bottom and the top

$$\rho_0 \beta V = \rho_0 f [w(\text{top}) - w(\text{bottom})] + \hat{k} \cdot \nabla \times [\tau(\text{top}) - \tau(\text{bottom})]$$

If the time average vertical velocity at the surface is assumed not to change and that velocity at the bottom is negligible, this leaves only the effect of the wind stress on the right hand side. Since the winds definitely do not exert a stress at the bottom this gives the famous Sverdrup balance

$$\rho_0 \beta V = \text{curl} \vec{\tau} \quad (7)$$

where $\text{curl} \vec{\tau} \equiv \hat{k} \cdot \nabla \times \vec{\tau}$ and $\vec{\tau}$ is the horizontal wind stress at the ocean surface. This is a fundamental and paramount result. It declares that the vertically integrated meridional transport of a water column is only dependent on the local wind stress. This is the most basic way in which winds can sustain a meridional transport.

The underlying assumptions are incompressibility, that the ocean can be treated as being a single layer, i.e. that the density does not vary with depth, that molecular friction and the acceleration are negligible, and that there is no interaction with the bottom.

This balance forms the basis of one of the hypothesis, which will be tested. In order to fully understand how the wind stress can drive a meridional overturning, certain topographic features needs to be taken into consideration.

3.3 Ekman pumping in the Southern Ocean

The further constraints provided by topography, will enhance the role of the wind by placing the above derived expression in an actual geographical context. Returning to equation 6 it is possible to split the velocity into two components sustained by each of the two components on the right hand side, i.e. the pressure gradient and the wind stress, such that $\vec{u} = \vec{u}_E + \vec{u}_G$, where the subscript E indicates the Ekman velocity and the subscript G indicates the geostrophic velocity, and

$$\rho_0 f \hat{k} \times \vec{u}_G = -\nabla p \quad (8)$$

$$\rho_0 f \hat{k} \times \vec{u}_E = \frac{\partial \vec{\tau}}{\partial z} \quad (9)$$

For mathematical clarification the geostrophic part will be split into its two vectorial components:

$$\rho_0 f v_G = \frac{\partial p}{\partial x}$$

$$\rho_0 f u_G = -\frac{\partial p}{\partial y}$$

Now we can imagine a transport in a zonally closed contour down to the depth of the shallowest sill - whatever this depth is. In this scenario the zonally integrated zonal pressure gradient must be zero such that

$$-\oint \rho_0 f v_G \partial x = \oint \frac{\partial p}{\partial x} \partial x = 0$$

which means the zonally integrated meridional geostrophic transport, v_G must as well be zero. If such a region still exhibits a net meridional transport it must be hence be driven by the winds. In order for the continuity equation to be obeyed a divergence of this meridional transport must be compensated by an upwelling taking place below this unspecific depth. This upwelling will accordingly also be driven by the wind.

In such a closed contour the only meridional transport will thus be the contribution of the Ekman transport. Vertically integrating this from eq 9 gives

$$\vec{U}_E = \int \vec{u}_E \partial z = -\frac{1}{\rho_0 f} \hat{k} \times \int \frac{\partial \tau}{\partial z} \partial z = -\frac{\hat{k} \times \vec{\tau}}{\rho_0 f}$$

which meridional component is

$$V = -\frac{\tau_x}{\rho_0 f} \tag{10}$$

The net upwelling in this region must therefore be caused by the divergence of only this transport.

$$\int_{-h_m}^0 \frac{\partial w}{\partial z} \partial z = w(0) - w(-h_m) = -\nabla \cdot \vec{U}_E \tag{11}$$

$$w(-h_m) = \frac{\partial V}{\partial y}$$

In this way specific topographic features can greatly influence the transport. The only place on Earth - besides the Arctioc Ocean - where a closed latitude band include no meridional boundaries, so that transport in a zonally closed contour is unhindered is the Southern Ocean, where Drake's Passage around $56^\circ N - 63^\circ N$ provides the narrowest gap and the shallowest sill on the ocean floor. Hence in this region no net meridional geostrophic flow can be sustained down to the depth of the Drake Passage (Toggweiler and Samuels, 1995)

This assymetric topography forms the basis of why the Southern Ocean winds will induce upwelling, and can therefore be hypothesized as the driver of the AMOC. This hypothesis will be elucidated in section 4.

3.4 Gyre circulation

The role of the subpolar gyre in the overall transport budget of the Atlantic has been addressed in several recent studies which will be shortly elucidated later. A theoretical basis comes from an earlier diagnostic study by Luyten et al. (1985), which highlights the result of a northward transport in the top 600 meters and a southward transport in the deepest part of the north Atlantic along with overall transport enhanced by sloping isopycnals and a sloping bottom topography. By assuming geostrophic and hydrostatic balance in a 3 layer model, it was showed that the sloping isopycnals and bottom topography modifies the Sverdrup balance greatly and allows for the layered transport.

Consider a 3-layer ocean where the depth of the first layer-interface is $h(x, y)$, that of the second is $D(x, y)$ and the bottom is $H(y)$. With the velocity in the bottom layer defining the pressure $p(x, y)$ the geostrophic velocities in layers 1, 2, and 3 are given by the thermal wind relation

$$\begin{aligned}\vec{u}_3 &= -\frac{g'}{f}\nabla p \\ \vec{u}_2 &= \vec{u}_3 - \gamma_2\frac{g'}{f}\nabla D \\ \vec{u}_1 &= \vec{u}_2 - \gamma_1\frac{g'}{f}\nabla h\end{aligned}\tag{12}$$

where $g' = g/\rho_3$ is the reduced gravity, and $\gamma_n = (\rho_{n+1} - \rho_n)/\rho_3$ are density contrasts between the layers. If the continuity equation is integrated vertically in a layer n one obtains

$$d \cdot \left(\frac{\partial u_n}{\partial x} + \frac{\partial v_n}{\partial y} \right) = w(z_n) - w(z_{n-1})$$

where d is the layer thickness, $w(z_n)$ is the vertical velocity across the n 'th interface and $w(0) = w_E$ is the Ekman suction. The vertical velocity across a sloping isopycnal can be expressed via a component normal to the interface and two horizontal components multiplied with the slope of the isopycnal itself. For the first layer we would thus have

$$w(z = -h) = w_1^* - u_1 \cdot \frac{\partial h}{\partial x} - v_1 \cdot \frac{\partial h}{\partial y}\tag{13}$$

In the bottom layer there is assumed to be no velocity normal to the bottom. If equation 12 is substituted into equation 13 one obtains an equation for each layer where the the sloping of isopycnals and bottom together with the bottom layer pressure controls the cross isopycnal velocities. For layer 3 the vertically integrated continuity equation becomes

$$(H - D) \left(\frac{\partial \vec{u}_3}{\partial x} + \frac{\partial \vec{v}_3}{\partial y} \right) = w(z = -H) - w(z = -D)$$

where the vertical velocities are given by equation 13 and the horizontal velocities by equation 12. This gives

$$\begin{aligned}
-w_2^* &= -(H - D) \left(\frac{g' \beta}{f^2} \frac{\partial p}{\partial x} \right) + u_3 \frac{\partial H}{\partial x} + v_3 \frac{\partial H}{\partial y} + \frac{g'}{f} \left(\frac{\partial p}{\partial y} \frac{\partial D}{\partial x} - \frac{\partial p}{\partial x} \frac{\partial D}{\partial y} \right) \\
-\frac{f}{g'} w_2^* &= -(H - D) \left(\frac{\beta}{f} \frac{\partial p}{\partial x} \right) - \frac{\partial p}{\partial y} \frac{\partial H}{\partial x} + \frac{\partial p}{\partial x} \frac{\partial H}{\partial y} + \frac{\partial p}{\partial y} \frac{\partial D}{\partial x} - \frac{\partial p}{\partial x} \frac{\partial D}{\partial y} \\
-\frac{f}{g'} w_2^* &= -(H - D) \left(\frac{\beta}{f} \frac{\partial p}{\partial x} \right) - \frac{\partial(H - D)}{\partial x} \frac{\partial p}{\partial y} + \frac{\partial(H - D)}{\partial y} \frac{\partial p}{\partial x}
\end{aligned}$$

Here the vertical velocity across the interface between the layers 2 and 3 are given only by the thickness of the layer, the sloping isopycnal and the bottom pressure. Similar equations would be obtained in layer 1 and 2, although these would contain velocities normal to the isopycnals at both the bottom and the top of the layer, i.e. two contributions on the left hand side. It is also worth noticing that in the model by Luyten et al. (1985) the bottom depth is only a function of y , so the zonal derivative of H is equal to zero.

The meridional transport per unit width is

$$\begin{aligned}
T_{top} &= v_1 h = h \frac{g'}{f} \left(\gamma_1 \frac{\partial h}{\partial x} + \gamma_2 \frac{\partial D}{\partial x} + \frac{\partial p}{\partial x} \right) \\
T_{middle} &= v_2 (D - h) = (D - h) \frac{g'}{f} \left(\gamma_2 \frac{\partial D}{\partial x} + \frac{\partial p}{\partial x} \right) \\
T_{bottom} &= v_3 (H - D) = (H - D) \frac{g'}{f} \frac{\partial p}{\partial x}
\end{aligned}$$

So the transport in the upper layer experiences a contribution from the sloping of both isopycnals and the bottom, whereas the transport in the middle layer only feels the contribution on the bottom and the second isopycnal, and the transport bottom layer is only influenced by the sloping of the bottom.

Using this set of equations Luyten et al. (1985) used table values to compute a meridional transport of 10 and 15 Sv in the two upper layers and -6 Sv in the bottom layer across the northern Atlantic. Their budget was thus not closed, but the highlight of Luyten et al. (1985) in regards to this thesis should be how the zonally sloping isopycnals in a layered model causes a meridional transport, that can shift direction with the layers. In the Atlantic Ocean there is a net northward transport in the upper ocean, and a net southward transport in the deeper ocean - simliar directions as those found by Luyten et al. (1985). It should also be highlighted that that southward motion in the bottom layer provides - because of the sloping bottom - the stretching needed by the water column to obey the Sverdrup relation.

The difference between the general Sverdrup relation and the result here obtained is universal. More layers could in principle be added and the meridional transport in each calculated. The fact that the result of a northward transport in the upper ocean and a

southward transport in the lower is obtained by table values of density is of course an accomplishment, since it shows the ability to construct models which outputs are consistent with observations.

Assumptions in this model include the geostrophic and hydrostatic balance. It is also worth noting the the height of the bottom is only a function of y , i.e. it has no zonal slope which could influence the flow.

4 Hypotheses

Following the introduction, this study imposes one simple yet complex question: What physical process controls the AMOC? What are the key mechanisms considered to be the drivers of the AMOC in terms of causality, and what are the uncertainties of the link between the AMOC and the respective hypothesized drivers. On the basis of the theoretical work described in section 3 and other recent research, the possible answers to these questions are outlined in the section below. The section should thus provide a sufficient basis to understand why a certain variable should be considered as a potential driver of the AMOC and an elaboration of how the knowledge of the respective connection have come into place. The hypotheses are as follows:

4.1 Hypothesis 1: The AMOC is controlled by the meridional density difference

As already outlined in section 3 this hypothesis stems from the pioneering theoretical two-box-model by Stommel (1961). Assuming the two boxes to be well mixed, so that density is uniform within each box, allows a calculation of the flow in equilibrium states. Not only did the work show the interdependence of a density flow and the temperature and salinity, which drives it, thereby highlighting the nonlinearity of the system, it also illuminated the requirement of certain conditions in order for the system to reach a state of equilibrium.

This box model, thus, offers a huge insight as to how flow between regions distinct in terms of temperature and salinity - and thus density - might take place, and by which mechanism an equilibrium can be reached. In the real world salinity and temperature *are* distinctly different in the subtropical and the subpolar regions of the Atlantic, and despite being an idealized case Stommel's box model experiment therefore contains very valuable information of how flow might be sustained between these regions. It is idealized in the sense that it only accounts for flow being controlled by density (since it is the only variable from the equations of momentum included) and that the geographical features of the Earth are completely disregarded, but nonetheless certain feedback processes are well elucidated. However, the fact that the Stommel box model only accounts for the motion caused by density difference, makes it impossible to compare this contributions to the possible (or rather, the very well documented) contributions by other forces. In other words, if the only force included in a physical oceanography model is one caused by density differences, this is also the only possible answer to the question of what drives the circulation.

In the theoretical work claiming the meridional circulation to be driven by density differences, the question of where and due to which forces upwelling has taken place has traditionally been answered by mixing in low latitudes. Internal waves brought about by tides

and winds will dissipate, and the associated mixing of heat will cause water in the deep ocean to rise in midlatitudes (Kuhlbrodt et al., 2007).

Another contribution to the claim that meridional density differences are the driver of the AMOC was made by de Boer et al. (2010). She finds an inverse relation between the meridional density gradient and the meridional overturning circulation and claims that this is due to a disconnect between the density gradient and the pressure gradient. When conducting a scaling analysis, the depth over which the overturning happens, is assumed to be constant, and de Boer argues that the most appropriate scaling depth is the depth of the maximum overturning. The best estimate of this maximum is obtained when it is taken to be the depth at which the derived meridional pressure gradient in the western boundary is zero. In this case the overturning can have an inverse relation with the meridional density difference. Since the conclusion in this work is, that despite the meridional density difference favouring a southward transport, the model study show a clear correlation between meridional density differences and the AMOC in perturbation experiments. In this sense de Boer et al. (2010) also supports the claim that the meridional density difference can drive the AMOC.

4.2 Hypothesis 2: The AMOC is controlled by the Southern Ocean winds

This hypothesis was first put forward by Toggweiler and Samuels (1995), and it concerns the claim that it is the upwelling branch caused by Southern Ocean winds which controls the AMOC. They argued that a northward induced Ekman transport came to happen due to meridional shear in the zonal wind over the Southern Ocean. Associated with this is the so-called Drake Passage's effect, which causes water to upwell south of the latitude with the strongest zonal winds in the Southern Ocean. Since the Southern Ocean is an open zonal passage spanning the entire globe the net zonal pressure gradient must be zero when averaged around the globe in this latitude band. This means there can be no net geostrophically balanced meridional flow at all latitudes and depths down to the shallowest sill in this band (Toggweiler and Samuels, 1995; Kuhlbrodt et al., 2007).

The Southern Ocean *is* subject to very strong westerly winds and the meridional shear in these causes a northward Ekman transport. South of the latitude with the strongest wind there will be a divergence of the Ekman transport which causes an upwelling. Because of the Drake Passage's effect (no net meridional geostrophic flow at all latitudes and depths down to the shallowest sill in the entire band) this means that all upwelling must happen south of the latitude with the strongest wind. Stronger winds will induce a stronger Ekman transport, and a stronger meridional shear in these winds will cause a stronger upwelling. In this sense it will be the strength of the zonal winds that control the upwelling and hence the AMOC.

Recent debate, however, have also focused on the possibility that non-eddy resolving models tend to overestimate the influence of the Southern Ocean winds on the meridional transport into the Atlantic. The claim is that the non-eddy resolving models underestimates the portion of the energy input from the winds which goes the formation of eddies. As a result the eddies removes less of the energy available for the northward Ekman transport, and this transport is thus overestimated (Jochum and Eden, 2015).

4.3 Hypothesis 3: The AMOC is controlled the strength of the deep water formation in the north Atlantic

The deepwater formation in the Atlantic occurs in the Labrador Sea and the Nordic Seas and is characterized by a transfer of energy to the atmosphere from the ocean via surface cooling facilitated by the northward decrease in temperature and the strength of winds. The depth and strength of the deep convection is thus determined by density stratification and these atmospheric conditions in the winter (Rhein et al., 2011). Böning et al. (1996) show how the Atlantic surface layer gradually cools in an east-northeast direction along the North Atlantic Current and afterwards north- and westward following the subpolar gyre until reaching the Labrador Sea. Here it obtains the lowest potential temperature around 3.5°C . This coincides with the largest value for the mixed layer depth, which is considered a measure for deep convection. Böning et al. (1996) also argues, however, that the influence of the formation of deep water in the Labrador Sea on the meridional overturning circulation is negligible and claims that it is the outflow from the Greenland and Norwegian Sea to the Atlantic which control the formation of North Atlantic Deep Water (NADW). However, this outflow in his model is represented as restoring boundary conditions and as such does not capture the physical process of deep water formation itself. The claim that the contribution by sinking in the Labrador Sea is less important is justified by the result that it only constitutes about $1/12$ of the total sinking north of 47°N in this study.

Delworth and Zeng (2016) performed perturbation experiments on the influence of the North Atlantic Oscillation (NAO) on the AMOC. They find that a positive NAO phase strengthens the AMOC by extracting heat from subpolar North Atlantic water thereby increasing surface density and mixed layer depths which ultimately leads to deep water formation. Thus the direct cause of the AMOC increase is deep water formation. In this study the impact of the heat flux perturbation exceeded that of the fresh water and momentum anomaly, why this was the justification of the increased mixed layer depths.

Lohmann et al. (2014) investigated the relative influence of the Denmark Strait overflow and the deepwater formation (measured as a deepwater formation index rather than mixed layer depths) on the AMOC. They find that variations in the subpolar deep water formation and the Denmark Strait overflow can explain half and one third of the variability of the AMOC at 30°N respectively. However north of 50°N variations in the Denmark Strait overflow becomes more influential on the AMOC than the deep water formation.

Claims that the deepwater formation is not important for the strength of the AMOC has also been made, however, by Pickart and Spall (2007). They find that the deep water formation in the Labrador Sea forms a mean overturning of merely 1 Sv compared with a horizontal transport of 18 Sv in a period of time of intense deep convection. Accordingly they claim that a part of the uncertainty of the influence of the Labrador Sea on the AMOC is due to a confusion around water mass transformation and Eulerian sinking, specifying that the formation of Labrador Sea mode water does not necessarily imply a net sinking of water.

All in all, the contributions to the influence of deep water formation on the AMOC have been many in recent years with a majority suggesting a positive correlation between an intense deep water formation and a strong AMOC.

4.4 Hypothesis 4: The AMOC is controlled by the strength of the subpolar gyre

The subpolar gyre as well has been a topic of much recent research. As a feeder of water to the deep water formation regions, it is directly linked to the sinking branch of the AMOC, but since its governing forces are fundamentally different from the actual deep water formation distinctions have to be made. According to Böning et al. (1996) one manifestation of the subpolar gyre is the deep western boundary current. Subsequent to the sinking in the Labrador Sea the strength of the subpolar gyre plays the role of removing water from the region of deep water formation. This was already highlighted by McCartney and Talley (1984) who estimated a southward transport off of New Foundland of 15 Sv highlighting also the deep water formation in this regard.

A different mechanism through which the subpolar gyre affects the AMOC is the feeding of saline water in the upper ocean to the deep water formation site. The poleward flowing water in the east Atlantic basin carries high salinity from the tropics. It gradually cools flowing northward, however, reaching a maximum density in the northern Atlantic and the Labrador Sea (Böning et al., 1996). Since the northward flow in the eastern part of the subpolar gyre counteracts the southward flow in the western, deep branch of the AMOC, the *ability to bring saline water* rather than the actual amount of water brought to the northern Atlantic, is highlighted as a key process. In this sense the amount of tropical water entering the subpolar gyre from the subtropical gyre is of great interest, since it has a higher salinity. The process of mixing across the intergyre boundary between the subtropical and subpolar gyre is, however, still not fully understood (Marzocchi et al., 2015).

Despite this uncertainty and the dual north/south flow of the subpolar gyre recent studies by both Hatun (2005) and Kleppin et al. (2015) highlight the importance of the subpolar gyre transport in regards to the strength of the AMOC by the means of transporting high salinity water to the deep water formation regions. Both Delworth and Zeng (2016) and Kleppin et al. (2015) mentions the North Atlantic Oscillation (NAO) is a key process in this regard.

4.5 Overview and a note on the subpolar gyre

It makes sense to address the driving mechanisms of the AMOC in terms of energy. However, only three out of the four hypothesized control mechanisms can be regarded as a driver in terms of energy. The Southern Ocean winds provide a mechanical energy input; the meridional density difference is associated with sea surface height differences and sloping isopycnals and therefore with available potential energy; the deep water formation is fundamentally caused by an inverse vertical density profile and thus also associated with potential energy; whereas the subpolar gyre does not contain a different kind of energy which can be transformed into kinetic energy in the AMOC.

In this view it is erroneous to talk about the subpolar gyre as a driver in the sense of an **energy provider**, despite the fact that this is one implicit meaning of the word driver. Therefore in the subsequent part of the study *a driver* will refer to one process or phenomenon causing a *reaction* of another. It still makes sense to address the subpolar gyre as a driver - or at least for now a potential driver - of the AMOC, since it provides key physical processes which can act as the first link in a causal chain that potentially governs the overall transport of the AMOC.

As for the energy input which drives the AMOC, it will - in the end - be provided by the gravitational and radiative forces of the Sun and the moon, and the rotation of Earth itself. Despite contributions towards the influence of all of the 4 hypothesized drivers a comparison of their relative impact on the AMOC is still missing in the literature.

5 Preliminary Analysis

This section will first of all contain timeseries of the AMOC and the four hypothesized drivers. In case a hypothesis can be rejected immediately on the basis of a comparison of timeseries with the AMOC alone no further investigation will be conducted of the particular variable. Subsequent to the initial timeseries analysis a cross correlation analysis will follow in order to give a quantitative measure of the respective correlation and to answer the question of, whether the variable in question is believed to be leading or lagging the AMOC. The section will hence first devote a short paragraph to the analysis of the AMOC itself, whereafter a paragraph focusing on each of the four hypothesized drivers will follow. In order to summarize an overview will be provided at last.

5.1 AMOC behavior

As mentioned in the introduction the AMOC is a geographically defined flow - the zonally integrated net north-/southward flow - so it will only change with latitude and depth. In the data the value of the AMOC at a certain depth index is given as the zonally integrated transport which is summed (unweighted) from the top of the ocean down to this particular depth index. The AMOC transport at the bottom most layer should thus be zero in order to avoid a piling up of water in either the southern or northern part of the Atlantic.

The most common latitude of evaluation in climate research has been at 30°N, but in order to compare the possible lag of the AMOC to any variable the latitude of evaluation is a critical point. Since the different possible drivers will influence the AMOC at different latitudes, it seems plausible that the lag of the AMOC to some variable will change depending on the latitude of evaluation. Moreover, because of the non-uniform grid used by the model a single latitude is not associated with a single latitude *index*, why each evaluation will be given at an index and a roughly corresponding latitude.

In figure 3 is shown a timeseries of the AMOC evaluated at four different latitudinal indices. At each latitude the AMOC has been evaluated at the depth of maximum (northward) transport at every timestep.

In general, this behavior is rather extreme. Even though the AMOC is projected to decrease in the next 100 years with - perhaps - 25 % it is - in this simulation with these initial conditions - seen to far more than double in 100 years at 35°N, where it also undergoes several rapid increases of about 10 Sv in the latter part of the simulation. This volatile behavior calls for an explanation.

Comparing the four latitudes it is clear that the AMOC transport is at all times the largest when evaluated at 35°N, whereas at the other three latitudes the strength of the AMOC are rather similar after the spin-up phase. Following the spin-up phase the transport can be characterized as showing first a steady then a rapid increase until approximately

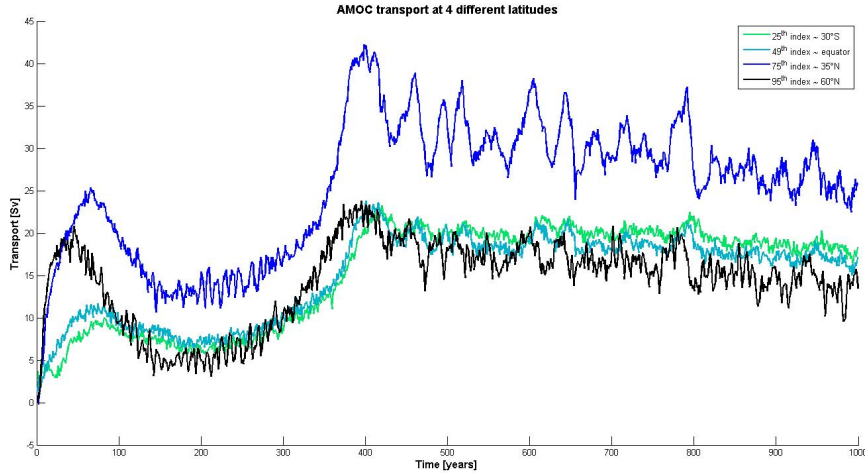


Figure 3: The AMOC evaluated at 4 different latitudes all at the depth of maximum transport at every timestep. The AMOC exhibits the largest transport at 34°N while the transport at the remaining four latitudes a similar in strength. After the spin-up phase the transport can be characterized by first a steady then a rapid increase until year ~ 400 , after which a somewhat linear decrease with oscillatory behavior is seen

year 400 of the simulation. Especially at 35°N this rapid increase is visible with the AMOC reaching a maximum transport of more than 40 Sv. After reaching this maximum the strength of the AMOC continues to decrease throughout the rest of the simulation in a somewhat linear fashion - although with large oscillations at 35°N . These oscillations are less pronounced at the other three latitudes but are also clearly visible at 60°N .

In fig 4 a transect of the AMOC is shown at six different years of the simulation with 100 years intervals, where the colorbar indicates transport in units of Sv with positive (negative) numbers indicating a clockwise (counterclockwise) transport. The fat line represents the line depth at which the AMOC is equal to zero indicating the shift in motion. Similar to fig 3 it is clear that the AMOC transport is rather low at year 200 and 300 after which a rapid increase in strength is seen. While the strength of the AMOC change quite substantially (especially from year 300 to 400) it is also clear that the spatial structure remains somewhat constant with neither the size of the clockwise nor the counterclockwise flowing cell changing significantly. Besides the sizes of these cells, it is worth noticing that the maximum of the AMOC transport is at all times found at the 75^{th} latitudinal index and close to $\sim 1000\text{m}$ depth.

Another interesting feature of figure 4 is that the meridional transport cease to exist completely around the 24^{th} latitudinal index. This roughly corresponds to 33°S . It seems plausible that the Antarctic Circumpolar Current (ACC) dominates the flow south of this region, but the fact that the feature remains so constant throughout the entire simulation given the difference in behavior of the AMOC is interesting. It has not been a scope of this study, though, and will not be examined further.

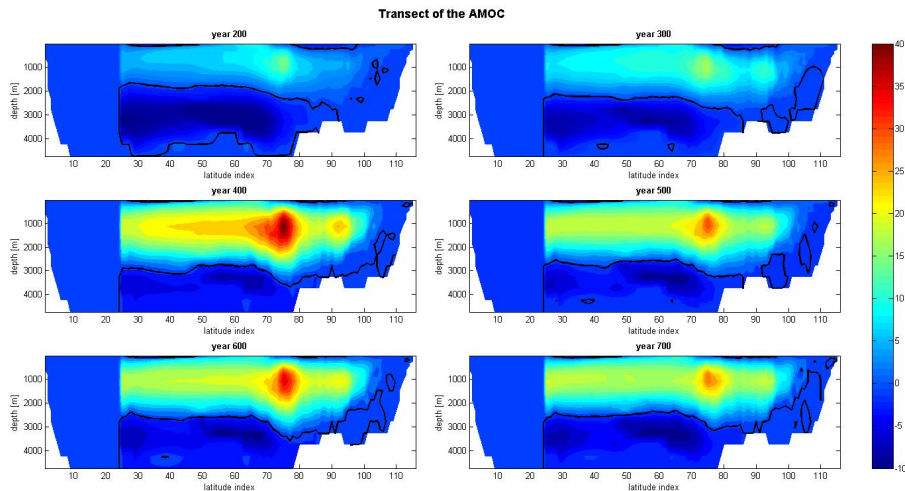


Figure 4: Transect of the AMOC at six different years of the simulation. The maximum strength is at all times found at the 75th latitudinal index and close to 1000 m depth. While the spatial structure remains somewhat constant throughout the simulation the strength varies substantially with an increase of more than 20 Sv from year 300 to year 400.

5.2 The correlation between the AMOC and the meridional density difference

Before directly investigating the correlation between the meridional density difference (MDD) and the strength of the AMOC, it is necessary to justify where the correlation should be examined, i.e. between which latitudes should the MDD be calculated and at which depths? And at which latitude and depth should the AMOC be evaluated in order to get the appropriate correlation?

Since the theories, which has historically claimed that the meridional transport was controlled by the meridional density differences, predicted or assumed an upwelling either uniform over the entire basin or in the low latitudes, the latitudinal interval over which the MDD has been computed were chosen to be 10°S - 10°N and the region of deep water formation which is between 62°N and 65°N. In both the northern and equatorial section the eastern and western boundary between which to compute the MDD were set accordingly as land boundaries.

Four different depth intervals over which to average the density in these latitude intervals were chosen. The first and second chosen on the basis of Stommel (1961), the third on de Boer et al. (2010), and the fourth were chosen on the basis of the spatial structure of the AMOC in this study - as seen in figure 4.

In the two box model study by Stommel (1961) the boxes are connected via tubes in the upper and lower part of the boxes, which are assumed to be well mixed to a constant density. The water thus flow through only the upper and lower most part, and inspired by this the first and second (interval 1 and 2) vertical interval used to compute the MDD are the top eight layers - which constitute the uppermost 100m - and the layers 19 and 20 which captures the depth interval of 1670 – 2555m. This is the bottommost layers at the deep water formation region.

de Boer et al. (2010) uses the upper most 1400m to support their final conclusion of how the meridional density gradient can control the AMOC. In this study this has been captured by the top 17 layers constituting the upper most 1280m (interval 3). Were 1400m to be used instead this would imply a interpolation of AMOC transport between layer 17 and 18, and this was deemed unnecessary.

The last vertical interval (interval 4) used is comprised of the layers 15 – 18. These layers constitute the part of the ocean which lies between 500 and 1690 meters depth. The reason behind this choice is as mentioned the spatial structure of the AMOC; it is seen that both in periods of low and high transport this is the proximity of the maximum of the AMOC, and should the meridional density difference control the AMOC a correlation between the two in this part of the ocean should be pivotal.

These intervals constitute both northern and southern, eastern and western, and upper and lower bounds for a northern and an equatorial part of the ocean and in all cases an average value (weighted by depth) of the density was found as a function only of time. Since the AMOC is defined as the total zonally integrated transport it makes sense to consider the average of the density over a complete latitude band in the Atlantic, when examining the influence of density.

Figure 5 shows timeseries for the meridional density difference (as the northern section subtracted the southern) for the four vertical intervals. It can be seen that the largest meridional density differences are found in the upper ocean (interval 1) and in all cases the MDD decreases with depth. During the first ~ 400 years of the simulation all four vertical intervals displays a behavior similar to that of the AMOC, whereas in the last ~ 600 years intervals 1 – 3 display a slight increase and only interval 4 experiences a decrease. In neither of the four intervals is the oscillatory behavior of the AMOC in the years 400 – 999 nearly as pronounced in the MDD as compared to the AMOC.

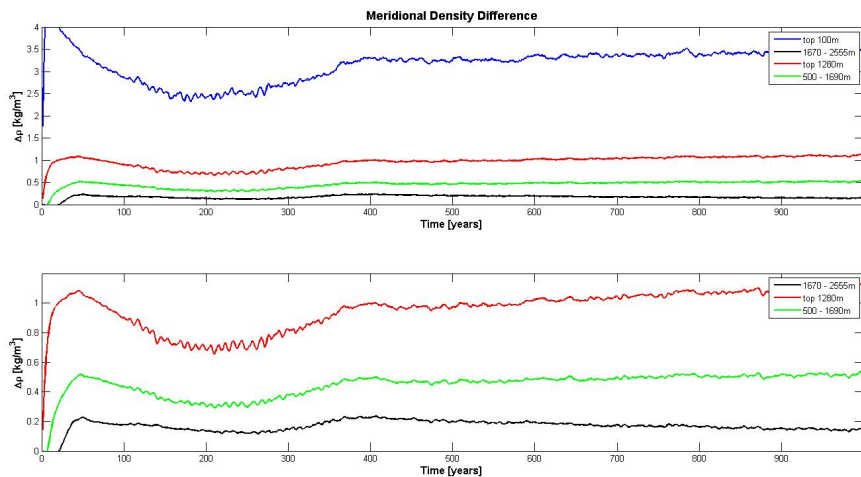


Figure 5: **a** Shows the MDD in the four vertical intervals. The largest meridional density differences is seen in interval 1 (top 100 meters) and the MDD decreases with depth. Interval 1 clearly exhibits a behavior similar to the AMOC until year ~ 400 after which an opposite behavior is seen. **b** A zoom in on the three deepest vertical intervals in order to see their behavior more clearly. It can be seen that interval 4 (1670 – 2555m) exhibits a behavior similar to the AMOC, whereas the intervals 2 and 3 (0 – 1280m and 500 – 1690m) shows a behavior similar to interval 1.

The fact that the AMOC and the MDD exhibit a similar behavior in the first ~ 400 years but distinctly different behavior in the last ~ 600 years is interesting because it can be seen as a possibility that the AMOC can exist in two different states, where one is related to the MDD and the other is not.

In order to compare the MDD and the AMOC a cross correlation coefficient has been calculated between the AMOC in the MDD in all four vertical intervals. For this purpose the AMOC was evaluated at the 75^{th} latitudinal index (which roughly corresponds to 33°N). This coincided with the maximum transport and had a latitude halfway between the northern and southern region used to calculate the MDD. Therefore it is theoretically appropriate in two logical ways; namely in the sense that should the MDD actually drive the AMOC, it would seem very nonplausible not to be seen at this latitude, and in the sense that if a correlation is seen at this grid point it seems plausible that the MDD could drive the AMOC.

In figure 6 is seen the correlation coefficient between the AMOC and the MDD in the four vertical intervals for the entire simulation (disregarding the spin-up phase which was set to the first 65 years) as a function of lag years where negative (positive) is taken to be the AMOC (MDD) lagging the MDD (AMOC). A correlation coefficient close to 0.8 obviously indicates a strong correlation, but the fact that there seems to be no significant difference in correlation of whether the AMOC lags the MDD by 10 years or the MDD lags the AMOC by 30 years blurs the overall picture.

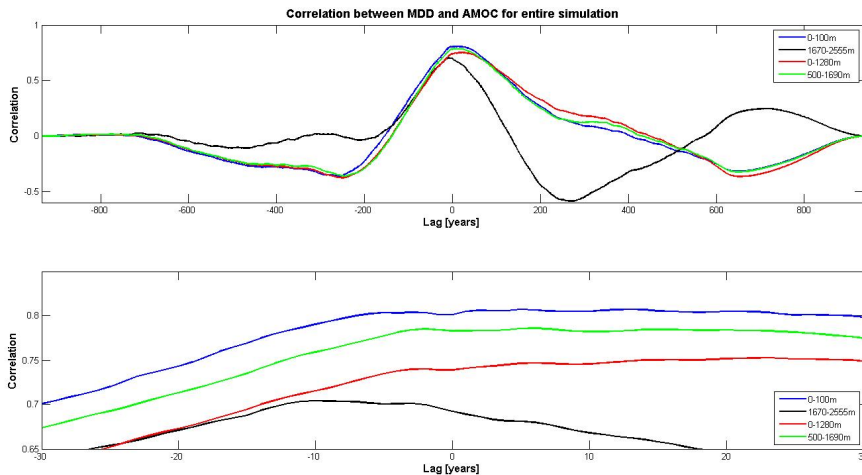


Figure 6: **a** Shows the correlation coefficient between the AMOC and the MDD in four vertical intervals as a function of lag years negative (positive) indicating a lag of the AMOC (MDD) to the MDD (AMOC) over the entire simulation. **b** A zoom in on the lagtime of maximum correlation.

The fact that the correlation is almost independent of lag years between -10 and 30 strengthens the claim already made by the difference in behavior prior and after year ~ 400 between the AMOC and the MDD; it calls for an separation into two temporal regimes, which can be investigated separately.

The 1^{st} temporal regime was defined as the years $65 - 395$ and the 2^{nd} as $395 - 999$ of the simulation. Figure 7 shows the correlation coefficient between the MDD and the AMOC as a function of lag years in the 1^{st} temporal regime, and figure 7b is a zoom in on the lag years -30 to 30 of figure 7a. In this part of the simulation the correlation between the MDD and

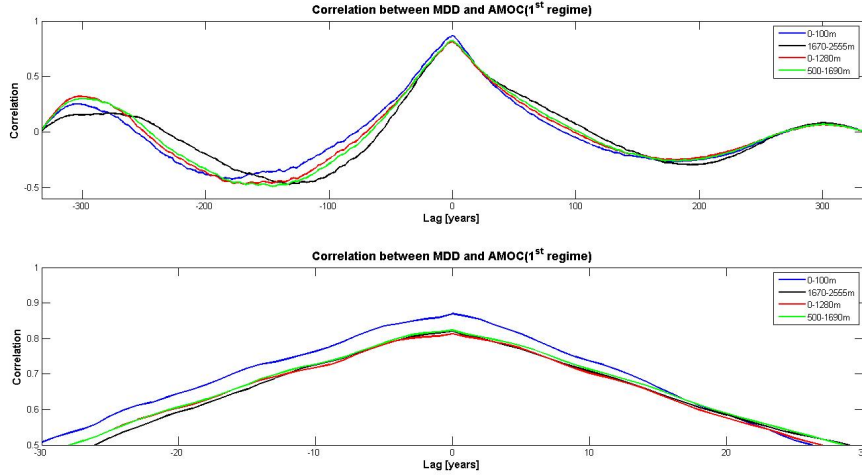


Figure 7: a shows the correlation between the MDD and the AMOC in the 1st temporal regime. This is highest when the MDD is evaluated in the top of the ocean with a maximum value of 0.8694. In all 4 vertical intervals the correlation is highest at 0 years lag, which makes it impossible to determine the direction of causality using this method. **Figure b** shows a zoom in on the years around maximum correlation.

the AMOC is highest when the MDD is taken over the top 100 meters reaching a maximum value of 0.8694 at 0 years lag. For all 4 vertical intervals the maximum correlation occurs at 0 years lag, which means that on the basis of this technique it is impossible to determine the direction of causality, i.e. whether the MDD should control the AMOC or vice versa, even though the correlation coefficient may be high.

Figure 8 shows the same correlation but for the 2nd temporal regime. In figure 8a it is clear that there is a correlation between the AMOC and the MDD in interval 2 but an anti-correlation in interval 1,3 and 4. Figure 8b shows a zoom in around the years of maximum (anti-)correlation where absolute values for the correlation in interval 1,3 and 4 have been used for the sake of comparison. It is clear that the highest correlation is in interval 2, i.e. the deep part of the ocean. The absolute values of correlation are not as high as in the first regime, and the maximum correlation still occurs at a lag of 0 years.

Overall the timeseries of the meridional density difference in the four different intervals show different behavior in two different periods of the simulation as compared to the AMOC. This breakdown in correlation implies a possibility for the AMOC to be driven by the meridional density difference in one part of the simulation, and by another variable (or another vertical interval of the MDD) in another part of the simulation, and therefore calls for a separation into temporal regimes, when examining the correlation. The correlation coefficient reaches a maximum of 0.8694 between the AMOC and the MDD in interval 1 in the first regime and 0.7457 between the AMOC and the MDD in interval 2 in the second regime. The fact that the highest correlation in both cases occur at a lag of 0 years makes the determination the direction of causality impossible. In all cases here has the AMOC been evaluated at the 75th latitude index, which roughly corresponds to 33°N.

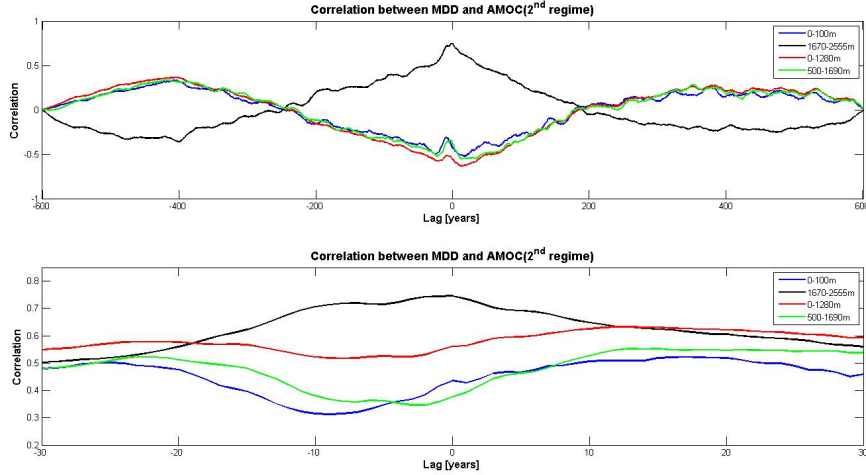


Figure 8: a shows the correlation between the AMOC and the MDD in the 2nd temporal regime. Whereas a positive correlation exists in the bottom part of the ocean, an anti-correlation exists in the other 3 intervals. In **figure b** the absolute values are shown for all 4 correlation coefficients for the sake of comparison. It can be seen that the correlation is highest for the lowest part of the ocean. In all cases the maximum correlation occurs at 0 years lag.

5.3 The correlation between the AMOC and the Southern Ocean winds

As mentioned in section 2 the atmospheric grid, on which the winds are defined, is different from that of the ocean. Directly in the data were the wind stress variables τ_y and τ_x which quantify the drag of the winds on the ocean in the meridional and zonal direction respectively. The latitudinal interval designed to represent the Southern Ocean were defined by the boundaries 64°S and 53°S which roughly correspond to that of the Drake's Passage. The coarser atmospheric resolution means that this interval contains only three latitude indices.

The total wind stress zonally averaged over the entire longitude band at each latitude index j has been numerically computed as

$$\tau_{avg} = \frac{\sum_{i=1}^{96} \tau_i(j) \cdot dx_i(j)}{\sum_{i=1}^{96} dx_i(j)}$$

where $\tau = \sqrt{\tau_x^2 + \tau_y^2}$ is the total wind stress experienced at a grid point. This is plotted in figure 9 for each of the three latitude indices

At neither of the three latitude indices in the Southern Ocean does the wind stress show a behavior similar to that of the AMOC.

The meridional Ekman transport caused by the wind stress as defined by equation 10 can be zonally integrated over the entire band to get the net meridional transport driven by the winds.

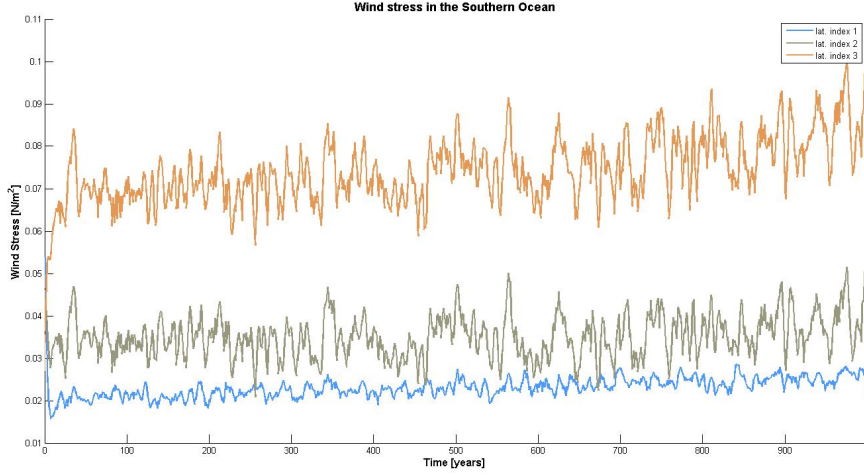


Figure 9: Average wind stress in the Southern Ocean latitude bands as defined by a northern boundary at $64^{\circ}S$ and a southern boundary at $53^{\circ}S$.

$$\oint V \partial x = - \oint \frac{\tau_x}{\rho f} \partial x$$

This was numerically zonally integrated at each latitude index j over the entire band at all longitude indices i

$$\sum_{i=1}^{96} V_i(j) \cdot dx_i(j) = - \frac{1}{f(j)} \cdot \sum_{i=1}^{96} \frac{\tau_{x_i}(j)}{\rho_i(j)} \cdot dx_i(j)$$

and is plotted in figure 10 for each of the three latitude indices

It is clear that the behavior of neither the wind stress or the meridional Ekman transport are similar to that of the AMOC. They do not show the same rapid increase up to year 400 and neither the negative trend or oscillatory behavior after year 400.

In order to completely establish the correlation - or lack thereof - between the AMOC and the Southern Ocean winds, the upwelling caused by the horizontal divergence of the Ekman transport (defined by equation 11) in the Southern Ocean was computed. As elucidated in section 3 the net upwelling in the Southern Ocean (at least down to the depth of the shallowest sill) must be caused only by the meridional Ekman transport, since this is a closed latitude band and the pressure gradient therefore zonally integrates to zero.

So the upwelling due to the divergence of the meridional Ekman transport is given as

$$w(-h_m) = \frac{\partial V}{\partial y}$$

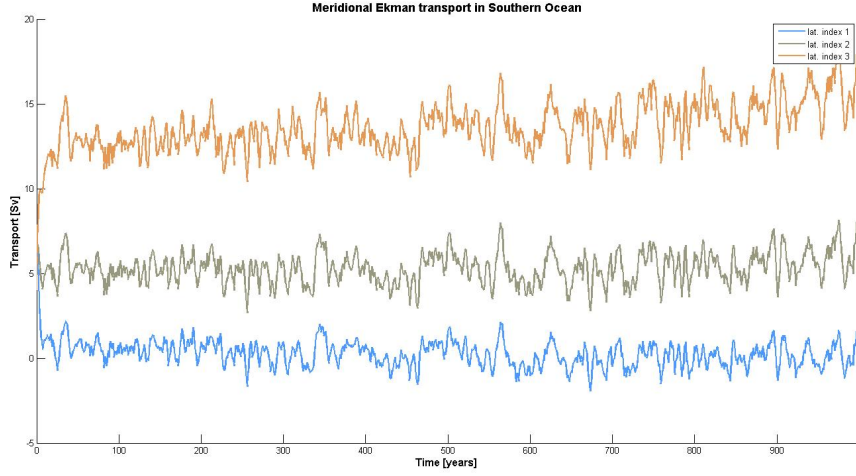


Figure 10: Zonally integrated meridional Ekman transport in the Southern Ocean latitude bands as defined by a northern boundary at $64^\circ S$ and a southern boundary at $53^\circ S$.

In order to compute the upwelling over the entire Southern Ocean the meridional divergence has been numerically integrated as

$$w_{total} = \sum_{i=1}^{96} \frac{\partial V_i}{\partial y_i} \cdot \partial x_i = \sum_{i=1}^{96} V_{E_i}(j=3) \cdot dx_i(j=3) - V_{E_i}(j=1) \cdot dx_i(j=1)$$

where $j = n$ indicates the n^{th} latitude index. The meridional difference at each latitude interface will vanish, and thus the only contributions remaining are those at the southern and northern most latitudes. The result of the upwelling is shown in figure 11

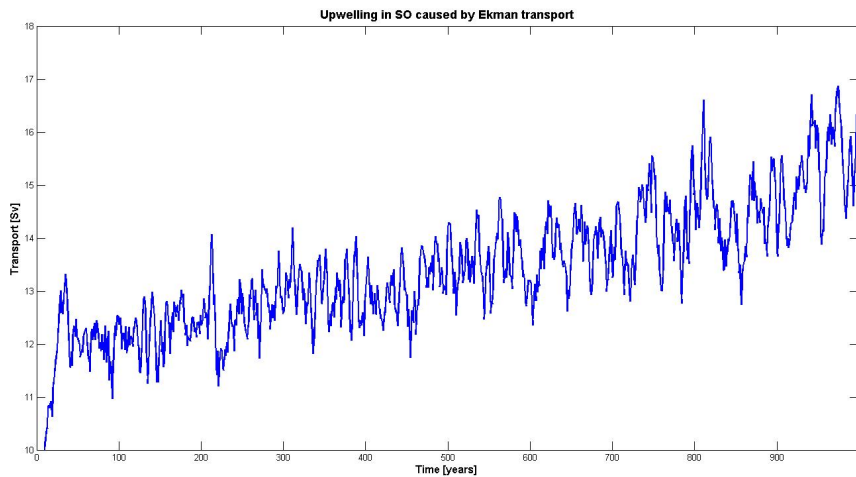


Figure 11: Total upwelling in the Southern Ocean caused by the divergence Ekman transport

Again it is clear that the behavior of the AMOC is not at all similar to that of the upwelling in the Southern Ocean. On the basis of this investigation the data show no apparent correlation between the AMOC and the winds in the Southern Ocean. All in all it is thus fair at this point to reject the hypothesis that the AMOC should be controlled by the winds in the Southern Ocean. Hence no further investigation between this correlation was made.

5.4 The correlation between the AMOC and the deep water formation

As a measure of the deep water formation was used the annual mean of the monthly maximum of the boundary layer depth - hereafter termed the XBLT. Although deep water formation is known to take place during winter time over periods of a few days (Kuhlbrodt et al., 2007), the annual mean was the best resolved variable available. This means that also summer time boundary layer depth has implicitly taken into account, when evaluating the boundary layer depth, even though convection does not take place in summer. A region in the north Atlantic was defined from which the XBLT values were used. This region encompasses both the Labrador Sea, the Denmark Strait, and large parts of the Norwegian and Greenland Sea, i.e. regions where the deep water formation is known to happen are all included.

In order to visualize the region from which the XBLT values were used figure 12 provides a filled contour plot of the XBLT in the north Atlantic at year 500 of the simulation, and it is clear that all the above mentioned regions are included.

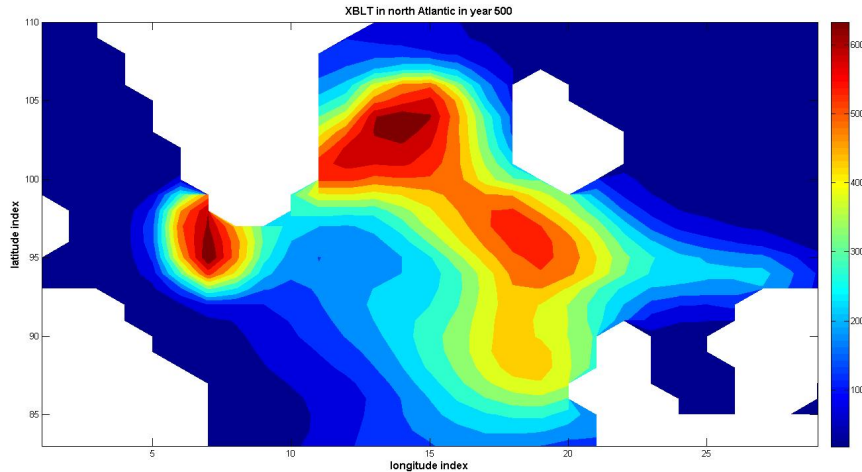


Figure 12: Shows the XBLT in the North Atlantic region, from which XBLT values were used, at year 500. The colorbar indicates XBLT in meters, white color indicate land, and the region shows Greenland in the north, Canada in the west, UK and Scandinavia in the southeast and Iceland in the northeast, and thus both the Labrador Sea and Denmark Strait are included.

From this region a maximum value of the XBLT were extracted only as a function of time and compared with the maximum value of the AMOC. In this analysis the AMOC was evaluated at the 95th latitudinal index - just south of where the maximum XBLT values

takes place in order to eliminate any travel time bias issues - and again at the depth of maximum transport. An explanation of exactly this index will be addressed later in this section. The timeseries of the maximum of the XBLT in this entire northern region and the AMOC can be seen in figure 13.

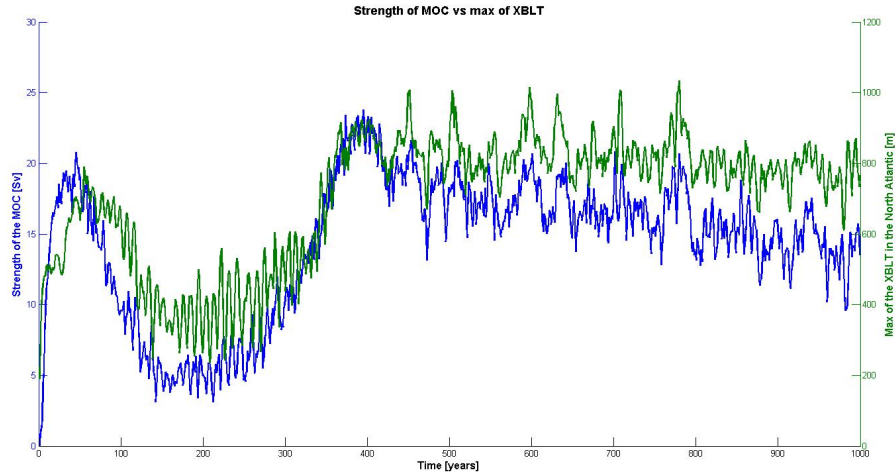


Figure 13: Timeseries of the maximum XBLT (green) in the north Atlantic and the AMOC transport (blue) at 95^{th} latitudinal index. A correlation between the two is clear, with the same rapid increase until year ~ 400 and same oscillatory behavior in the late part of the simulation. The decreasing trend in the late part of the simulation of the AMOC is, however, not as pronounced in the XBLT. The XBLT values are the result of a 5-year running mean.

It is shown that the XBLT reaches maximum depths of around 1000m which is lower than Holdsworth and Myers (2015) but not inconsistent with Böning et al. (1996) and Lohmann et al. (2014). At this latitude it is also worth noticing that the AMOC transport is significantly lower than further south shown previously. The overall behavior of the two are similar showing the rapid increase before year 400 and the oscillatory behavior in the later part of the simulation. The decreasing trend after year 400 of the AMOC is, however, not nearly as pronounced in the deep water formation. In computing figure 13 the XBLT maximum have been subjected to a 5-year running mean.

A correlation coefficient as a function of lag years was also calculated between the XBLT and the AMOC. In doing this calculation the AMOC was again evaluated at the 95^{th} latitudinal index. As with the correlation between the AMOC and the MDD the correlation between the AMOC and the XBLT were also calculated for both the full simulation, and the 1^{st} and 2^{nd} temporal regime alone, the result of which can be seen in figure 14

First of all, it can be seen that the correlation is very high when considering the full simulation and the first regime. Here the correlation coefficient reaches a maximum value of 0.8273 and 0.7665 at 2 and 3 years lag respectively. In contrast to the correlation between the AMOC and the MDD it is encouraging that the maximum correlation occurs when the AMOC is lagging the XBLT by 2 or 3 years. The fact that both the correlation in the 1^{st} and the 2^{nd} regime are lower than when considering the entire simulation would imply, however, that the correlation between the AMOC and the XBLT is not elucidated further by separating the timeseries into two regimes.

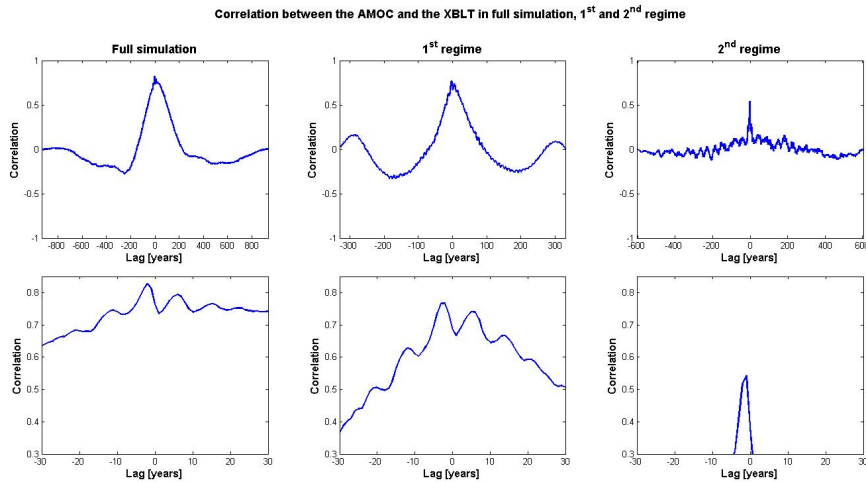


Figure 14: Correlation coefficients as a function of lag years between the AMOC and the XBLT. **Left panel** shows values for the full simulation, **center panel** for the 1st regime, and **right panel** for the 2nd regime.

In order to further investigate the influence of deepwater formation on the AMOC a more precise location of where the deep water formation takes place were examined. At each year in the simulation the long- and latitude index of the maximum XBLT were counted and recorded into a 2-dimensional histogram. The result of this for the entire simulation can be seen in figure 15. The colormap in this figure is logarithmic in order to favor the exposure of grid points where the the maximum XBLT takes place only a few number of times, and the darkest blue color thus indicates places where the maximum XBLT occurs not even once during the entire simulation. This shows three distinct regions of deep water formation; the Labrador Sea, the Denmark Strait and the northeast Atlantic from left to right.

These three regions (the Labrador Sea, the Denmark Strait, and the northeast Atlantic) were then separately defined and the XBLT maximum in each were found only as a function of time. This can be seen in figure 16 along with the AMOC transport. From this it is clear that in periods of time with low AMOC strength the deep water formation mainly take place in the northeast Atlantic, and it is furthermore remarkable that in this period of time no deep water formation at all take place in the Labrador Sea. The rapid increase in AMOC strength until year ~ 400 is best resembled by the XBLT in the Denmark Strait, whereas the decreasing trend and oscillatory behavior in the late part of the simulation is perhaps better mirrored in the XBLT in the Labrador Sea. However, this region also clearly shows the most volatile behavior with values changing from $\sim 1000\text{m}$ to below 200m in the matter of about 15 years. In this plot XBLT values from all three subpolar regions have been subjected to a 5-year running mean to filter out high frequency changes.

The vertical grey lines in figure 16 indicate the years at which the simulation has been separated into the two aforementioned temporal regimes (the first 65 years are considered a spin-up phase). Since the behavior of the XBLT in the three deep water formation sites are significantly different in both first and second temporal regime, it makes sense to compare the correlation coefficient as a function of lag years between each of them and the AMOC in both regimes. It was, however, considered that the XBLT behavior in none of the three deep water formation sites resembled that of the AMOC for the *entire* simulation, why the

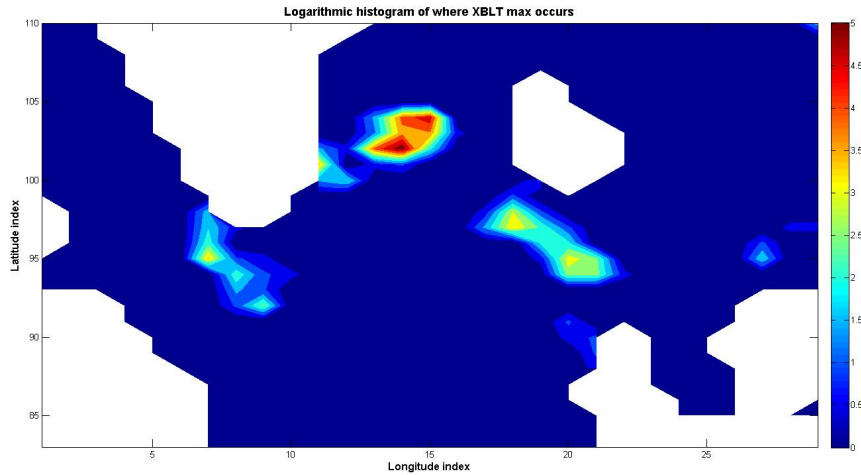


Figure 15: 2-d histogram of where the maximum XBLT occurs. Values are logarithmic; dark blue indicates places where XBLT not even at a single timestep obtains the maximum value, red indicates places where XBLT often obtains maximum value throughout the entire simulation. From this three distinct regions where deep water formation occurs can be extracted; the Labrador Sea, the Denmark Strait and the northeast Atlantic.

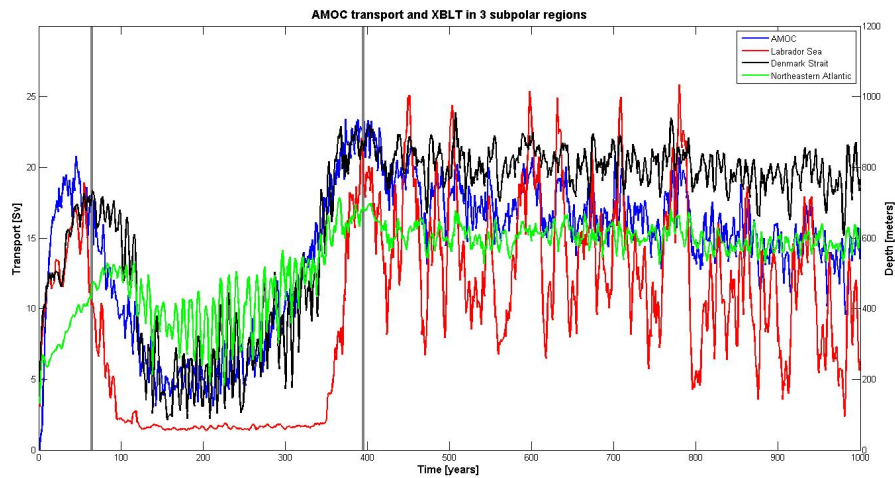


Figure 16: Timeseries of the AMOC transport (left side y-axis) and the XBLT maximum (right side y-axis) in three regions in the north Atlantic where deep water formation takes place. It can be seen that deep water formation occurs mainly in the northeastern Atlantic in the first 350 years of the simulation, whereafter it is shifted further northward to the Denmark Strait. Whereas the deep water formation in the northeastern Atlantic and the Denmark Strait remain somewhat steady from year 400 that of the Labrador Sea displays large oscillations and a decreasing trend similar to the AMOC transport. Vertical grey lines mark the regime separation years

correlation coefficient for each of the three sites was only found for the first and second regime and not for the entire simulation.

In figure 17 can be seen the correlation between the AMOC transport and the XBLT maximum in the three subpolar regions as a function of lag years. The left panel and right shows the correlation coefficient in the first regime and second regime respectively and the lower panel is a zoom in on the years of max correlation of the upper. First of all it is clear that the general correlation is higher in the first regime than in the second. Second of all it is interesting that the correlation for Denmark Strait is the highest in the first regime, whereas that of the Labrador Sea is highest in the second. It is furthermore worth noticing that in both first and second regime the maximum correlation occurs at a negative number of lag years, i.e. the AMOC lagging the deep water formation. In the first regime this is 0.7962 between the AMOC and the XBLT in the Denmark Strait at -2 years lag while it is 0.6855 between AMOC and the XBLT in the Labrador Sea at -1 years lag.

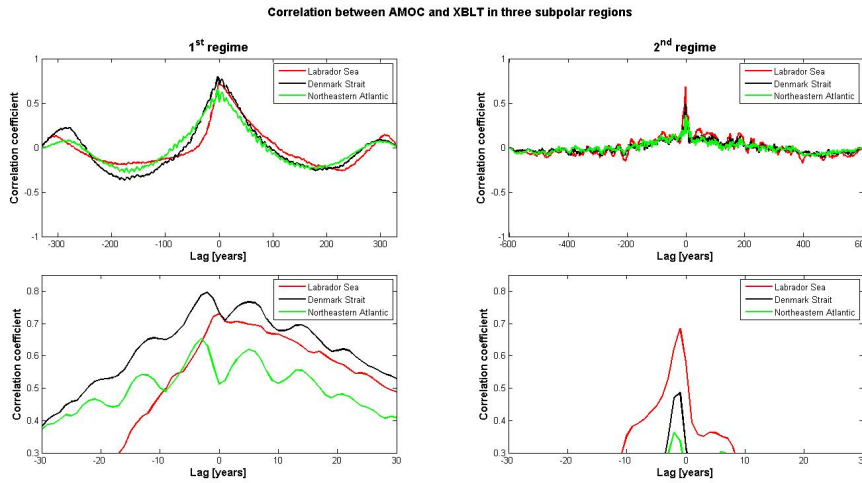


Figure 17: Correlation coefficient between the AMOC transport and the XBLT in three subpolar regions in 1st and 2nd regime. **Left panel** shows the 1st and **right panel** the 2nd regime.

Overall it is encouraging that no matter how the simulation is split up, the maximum correlation always occurs when the AMOC is lagging the XBLT. The correlation analysis between the AMOC and the XBLT shows a maximum correlation between the two when considering the maximum of the XBLT in the entire North Atlantic and the entire simulation. It is interesting, however, that when splitting the simulation into two temporal regimes the correlation coefficient reaches a higher value when also splitting the XBLT into three subregions in the North Atlantic, and furthermore that the subregion which shows the highest correlation coefficient changes with the temporal regime. This enables the possibility, that deep water formation in different regions can control the AMOC at different times, while the AMOC is still best represented by a maximum deep water formation in the North Atlantic. In the first regime - where the AMOC is low at first and the experiences a rapid increase - it is best represented byt the XBLT in the Denmark Strait, and in the second regime - where the AMOC is characterized by a decreasing trend with large oscillations - it is best described by the XBLT in the Labrador Sea. The fact that the year of maximum correlation in these two cases changes from 2 to 1 can possibly be explained by the increase in advection time in the counter clockwise motion, that is associated with the subpolar gyre, before reaching the latitude at which the AMOC has been evaluated. The volatile behavior shown by the XBLT in the Labrador Sea - shown both as the sudden "turn on" close to year 350 and the large oscillations in the second regime - is interesting because it implies that the deep water formation in this region can change by a very large amount in very few years,

something which would most plausibly have a large effect on the AMOC. The fact that the AMOC changes behavior shortly after such a sudden increase in XBLT in a very specific region, furthermore enables the possibility that the AMOC undergoes a state transition due to a change in the location of deep water formation.

5.5 The correlation between the AMOC and the subpolar gyre

As a measure of the subpolar gyre transport was used the barotropic streamfunction (BSF), which quantifies the depth integrated transport in the entire water column. To give an overview of the subpolar gyre transport a snapshot of the barotropic streamfunction at year 500 is shown in figure 18. The region depicted is the same as in figure 12. The differences in land area are due to the different grid on which the XBLT and BSF are defined. It can be seen that the minimum (negative values indicate a counterclockwise transport) of the BSF is located south-southeast off of the Cape Farewell reaching a local transport close to 35 Sv. The fat black line is the 0^{th} contour line indicating a transition between a clockwise and counter clockwise motion.

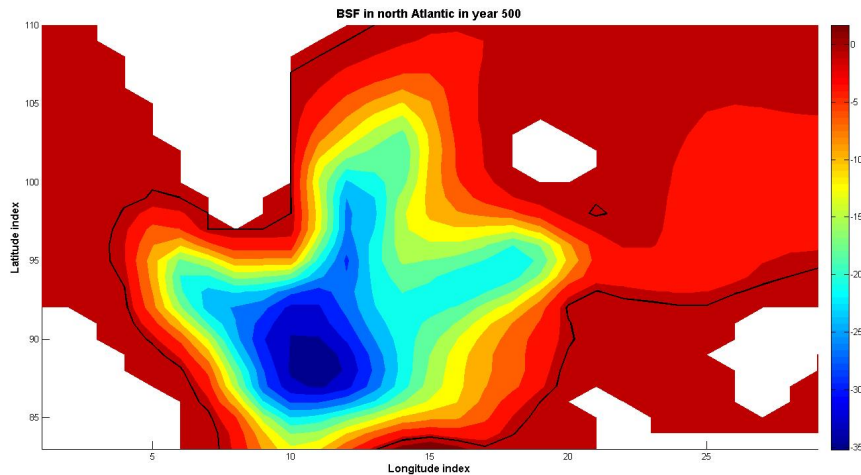


Figure 18: Values of the barotropic streamfunction in the subpolar north Atlantic in year 500. The counter clockwise motion of the subpolar gyre is clearly visible with a minimum located south-southeast off of Cape Farewell reaching 35 Sv. The heavy black line is the 0^{th} contour line indicating the transition between clockwise and counter clockwise motion.

In order to compare the subpolar gyre transport with the strength of the AMOC the subpolar gyre transport was found only as a function of time as the minimum of the barotropic streamfunction (since the transport is counter clockwise and the BSF values therefore negative) in the region shown in figure 18. Absolute values were taken and together with the AMOC transport this is shown in figure 19. For this comparison the AMOC was evaluated at the 95^{th} latitudinal index - (same procedure as used to generate figure 13).

The 95^{th} latitudinal index was computed as the mean of the indices where the maximum of the XBLT and the minimum of the BSF take place respectively. In this way neither the XBLT or the BSF have been biased by advection travel time

The correlation between the two is clear with both showing the rapid increase until \sim

year 400. In contrast to the comparison between the AMOC and the XBLT (figure 13) the decreasing trend of the AMOC in the late part of the simulation is better mirrored by the BSF. Here the BSF values are depicted as 5-year running mean values.

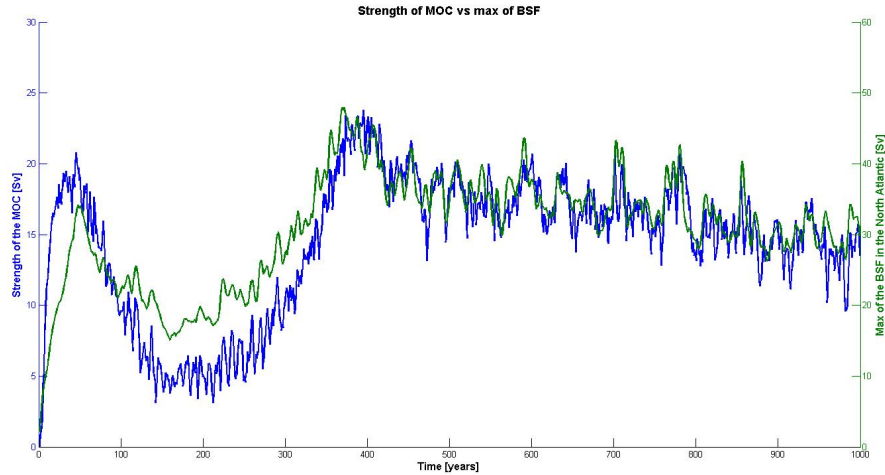


Figure 19: Timeseries of the maximum BSF in the north Atlantic and the AMOC transport at 95th latitudinal index. A correlation between the two is clear, with the same rapid increase until year ~ 400 and same decreasing trend in the last part of the simulation. The BSF values are the result of a 5-year running mean.

A cross correlation between the AMOC and the BSF have also been computed for both the entire simulation, and the first and second regime, the result of which can be seen in figure 20. In contrast to the correlation between the AMOC and the XBLT the maximum correlation in this case occurs when only considering the first regime. Here the correlation is 0.9406 at 0 years lag. Considering the fact that the north/south transport captured by the AMOC is also captured by the BSF while keeping in mind that the maximum correlation occurs at a lag of 0 years makes it impossible with this quantitative measure to determine the direction of causality.

All in all there is a strong correlation between the AMOC transport and the values of the barotropic streamfunction in the north Atlantic. As will be elaborated later in the report, however, there is also a natural quantitative bias in this particular measure since both the barotropic streamfunction and the AMOC capture meridional transport, so a high correlation coefficient was to be expected. This will be further addressed in section 7. Furthermore, the fact that the maximum correlation occurs at 0 years lag - when considering both the first, and second regime or the entire simulation - causes the determination of causality impossible with this quantitative method.

5.6 Summary of the preliminary analysis

On the basis of the quantitative analysis of the correlation between the AMOC and the four hypothesized drivers there seem to be no apparent correlation between the AMOC and the Southern Ocean wind and the according hypothesis is therefore rejected. The correlation between the AMOC and the remaining three possible drivers were all positive and significant.

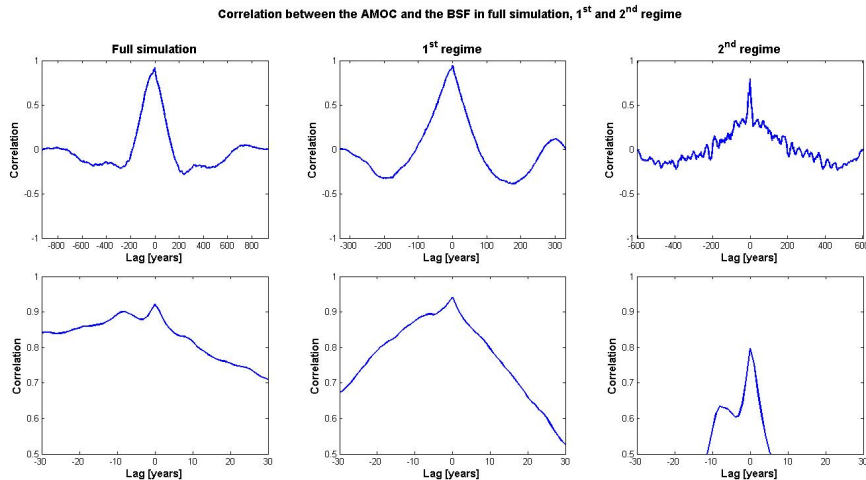


Figure 20: Correlation between the BSF and the AMOC in the full simulation (**left panel**), first regime (**center panel**) and second regime (**right panel**). The highest correlation occurs when only considering the first regime - reaching a maximum of 0.9406 at 0 years lag - while only considering the second gives the lowest correlation. In all matters the maximum correlation occurs at a lag of 0 years.

This correlation analysis has been presented only evaluating the AMOC at a single latitude for each variable. For the MDD this was the 75th index, since it is half way between the two regions used to compute the MDD. For the XBLT and the BSF the 95th latitude index was used. This index was calculated as the mean of the time averaged latitudes of where the max BSF and XBLT occurs. The only variable which the AMOC seemed to be lagging was the XBLT, and this particular correlation was not very strong, however. In order to get a complete overview of the maximum correlation between the AMOC and each variable the correlation was at last computed as a function of both lag years and the latitude at which the AMOC was evaluated. This is showed for each variable and for the full simulation, the 1st and the 2nd regime in figures 21, 22 and 23 below with the color indicating the value of the correlation coefficient. In each figure are showed white dashed lines, which marks the latitudinal extent of the deep water formation regions, and a white marker which shows the lag and latitude at which the correlation is highest. This is done for the sake of retaining a sense of geographic location of the correlation.

From figure 21 it is clear to see that the correlation between the AMOC and the MDD is much higher in the first than in the second regime. It is also interesting that the latitude of maximum correlation changes from the 80th latitude index (roughly 43°N) to just north of the deep water formation region going from regime 1 to regime 2. This would point to the possibility that changes in density occur predominantly in the deep water formation region. In the second regime the correlation south of the deep water formation region is significantly weaker than in the first regime.

The first thing to notice in figure 22 is that the correlation between the AMOC and the XBLT is actually higher than originally proposed by evaluating the AMOC at the 95th latitude index. Just south of the deep water formation region it reaches a value of ≈ 0.82 for the full simulation. When splitting the correlation analysis into the two regimes the correlation drops in both cases, but it is worth noticing that the location of maximum correlation also

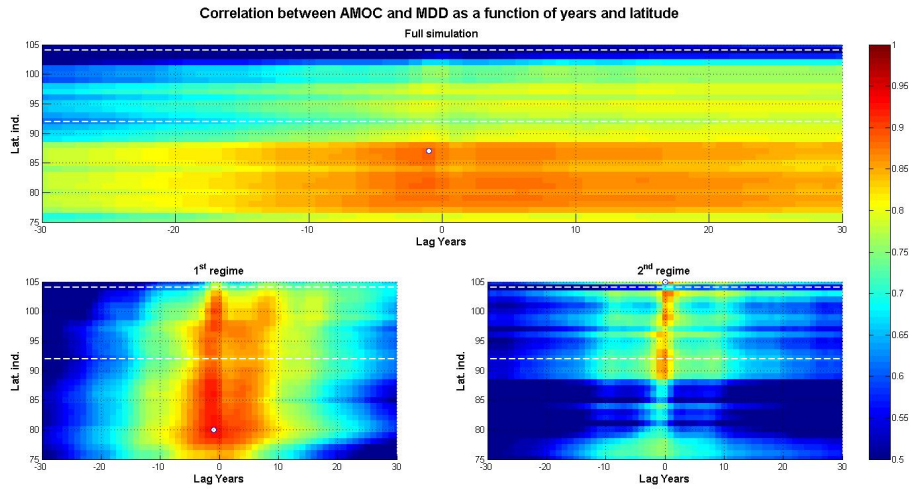


Figure 21: Correlation coefficient between the AMOC and the MDD as a function of lag years (horizontal axis) and the latitude at which the AMOC is evaluated (vertical axis). **Upper panel** shows the correlation coefficient for the full simulation, **lower left panel** the 1st regime, and **lower right panel** the 2nd regime. In each regime the depth interval which showed the highest correlation is plotted. White dashed lines indicate the region in which the deep water formation occurs, and the white marker shows the maximum correlation.

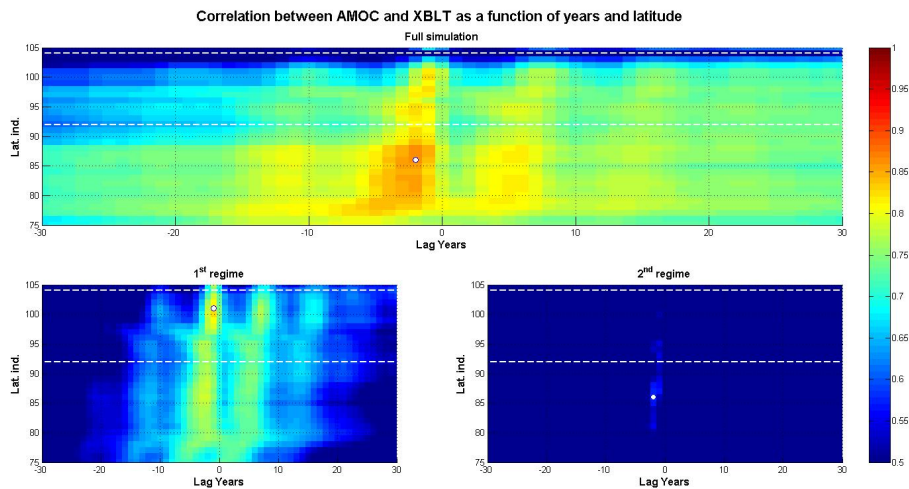


Figure 22: Correlation coefficient between the AMOC and the XBLT as a function of lag years (horizontal axis) and the latitude at which the AMOC is evaluated (vertical axis). **Upper panel** shows the correlation coefficient for the full simulation, **lower left panel** the 1st regime, and **lower right panel** the 2nd regime. White dashed lines indicate the region in which the deep water formation occurs, and the white marker shows the maximum correlation.

changes indicating that the source of deep water affecting the AMOC changes.

In figure 23 the most striking aspect is that the location of maximum correlation does not change at all between the two regimes. This could again be caused by the mathematical

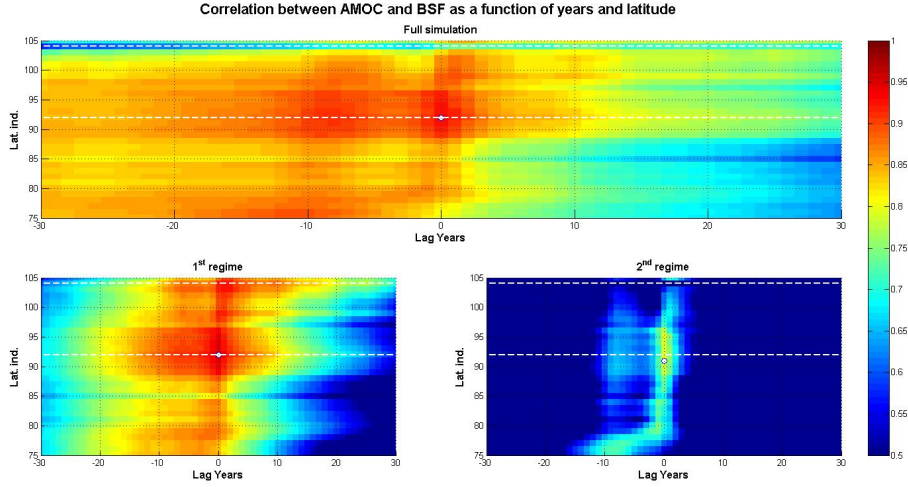


Figure 23: Correlation coefficient between the AMOC and the BSF as a function of lag years (horizontal axis) and the latitude at which the AMOC is evaluated (vertical axis). **Upper panel** shows the correlation coefficient for the full simulation, **lower left panel** the 1st regime, and **lower right panel** the 2nd regime. White dashed lines indicate the region in which the deep water formation occurs, and the white marker shows the maximum correlation.

inclusion of the meridional transport in the definition of the barotropic streamfunction, and as mentioned previously, this is a bias towards a higher correlation coefficient.

In order to give a clear picture and an overview of the correlation between the AMOC and the MDD, XBLT and the BSF, and to provide the details of how each quantitative analysis was performed the important most results of the entire analysis have been summarized in the tables 1, 2, 3, and 4 below.

The tables are arranged as follows: in the most left column are listed each variable; in a specific row going to the right through each column the first numbers indicates the highest correlation coefficient when analyzing the full simulation, the first, and the second regime respectively; the next three numbers are the lag years at which the maximum correlation coefficient occur in the full simulation, first and second regime; table 4 furthermore includes the latitude at which the AMOC was evaluated, when the maximum correlation coefficient occurs, in the last three values.

Variable	Max correlation			Lag years		
	full	1 st	2 nd	full	1 st	2 nd
MDD	0.8074	0.8694	0.7457	13	0	0
XBLT	0.8273	0.7665	0.5423	-2	-3	-1
BSF	0.9212	0.9406	0.7984	0	0	0

Table 1: Correlation between the AMOC, MDD, XBLT and BSF. For the correlation between the AMOC and XBLT and BSF the AMOC was here evaluated at the 95th latitude index in both full simulation, 1st, and 2nd regime. For the correlation between the AMOC and the MDD the AMOC was evaluated at the 75th latitude index. The correlation values for MDD have been obtained using the depth interval which gave the highest correlation

Depth interval	Max correlation			Lag years		
	full	1 st	2 nd	full	1 st	2 nd
0-100	0.8074	0.8694	0.5222	13	0	20
1670-2555	0.7042	0.8208	0.7457	-10	0	0
0-1280	0.7526	0.8133	0.6324	22	0	13
500-1690	0.786	0.823	0.5522	6	0	13

Table 2: Correlation between the AMOC evaluated at the 75th latitude index (roughly 33°N) and the MDD in specific depth intervals and in the two temporal regimes

Region	Max correlation		Lag years	
	1 st	2 nd	1 st	2 nd
Labrador Sea	0.7314	0.6855	0	-1
Denmark Strait	0.7962	0.4859	-2	-1
Northeastern Atlantic	0.6539	0.3636	-3	-2

Table 3: Maximum correlation coefficients between AMOC at 95th latitude index and XBLT in specific regions and temporal regimes. The two right most columns indicate at how many lag years the maximum correlation occurred.

Variable	Max correlation			Lag years			Latitude		
	full	1 st	2 nd	full	1 st	2 nd	full	1 st	2 nd
MDD	0.8839	0.9305	0.9048	-1	-1	0	87	80	105
XBLT	0.8652	0.8276	0.5862	-2	-1	-2	86	101	86
BSF	0.9327	0.9584	0.7992	0	0	0	92	92	91
XBLT in LS	-	0.8560	0.6998	-	0	-2	-	72	86
XBLT in DS	-	0.8626	0.5241	-	-1	-1	-	100	100
XBLT in NA	-	0.7648	0.4596	-	-1	-1	-	105	105

Table 4: Results of correlation analysis between the AMOC and the MDD, XBLT, and BSF as a function of lag years and latitude of evaluation of the AMOC. The values for the correlation with the MDD have been obtained using the depth interval which showed the highest correlation. For the full simulation and the first regime this is from 0 – 100 meters, while for the second regime it is the interval spanning 1650 – 2555 meters.

Tables 1, 2, and 3 summarize the analysis performed, when only evaluating the AMOC at a single latitude, whereas table 4 includes the dependence of the correlation coefficient on the latitude at which the AMOC was evaluated. Comparing table 1 and 4 it is clear that there is actually a very high correlation between the AMOC and the MDD at a lag of -1 year in the first regime when the AMOC is evaluated at the 87th latitude index which is roughly at 53°N. However, the fact that maximum correlation between the AMOC and the MDD occurs at the 105th latitude index, which is just north of the Denmark Strait, in the second regime and that this correlation in the regime is generally much higher in the deep water formation region than south of it, somewhat blurs the picture of the causal relation between the two. If the MDD should drive the AMOC the correlation coefficient should be high south of the deep water formation region which it is not. Furthermore, it is also

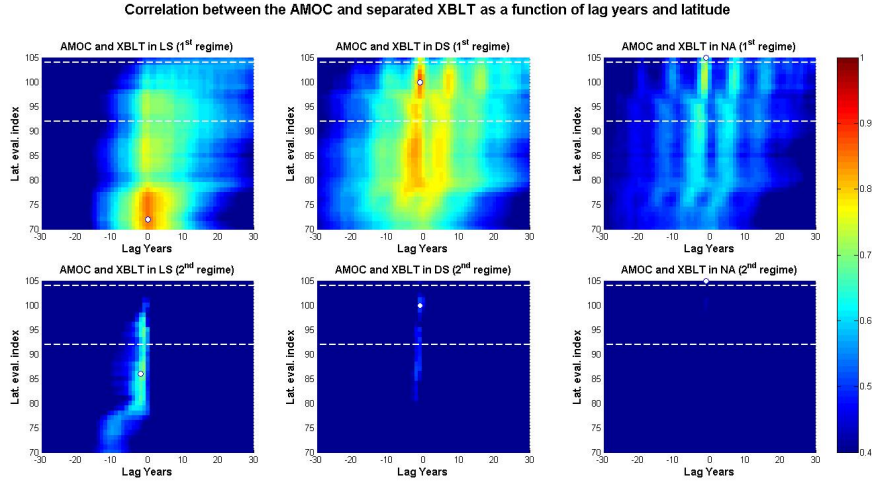


Figure 24: Correlation coefficient between the AMOC and the XBLT in three regions in the first (**upper panel**) and second regime (**lower panel**). **Left column** shows correlation from the Labrador Sea, **center column** the Denmark Strait and **right column** the northeast Atlantic.

clear from table 4 that the AMOC/MDD correlation in the second regime is highest when there is no lag between the two. On the basis of this, it is still deemed relevant to split the analysis into two regimes. What is also important in regards to the further analysis in this study, is that the MDD in the intervals 0 – 1280m and 500 – 1690 are in all cases lagging the AMOC and in no cases do they exhibit the highest correlation coefficient. They are therefore deemed irrelevant.

Table 4 still leaves only the XBLT preceding the behavior of the AMOC although with a much lower correlation coefficient in the second regime, but if the XBLT is investigated in separate regions, it can be seen from table 3, that the correlation between the AMOC and the XBLT in the Labrador Sea in the second regime is actually higher than if looking at the XBLT as a single variable.

This prompted the correlation between the AMOC and the XBLT in the three separated regions to be performed as a function of the latitude at which the AMOC as well. The results from this analysis is shown in figure 24 and the most important details are included in table 4

The conclusions from the preliminary analysis should then be as follows: Because of the AMOC behavior and the fact that the relation between the AMOC and the MDD in all but three depths interval breaks down just prior to year 400 of the simulation it seems necessary to split the correlation analysis into two temporal regimes.

Even though the correlation between the AMOC and the BSF is the highest it is not possible via this method of analysis to determine whether the BSF controls the AMOC, since this maximum correlation occurs when there is no lag between the two, thus rendering the distinction between the direction of causality impossible. Furthermore, because of the inclusion of the meridional transport in the mathematical definition of the barotropic stream-function there is a natural bias toward a high correlation, even though no causal relation is implied.

In the first regime the correlation between the AMOC and the MDD reaches a maximum of 0.9305 at a lag of -1 year at the 80^{th} latitude index (roughly corresponding to 43°N) when the meridional density difference is calculated in the top 100 meters. Since this is the highest correlation occurring with a lag of the AMOC, this analysis technique points to the conclusion that the meridional density difference drives the AMOC in the first regime.

Interestingly the correlation between the AMOC and the XBLT seems in all cases to increase if the XBLT is separated into the three exact regions where the deep water formation occurs rather than simply using a total maximum value of the XBLT. This could highlight the possibility that the influence of deep water on the AMOC comes from specific regions rather than simply from the entire subpolar Atlantic.

In the second regime only the correlation between the AMOC and the XBLT displays a maximum when the AMOC is lagging. Here the maximum correlation occurs between the AMOC and the XBLT in the Labrador Sea at a lag of -2 year when the AMOC is evaluated at the 86^{th} latitude index (roughly corresponding to 51°N). This points to the conclusion that it is the deep water formation in the Labrador Sea which drives the AMOC in the second regime.

6 Qualitative analysis

The analysis performed in section 5 had a quantitative character and focused on a measure of the correlation between the AMOC and the hypothesized drivers. Whereas this sort of analysis has the advantage of being able to quantify how well one variable relates to another via the correlation coefficient, it suffers from not being able to address and elaborate on the issue of a causal direction and even more importantly the causal relation between the two variables under investigation.

The content of this section, on the other hand, should elaborate further on the details of *how* and *why* these physical mechanisms actually influence the behavior of the AMOC, and what can be learned through such examinations. So where the questions of the previous section related to *how well* a variable correlated with the AMOC, this section will have a more qualitative character and address the issues of *why* the behavior of a certain variable relates to the AMOC.

Regarding the behavior of the AMOC, it proved fruitful to split the correlation analysis into two temporal regimes. Following this structure, the first part of this section will thus predominantly focus on explaining the behavior of the AMOC leading up to the arrest of the rapid increase just prior to year 400 of the simulation. The objective of the first part will be to explain the behavior in the first regime and what causes the regime transition. The second part of this section will focus on the behavior of the AMOC in the second regime and have an emphasis on explaining the large rapid increases/decreases, referred to as the oscillatory behavior or the oscillations.

6.1 First regime behavior and regime transition

As mentioned previously (and as can be seen in figure 3 the AMOC behavior in the years 350 – 400 are characterized by an increasingly rapid increase, and the three remaining hy-

pothesized drivers all showed similar characteristics. Subsequent to this rapid increase the AMOC is relatively steady displaying only small fluctuations for roughly 20 years perhaps with a slight increase, before a significant decrease is once again shown. Because of this behavior and in order to answer the question of *what causes the transition from one state to the other*, the behavior of these possible drivers (the meridional density difference, barotropic stream function, and XBLT) were analyzed on annual and decadal time scales. The underlying assumption when performing this investigation was that, *the variable which stops to increase first, is the one causing the total arrest in increase*, and this variable will hence be considered as the first link in a causal reaction.

Since the meridional density difference in the depth intervals 0 – 1280 m and 500 – 1690 m and the XBLT in the northeast Atlantic were deemed irrelevant (as compared to the other two depth intervals and regions of deep water formation in section 5) they have been omitted from the analysis that follows unless the opposite is explicitly stated.

From the same timeseries that were used to compute the correlation coefficient (i.e. as showed in figures 5, 13, 16, and 19) the years at which each of the variables ceased to increase rapidly were extracted. An overview of these years are presented in table 5.

Variable	Year of rapid increase stop	Year of maximum
AMOC	373	395
MDD (0 – 100)m	367	392
MDD (1670 – 2555)m	368	405
XBLT	367	402
XBLT in DS	367	402
XBLT in LS	378	392
BSF	371	371

Table 5: Years at which AMOC and possible drivers stops rapid increase prior to year 400 and at which the overall maximum is reached.

The fact that the meridional density difference in the top layer are the first variable to cease to increase corresponds well with the hypothesis, that this is the primary driver of the AMOC in the first regime. The deep water formation in the Denmark Strait cease to increase in the same year, however. It is seen that the BSF also experience a stop of the rapid increase prior to the AMOC, but this is a global maximum, which means that when the BSF starts to decrease the AMOC still increases, if only by a small amount. So we proceed with the notion that an arrest of the increase in the meridional density difference and the deep water formation in the Denmark Strait are to be considered as the first link in a causal chain, which should explain the transition of the AMOC.

In order to obtain a values for the meridional density difference only as a function of time and depth, an average was computed at each time step in two different regions; one bounded by the latitudes $[62^{\circ}N; 65^{\circ}N;]$ and the longitudes $[64^{\circ}W; 10^{\circ}E]$ dubbed the northern region, and one bounded by latitudes $[10^{\circ}S; 10^{\circ}N;]$ and the longitudes $[60^{\circ}W; 13^{\circ}E]$ dubbed the equatorial region. The first step to elaborate on the AMOC behavior was to compute the density in these two regions separately. This is showed in figure 25. Here it is very clear that the changes occur in the northern region and not in the equatorial region.

Due to this assymetry timeseries of both temperature and salinity were computed in the

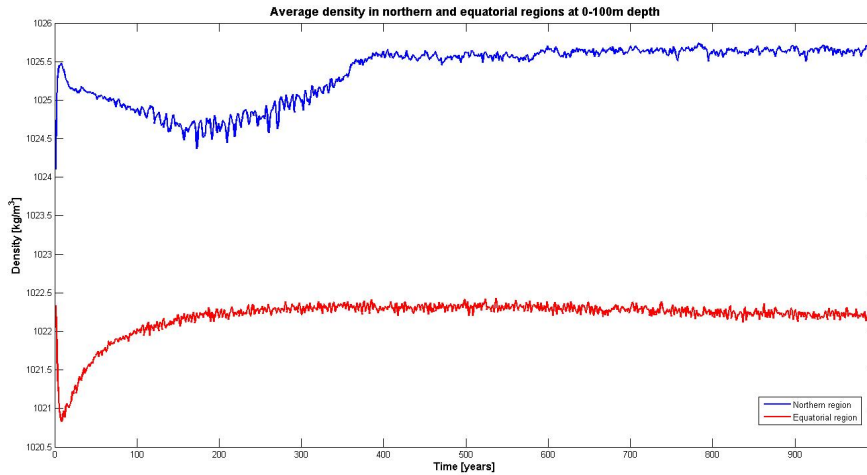


Figure 25: Depth averaged density in depth interval 1 (0 – 100m depth) in the northern and equatorial region. The northern region displays a distinct increase in density similar to that of the AMOC, whereas the density in the equatorial region remains steady in the same period of time.

northern region in order to explain the behavior of the changes in density in the northern region. Figure 26 shows the depth averaged salinity and temperature in the northern region in depth interval 1. Both salinity and temperature shows similar behavior as the MDD and the AMOC, i.e. a rapid increase up to year 400, but because of their opposite impact on density as given by the equation of state, the increase in density must take place due to the increase in salinity.

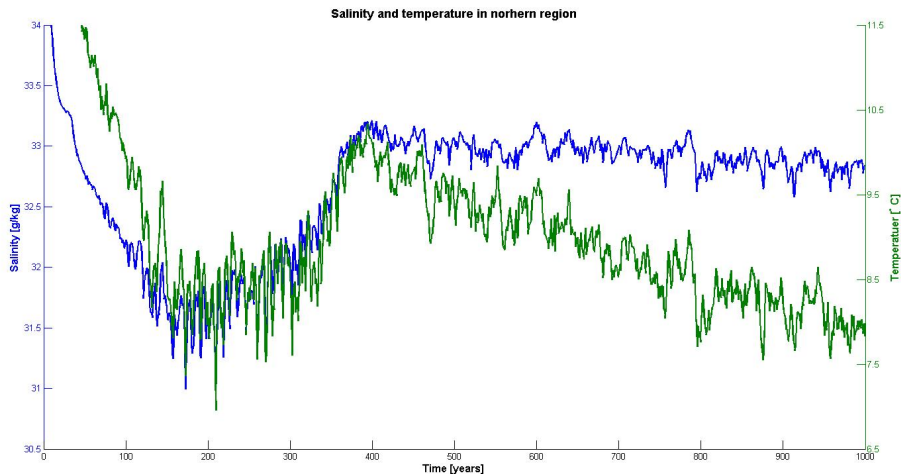


Figure 26: Timeseries of the depth averaged salinity and temperature in depth interval 1 (0 – 100m depth) in the northern region

It is clear then that the meridional density difference in the upper most 100 meters increase because of a large increase in salinity in the northern part of the Atlantic. The same vertical interval of the equatorial part of the Atlantic does not show any increase in

density. The density in this part, on the other hand, is extremely stable. Since the northern region also displays a large increase in temperature, the increase in MDD is attributed to the salinity increase in the northern region. The influence of temperature will be elaborated in due course.

A number of possible causes for this was examined but here is only presented the most prominent results. A discussion of other theoretically possible factors are presented in section 7. As mentioned previously the meridional density difference, deep water formation and the barotropic streamfunction in the northern Atlantic all display similar behavior just prior to year 400 of the simulation. This simultaneous increase is attributed to an internal feedback in the system best visualized by the salinity and the barotropic streamfunction in the northern Atlantic in figure 27. Here salinity is plotted as colour filled contours and overlaid by black lines of constant values of the barotropic streamfunction. The figure shows the northern Atlantic basin where white patches indicate land. As such Greenland is shown in the northern boundary, Canada in the western, the European and African continents in the southeastern and Iceland in the northeastern part. The horizontal and vertical axes are longitude and latitude indices, and it is important to notice, that these are not directly translated into longitude and latitude because of the irregularity of the grid.

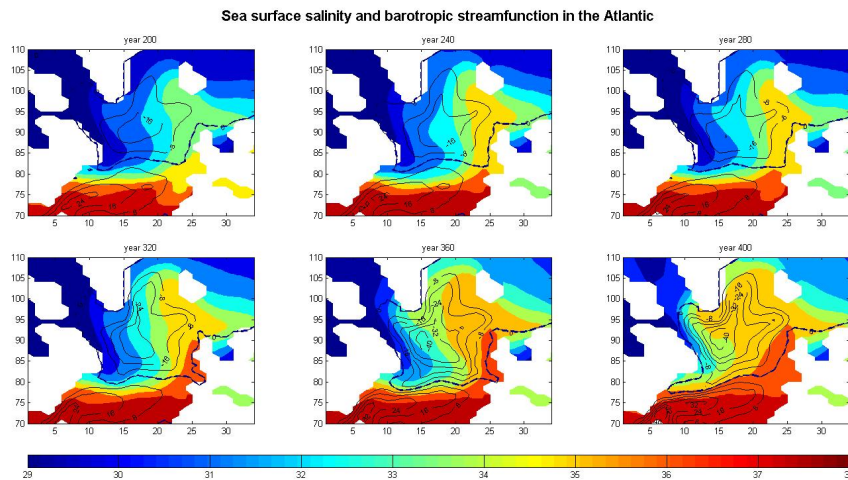


Figure 27: Filled coloured contour plot of the sea surface salinity overlaid by black contour lines of constant barotropic streamfunction values at 6 different years separated each by 40 years leading up to the arrest of the rapid increase of the AMOC. Salinity values are indicated by the colorbar. The heavy black line is where the barotropic streamfunction is zero indicating a change between clockwise and counterclockwise transport

From here it is clear that the changes in sea surface salinity starts in the eastern part of the north Atlantic basin, while the western part exhibits no significant increase until year 320. The increase in salinity the eastern part occurs simultaneously as an increase in subpolar gyre transport (manifested as an increase in the barotropic streamfunction), and the change in these two can be difficult to separate from the figure. However, since the meridional flow should be caused by the zonal density gradient, it is natural to point to the increase in salinity in the eastern basin to cause an increase in subpolar gyre transport.

Overall, the northward salinity fluxes from the eastern midlatitudes are seen to increase and follow the flow of the subpolar gyre, so the flow accelerates itself. These waters seen

following the flow of the subpolar gyre, reach first the Denmark Strait between year 320 and 360 and later the Labrador Sea. Since the deep water formation is dependent on the vertical density difference in the region, and therefore to a large degree on sea surface density and salinity, this behavior also corresponds well with the fact that the XBLT in the Labrador Sea cease to increase significantly later than that of the Denmark Strait.

A similar behavior as depicted in figure 27 is shown in figure 28. Salinity values are the same, but instead of values of the barotropic streamfunction velocity arrows are shown.

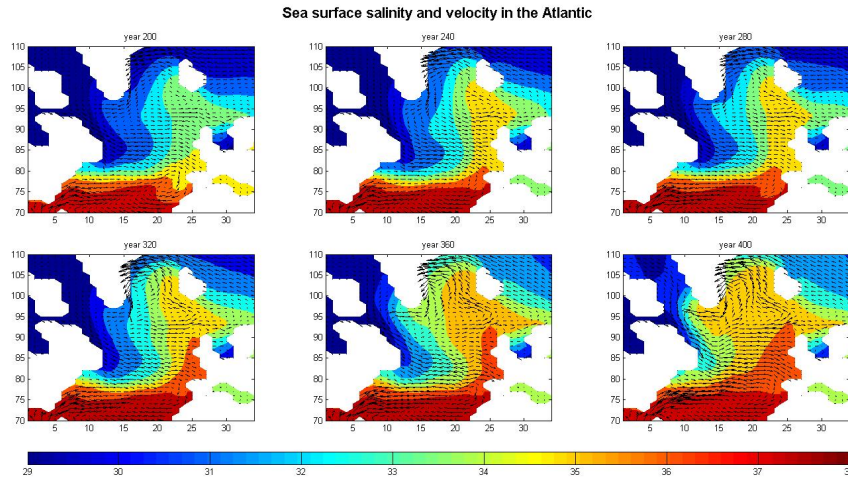


Figure 28: Filled coloured contour plot of the sea surface salinity shown along with velocity arrows at 6 different years separated by 40 years. Sea surface salinity values are indicated by the colorbar.

Several elements can be noticed from this figure. First, the meridional velocity in the eastern part of the basin off the coast of Ireland is predominantly negative in all images, but have a distinctive positive value at the years 320 and 360. This is what brings the saline water northward.

Second, the zonal velocity south at the southern tip of Greenland (Cape Farewell) is seen to be almost non-existing until year 320 and still increases significantly until year 400. The changes here is what brings the saline waters to the Labradors Sea, where the salinity increases greatly from year 320 to year 400

Third, the velocity south and southeast of Cape Farewell in the center of the subpolar gyre is seen to change direction. At year 200 the velocity here is mostly southeastern, but this clearly changes to a northeaster direction in year 360 and especially in year 400. This change in direction of the flow means a recircling of water to the Denmark Strait occuring very far north. This feature could play a part in actually stopping the increase of the deep water formation, since it surpresses the northward flowing very saline water from the most easter part of the Atlantic basin.

The first aspect pointed out from figure 28 - the change in meridional velocity in the eastern part of the basin - is best visualized, however, in a cross section. Figure 29 displays a cross section of the Atlantic from New Foundland to Ireland (61°N in the west to 67°N in the east due to the skewness of the grid). Here salinity is again showed as a colour filled contours and is overlaid by valued black contour lines of meridional velocity. All values

shown are taken from the same timesteps as those in figures 27 and 28. The vertical axis of the plot is the depth index and not the actual depth at which values are computed. This is for clarification purposes - the northward flowing cell in the eastern part of the basin is clearly visible - but this way of depicting the cross section also creates a false image of the depth of each layer, since every layer is depicted as having the same thickness. The result is that what is actually the upper part of the ocean seems to extend to much greater depth than it does.

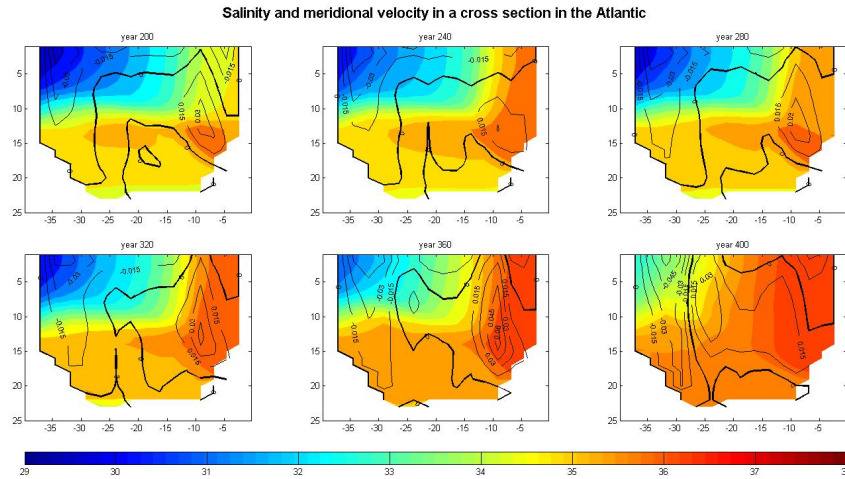


Figure 29: Salinity and meridional velocity in a cross section of the Atlantic at 6 different years separated by 04 years. The latitude of western boundary is 61°N while the latitude in the eastern boundary is 67°N . This is due to the skewness of the grid. The horizontal axis is degrees of west and the vertical axis is the death index. Salinity is showed as filled coloured contours and values are indicated by the colorbar. The meridional velocity is showed as black contour lines. The heavy black contour line shows the line of 0 meridional velocity.

The conclusion that should be drawn on the basis of this image, though, is that the velocity in the eastern part of the basin has a much stronger northward component in the later years displayed than the earlier. The meridional velocity thus reaches 0.06m/s in year 360. This is the cause of the northward salinity flux.

As mentioned, however, the sense of depth in figure 29 is distorted and the cause of the northward flow is the increased strength of the subpolar gyre.

What is also possible to notice in figure 29 is that the region in which the flow is distinctly northward is shifted westward from year 360 to 400 to a region where salinity is significantly lower. This change of flow direction is part of the recircling of water to the Denmark Strait taking place very far north, which, as mentioned, suppress the northward flow occurring in the eastern part of the basin, and is partially responsible for the very saline waters not reaching the Denmark Strait. The fact that the very saline waters do not reach the very northern part of the basin is shown in figure 27 and 28 as the red tongue ($S > 36.5 \text{ g/kg}$) in the eastern part of the basin from year 320 not reaching farther north than the British Isles.

As mentioned, the vertical extent of the flow is distorted in figure 29 in order to better depict the northward transport in the eastern part of the basin reaching a maximum strength

in year 360 and shifting westward going to year 400. The same values of salinity and meridional velocity is depicted in figure 30 where the vertical axis is the actual depth, so as to give a truer sense of the depth.

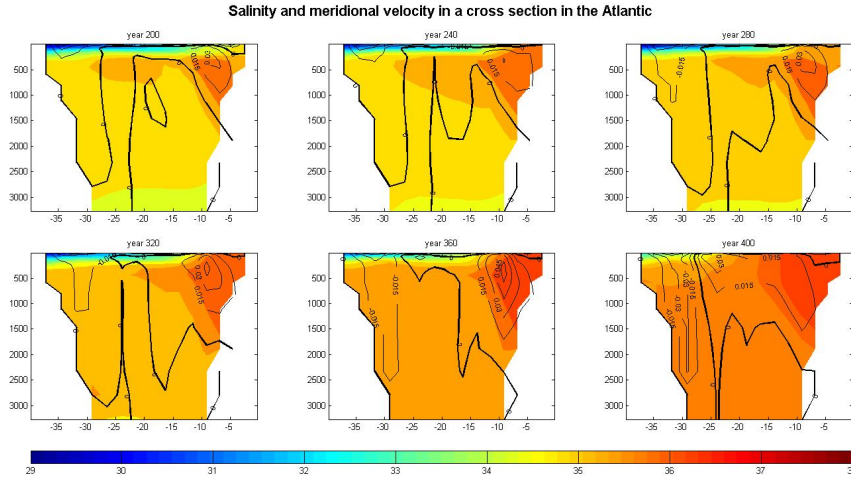


Figure 30: Same as figure 29 but shown with the actual depth on the vertical axis. Only the upper most 22 layers are displayed,

Figure 30 depicts the actual vertical extent of the northward flowing brach in the eastern part of the basin reaching a maximum strength at year 360, and how this northward flow is shifted westward at year 400. This saline branch reaches a vertical extent of about 1500 meters at year 360. The strong northward flow ($v > 0.03$ m/s) in the central Atlantic at year 400, however, is confined to the uppermost 500 meters on the other hand. This is the effect of the increase in subpolar gyre strength. The shift of the location of the flow ensures a larger recircling of water in the upper part of the ocean contributing to an arrest of the increase in upper ocean salinity - and thus density - which inhibits a further increase in deep water formation.

The previous figures clearly highlight the role of the subpolar gyre to bring saline water northward to the deep water formation sites, where an increased surface density raises the potential for deep water formation. The initial relatively small increase in salinity in the eastern part of the basin increases the zonal pressure gradient, which in turn - according to Luyten et al. (1985) - should enhance the meridional flow. In the end a shift in the direction of the flow in the upper ocean stops the increase in density here. Figure 30 show the maximum northward velocity at around 500m depth. This corresponds to the 13th layer of the model, and the velocity in this layer was therefore also plotted along with the salinity in figure 31.

First of all, the velocities in this layer is smaller and a bit more irregular than those in the surface layer. A comparison of the images of year 360 and 400 still show a shift in velocity in the central-eastern part of the region. In year 360 velocities here are distinctly northwestern bringing in saline waters to the central part of the gyre, whereas in year 400 they are northeastern. In year 400 the northward transport is taking place in a more central region of the north Atlantic where the salinity is not as high.

Despite some irregularities in the trajectory of the saline waters, an increase in the

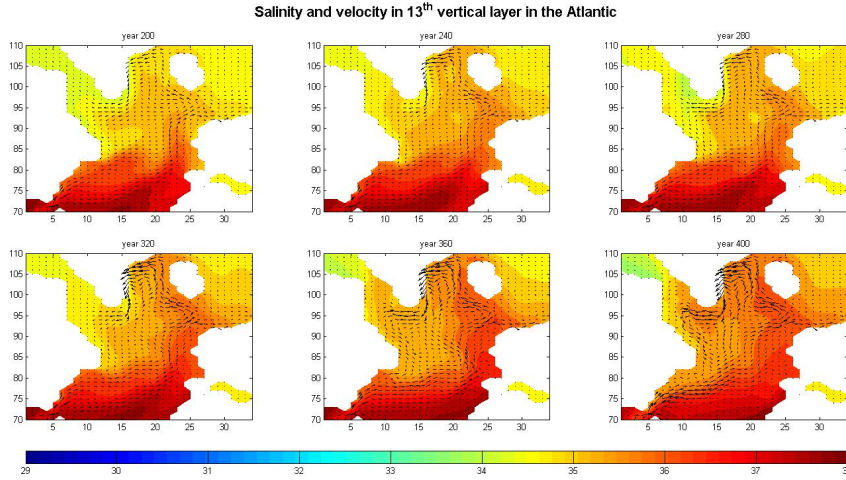


Figure 31: Salinity and velocity in the layer of maximum northward velocity in north Atlantic

deepwater formation is still seen to be caused by increasing salinities. How the increased upper ocean salinity will cause an increase in deep water formation is elaborated below.

Since energy is required redistribute density vertically, be it by direct motion or mixing, the potential for deep water formation is to a high degree set by the vertical density difference. A large vertical density difference requires a larger amount energy to inverse the vertical density profile in order to enable convection, whereas a small vertical density difference require less energy input. The vertical density difference in the deepwater formation sites is therefore of interest when elucidating the role and effect of the deep water formation on the general circulation.

The vertical potential density difference, $\Delta\rho_\theta$, calculated as

$$\Delta\rho_\theta = \rho_\theta(d = 1) - \rho_\theta(d = 16)$$

where d is the depth index, is showed in figure 32, where the colorbar indicates the density difference, i.e. between the layers 1 and 16. The 16th layer constitutes the depth interval 686 – 947 and the middle of the layer is situated at a depth of 815 meters, and the top layer has a depth of 8 meters. The white patches of land now indicate land or grid points where the bottom of the sea is located at or above the 16th layer. Thus Greenland is connected to Iceland via the Greenland-Iceland sill and to Canada via the Davis Strait sill. Blue colors indicate a large absolute vertical density difference a red colors low.

The important thing to notice here is the decrease (in absolute terms) in vertical density difference in first the Denmark Strait and next the Labrador Sea. This enables deep water formation and is - at least partially - attributed to the incoming saline waters from the eastern basin. A timeseries for difference in the spatially averaged potential density in the 1st and 16th layer in the three deep water formation regions was computed in order to visualize the changes at these exact regions. This is shown in figure 33, from which it is clear that the three deep water formation regions experiences changes also inferred from

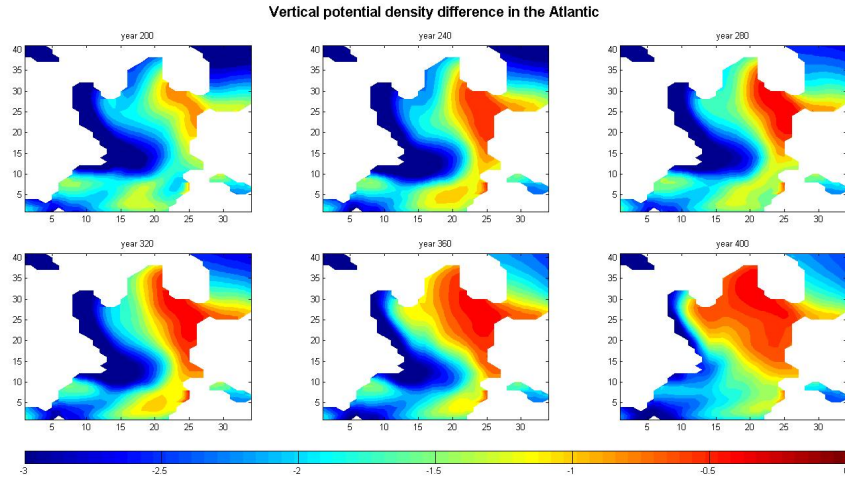


Figure 32: Vertical potential density difference between the 1st and 16th layer (corresponding to a difference between depths of 4 and 815 meters) in the Atlantic. White patches indicate land or sea bed.

figure 32.

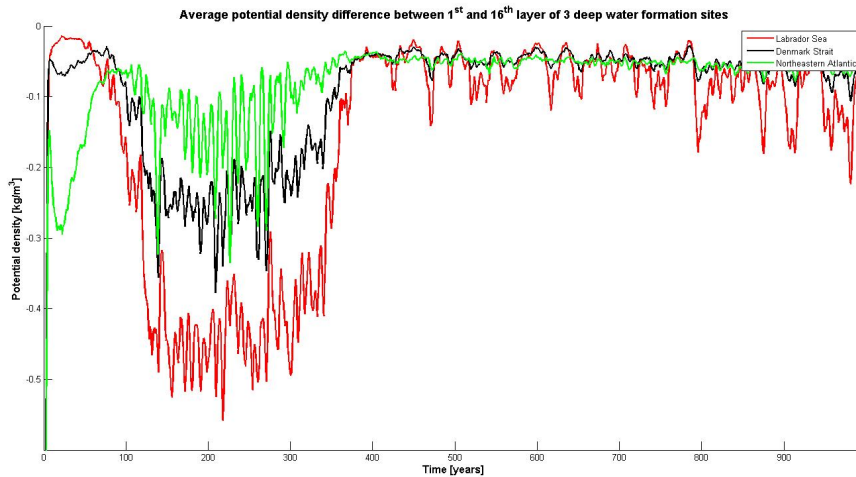


Figure 33: Vertical potential density difference in the three deep water formation sites only as a function of time.

To distinguish the changes occurring in the upper ocean from those in the deeper parts timeseries of potential density in the 1st and 16th layer have been separated and are shown in figure 34. This clearly show that the potential density increases in both.

Since an increase in potential density in the deeper part of the ocean should act to increase stratification and therefore inhibit deep convection, it must be the changes in the upper part of the ocean, which is the key process of why the deep water formation increases. It is also worth mentioning however, that the upper ocean salinity seems to continue to

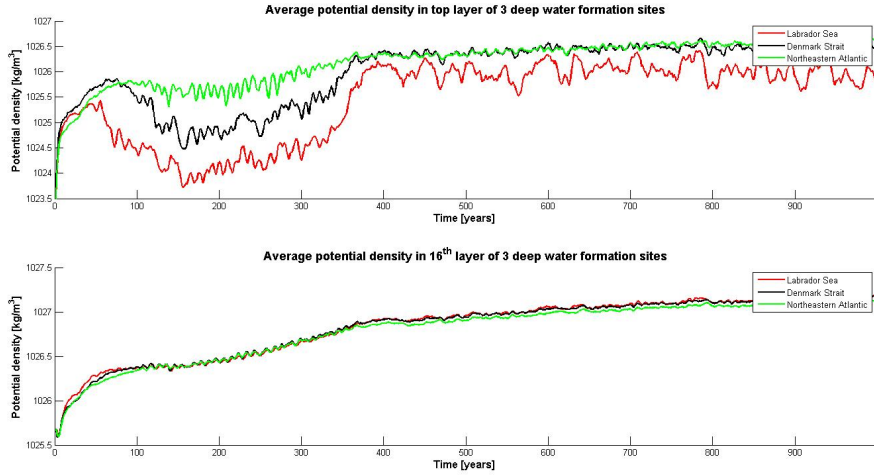


Figure 34: Potential density in the three deep water formation regions in 1st (**upper panel**) and 16th layer (**lower panel**).

increase even though the maximum of the deep water formation has been reached. This is in fact also depicted in figure 28, where salinity in the Labrador Sea is higher in year 400 than in year 360. The increase in deep ocean salinity must therefore also contribute to set a limit on the deep water formation, since it acts to increase stratification. To which degree the deep water formation itself acts to increase deep ocean salinity also remains an open question, but it must be noted that at all times during the increase in AMOC strength (and that of deep water formation) is the potential density in the 16th layer seen to increase.

Furthermore, though, the fact that the density in the deeper part of the northern Atlantic increases is interesting, because it contributes to setting up a meridional density gradient in the deep ocean possibly capable of driving a deep return flow southward. Figure 34 also shows how the region in which the southward return flow develops. Especially at year 360 and 400 the southward flowing cell in the western part of the basin increases.

It is well known that water flowing north in this region cools, which increases the density as well. The respective effect, of cooling of the moving water parcel as seen from a Lagrangian point of view and the increasing salinity at the deep water formation site as seen from an Eulerian point of view, is difficult to determine because of the flow field. This has to be done by tracing the moving water parcel, and this kind of analysis has been not been performed. Because of the fact that the temperature has been evaluated to increase in the northern region (from an Eulerian) and that the density in the southern region was extremely stable, the cooling of the moving water parcel was deemed irrelevant to the deep water formation. Nonetheless, a brief estimate of the effect of temperature on vertical density difference and thereby deep water formation was made. Figure 35 and 36 shows the temperature in the north Atlantic in the top and 13th layer respectively. From these figures it should be clear that the temperature differences between the eastern midlatitudes and the deepwater formation sites are larger in the years 200 – 320 than in 360 – 400 of the simulation. Therefore a moving water parcel would seem to cool less in the later years, which would not act to increase deep water formation.

All in all, this paragraph suggest that an internal feedback of the system - involving

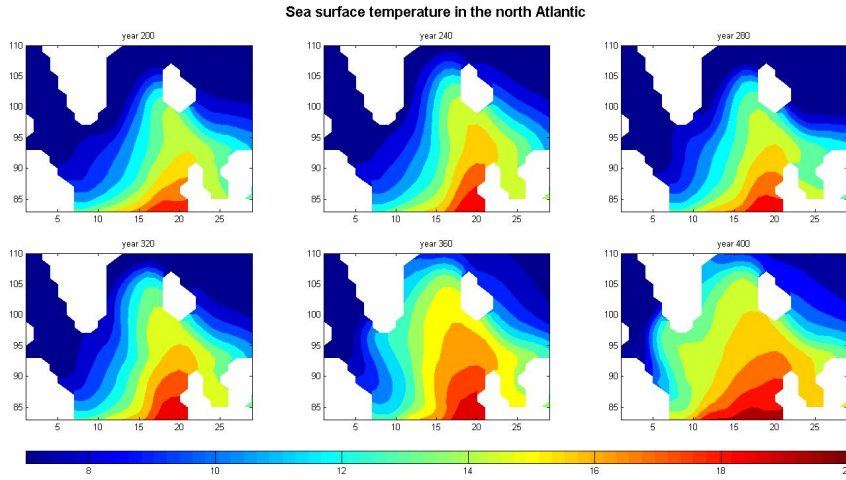


Figure 35: Sea surface temperature in north Atlantic

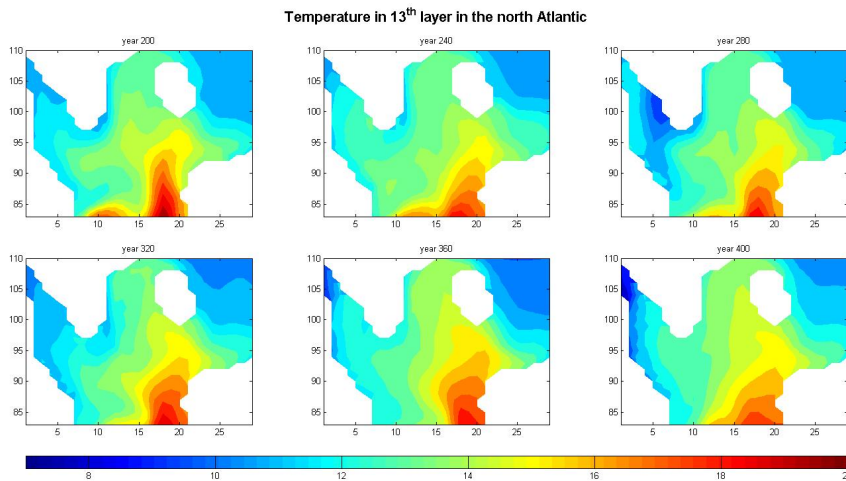


Figure 36: Temperature in the 13th layer in north Atlantic

the deep water formation and a northward salinity flux attributed to the transport of the subpolar gyre - is responsible for the rapid increase of the AMOC. A northern salinity flux in the eastern part of the basin causes a density increase here. Since the western part of the basin does not experience this, a larger zonal pressure gradient is set up, and this should further enhance the northward flow. This is manifested as an increase in the subpolar gyre circulation. This salinity flux reaches first the Denmark Strait and later the Labrador Sea where upper ocean density increases. This further enables deep water formation, which again increases the meridional overturning. A shift in the circulation of the subpolar gyre means that a larger portion of the water reaching the Denmark Strait comes from recirculation of water from the central part of the gyre, where the salinity is lower, rather than from the eastern Atlantic. Hence the upper ocean density ceases to increase, which also inhibits a further increase in deep water formation. This is supported by the fact that the maximum

of the XBLT in the Denmark Strait at year 367 and in the Labrador Sea at year 378. This shift along with the natural maximum limit on salinity - which comes from the salinity in the subtropical region, from where the salinity flux originated - is what seems to bring the rapid increase to a stop.

So whereas the preliminary quantitative analysis pointed to the meridional density difference as having the highest correlation with the AMOC and still leading it in the first regime, this elaborating qualitative analysis highlights the role of the subpolar gyre in bringing the saline, heavy water to the deep water formation sites and therefore being responsible for the increase in meridional density difference rather than an effect of it. This increasing northward flux of heavy water is what enables deep water formation and therefore sets the potential of the sinking branch of the AMOC, whereas a recirculation suppresses the very saline water from the east and brings the increase in deep water formation to a stop. The fact that the water reaching the deep water formation sites seems to cool less on way in the period of time, where deep water formation is high, further highlights the role of salinity fluxes on the deep water formation and therefore the AMOC.

6.2 Oscillatory behavior in the second regime

As depicted in figure 3 the AMOC undergoes several heavy increases and following decreases all occurring in a very short time span in the second regime. These events will henceforth be referred to as the oscillations. Depending on the latitude of evaluation these oscillations have different amplitudes. If one is to measure or evaluate the influence of a possible driver on the AMOC, it is necessary to do this at a latitude as close to the driver itself as possible. Otherwise a signal of the possible driver will get diluted with advection, while signals of other local drivers can also be thought to bring noise to it. Another principle used to determine the cause of the large oscillations is that of 'extreme behavior calls for extreme explanations', in the sense that such short-lived but yet large oscillations, should be caused by oscillations of more or less equal amplitude - at least proportionally - of which ever driver in question. The correlation analysis presented in section 5 pointed to the deep water formation in the Labrador Sea as the most likely driver. This was also the only hypothesized driver which showed nearly as large oscillations.

In figure 37 is plotted the XBLT (in red) in the Labrador Sea and the maximum AMOC transport (in blue) at the 89th latitude index (corresponding to roughly 55°N) in the second regime, where the vertical black lines indicate the timing of six oscillation events of the AMOC all of which are preceded by a very large increase in the XBLT by respectively 2, 5, 3, 8, 2 and 5 years. Taking into account the fact that the 4th and 6th oscillation event in the AMOC (the events where the delay between the XBLT and AMOC peaks are the longest) show very broad peaks, the delay between the XBLT and the AMOC is very consistent.

If this AMOC behavior is compared with the BSF in the northern Atlantic - which also showed a very large correlation coefficient but at a lag of 0 years in the preliminary analysis - the causal relation is not depicted with nearly as much clarity. This is shown in figure 38, where the same AMOC timeseries is plotted along with the absolute maximum of the barotropic streamfunction in the north Atlantic. Here it is clear that the timing of the peaks are not nearly as well correlated.

The two first peaks in AMOC transport precede those of the BSF. The third peak of the AMOC can be characterized as a "double event" since the local maximum at year 600

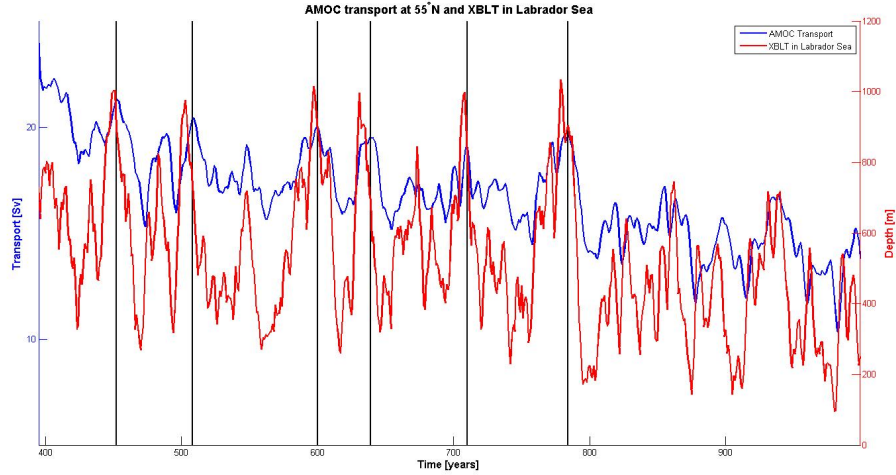


Figure 37: Maximum AMOC transport at the 89^{th} latitude index (or 55°N) and XBLT in the Labrador Sea in the second regime. Vertical black lines indicate the timing of 6 oscillation events in AMOC transport, which are all preceded by similar behavior in the XBLT.

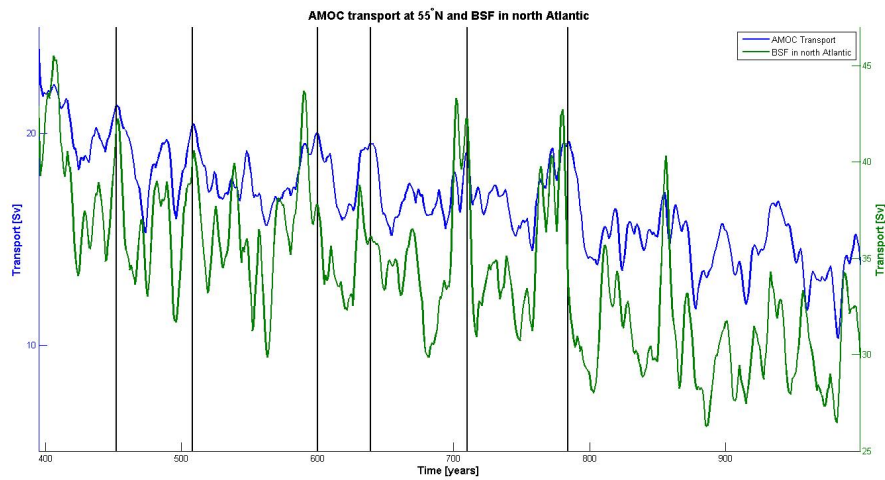


Figure 38: Maximum AMOC transport at the 89^{th} latitude index (or 55°N) and absolute maximum of the BSF in the north Atlantic. Vertical black lines indicate the timing of 6 oscillation events in AMOC transport.

is preceded by a lesser one at year 590. At this event both of these two local maxima falls at the same year as a local maxima of the BSF, but whereas the second local maxima of the AMOC is larger than the first, the opposite is true of the BSF. This image of the timing is similar in the last 3 events as well.

In this regard the respective latitudes of evaluation of the AMOC and of the BSF maximum is important as it indicates whether a signal is travelling northward or southward. in the above timeseries the maximum of the BSF occurs at the 91^{st} , 91^{st} , 91^{st} , 92^{nd} , 89^{th} and 91^{st} index, i.e. all but one farther north than the AMOC was evaluated, and never farther

south. Since the transport in the upper ocean (or rather since the AMOC transport in this evaluation) is northward, the local maximum of the BSF should occur before that of the AMOC were the BSF to drive the AMOC. This again points to the importance of the deep water formation rather than the subpolar gyre strength in setting the AMOC.

A similar analysis of potential density and salinity as employed in section 6 were performed to investigate the cause of the AMOC oscillations in the second regime. For the six aforementioned events the potential density in the top layer of the north Atlantic were evaluated before the rapid increase, at the local peak and after the following decrease of the AMOC transport. These are shown for the first three events in figure 39 and for the last three in figure 40. In all images are inserted a block box. This box indicates the region of the Labrador Sea from which the XBLT values were used.

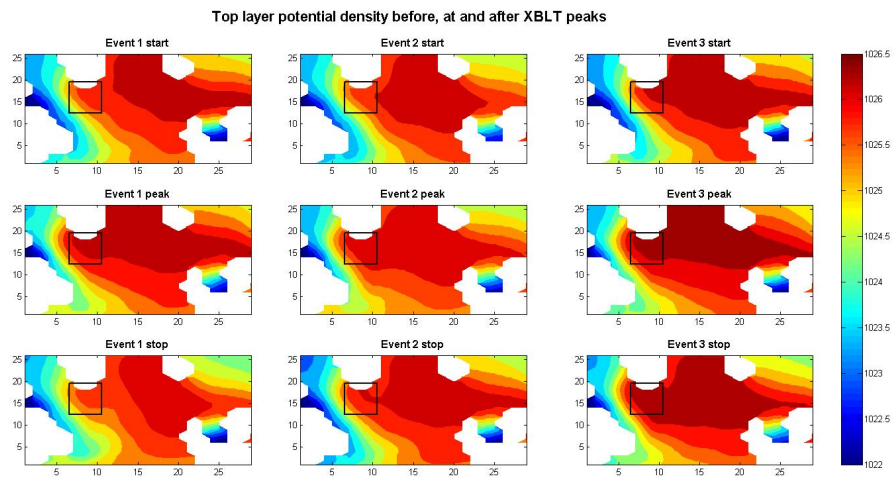


Figure 39: Potential density in uppermost layer before, at the peak of and after the first three oscillations in the second regime.

These two figures are constructed in such a way that the different events are aligned in columns and the start, peak and end of each event are aligned in rows. Comparing the start, peak and end of all events it is clear that a plume of dense water enters the Labrador Sea whereafter it withdraws again. Only the third event (the max AMOC transport of this event occur at year 600) show a different behavior. Here the potential density does not decrease in the Labrador Sea in the same way as in the other events. What is important to notice about exactly the third event, though, is that both the XBLT and the AMOC experiences a slight rebound after the decrease of the local peak before plummeting to a much lower value. The potential density shown in figure 39 is evaluated before this rebound, why it is more natural that the potential density is maintained high.

As was the case with the analysis of the regime transition, the upper ocean salinity anomalies also proves a key parameter in setting the deep water formation maximum in the second regime. Similar to figure 39 and 40 sea surface salinity are displayed at the start, peak of and at the end of each of the 6 events in figure 41 and 42

Here the overall picture is the same - namely that the increase in potential density is caused by salinity fluxes into the Labrador Sea. All in all this analysis points to the upper ocean salinity anomalies in the Labrador Sea causing an increase in deep water formation

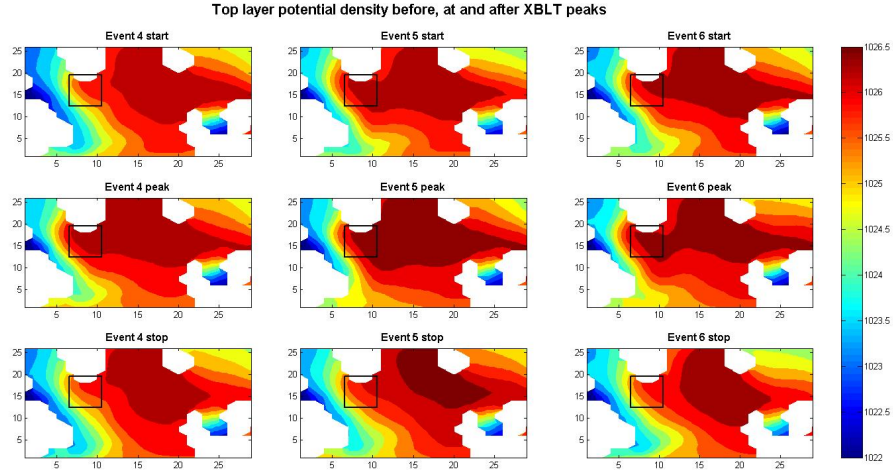


Figure 40: Potential density in uppermost layer before, at the peak of and after the last three oscillations in the second regime.

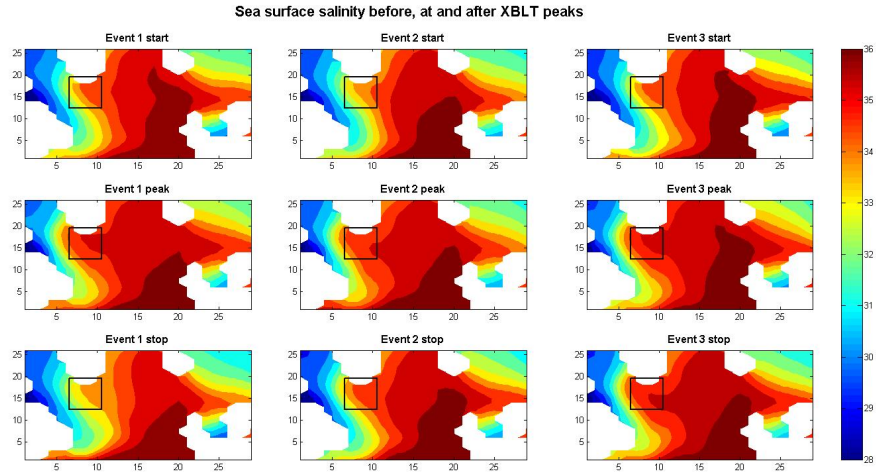


Figure 41: Sea surface salinity in uppermost layer before, at the peak of and after the first three oscillations in the second regime.

that strengthen the AMOC. The fact that the timing of the maximum subpolar gyre transport - as measured by the barotropic streamfunction - relative to that of the AMOC are significantly more inconsistent blurs the explanation of which mechanism is important for causing the salinity anomalies. At all events both potential density and sea surface salinity are relatively stable in the eastern part of the basin. Along with the irregularity in the timing of the maximum BSF values this seems to render the subpolar gyre less influential as compared to the event of the global maximum in AMOC transport around year 400. The oscillations in both AMOC transport and deep water formation are furthermore so short-lived, that the spin-up of the subpolar gyre becomes difficult to evaluate. Nonetheless, these results show that also in the second regime does an increase in deep water formation due to upper ocean salinity increases in, especially, the Labrador Sea look like a very plausible

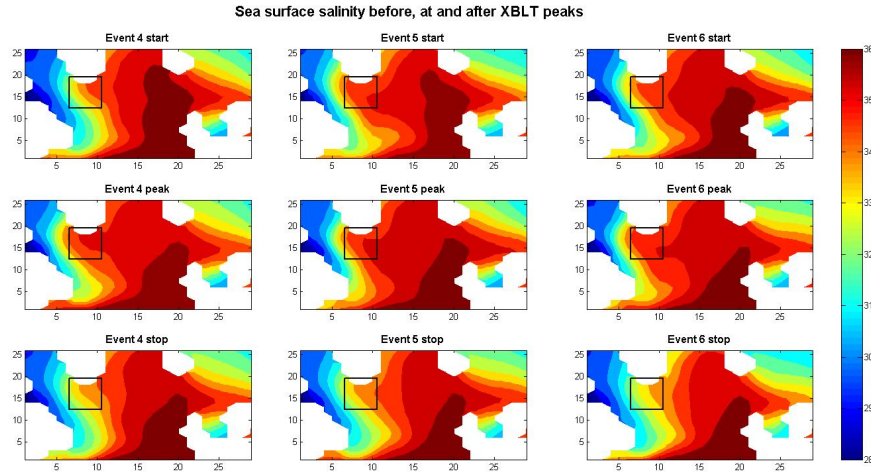


Figure 42: Sea surface salinity in uppermost layer before, at the peak of and after the last three oscillations in the second regime.

driver of the AMOC.

6.3 Summary of the analysis

In total the analysis consisted of three main parts.

The first, preliminary analysis focused on the correlation coefficient as a quantitative measure of the correlation between the AMOC and the respective hypothesized drivers. Here it proved illuminating to split the analysis into two temporal regimes, which were separated at year 395, and in which the AMOC displayed qualitatively different behavior. The choice for splitting the analysis into these regimes were furthermore justified by the breakdown in correlation between the AMOC and the meridional density difference. Results of this analysis pointed towards the meridional density difference being the main driver of the AMOC in the first regime, and the deep water formation in the Labrador Sea being the driver in the second regime, since these particular relations had the highest correlation coefficient, while the (possible) driver was still leading the AMOC.

The second part showed mechanisms through which the AMOC experienced a rapid and very large increase, which very abruptly came to an end, and after which the regime transition took place. Highlighted here was the role of the subpolar gyre in bringing saline water to the north Atlantic resulting in an increased deep water formation specifically in the Denmark Strait and the Labrador Sea. Limited by the salinity in the midlatitude eastern Atlantic and a westward shift of the northward flow of the subpolar gyre, to a region with lower salinity, the maximum of the deep water formation occurred in the Denmark Strait at year 367 and in the Labrador Sea in year 378 whereafter it decreased. The shift in the subpolar gyre flow caused a larger recirculation of water from the central to the northern part of the gyre, which suppressed the flow of high salinity water coming from the southeastern part of the gyre. The fact that temperature differences between the deep water formation sites and the southern part of the gyre were lower in times of high deep water formation seems

to indicate, that a water parcel, at these times, would cool less along its path to the deep water formation sites. This supports the conclusion that salinity rather than temperature has the largest influence on the deep water formation. The overall behavior showed by AMOC, barotropic streamfunction and XBLT in the northern Atlantic seems to underline the importance of a positive salt-advection feedback; an increase in northward transport brings in saline water from the southeastern part of the subpolar gyre, which raises the sea surface density in the deep water formation sites. A larger deep water formation in turn increases the overturning. It is furthermore worth emphasizing that the initial small perturbation brings about changes of an amplitude far larger than itself by this internal feedback and not via external forcing - a feature which underlines the ability of the ocean to act as an amplifier of climate signals - and that a different perturbation (the shift in subpolar gyre circulation) though with a comparably small amplitude is able to bring the feedback to an end.

The third part tried to explain the oscillatory behavior of the AMOC in the second regime. An emphasis was again given on the role of the deep water formation and on the sea surface salinity, but the fact that the timing of maxima of the subpolar gyre and AMOC does not match seems to undermine the role of the subpolar gyre. The fact that the preliminary analysis in section 5 gave a much more precise estimate of the role of deep water formation - namely that the deep water formed in the Labrador Sea correlates to a much higher degree with the AMOC transport - allowed for a better understanding of the AMOC oscillations. In 6 oscillation events all peaks in the AMOC transport were preceded by similar peaks in the XBLT in the Labrador Sea. Moreover, the behavior of the sea surface salinity in the Labrador Sea at the start and end of the oscillation events, seems to explain to a large degree why XBLT displays the sudden oscillations.

All in all the analysis and results presented here points first and foremost to the deep water formation in the northern Atlantic in setting the AMOC strength. This is mainly due salinity anomalies in the upper ocean in the Denmark Strait and the Labrador Sea. It must be stressed, though, that the subpolar gyre plays a large role in transporting the saline waters to the deep water formation regions, and that internal feedbacks in the system as a whole acts to amplify initial perturbations.

7 Discussion

This section will serve as an overall discussion of the report. Included in this will be an elaborating comment on both the impact and the validity of the results. This implies a critical assessment of both strength and weaknesses of the way in which the analysis have been performed, of how the hypothesized drivers could otherwise have been examined, and which other physical processes and variables should be taken into consideration. Comparison with recent research and suggestions for further research will also be presented.

7.1 Discussion of the quantitative and qualitative analysis

The general results highlight the role of the subpolar gyre and the deep water formation in the north Atlantic in setting the AMOC strength. Even though neither the correlation coefficient between the AMOC and the XBLT in the Denmark Strait nor the Labrador Sea are higher than that of the BSF or MDD in the first regime, the qualitative analysis points to

the fact that an increased downwelling here contributes significantly in driving a northward transport. This conclusion is, however, also heavily supported by the XBLT in the Denmark Strait having the highest correlation coefficient when leading the AMOC.

It is naturally a problem, however, when the results of these two methods of analysis contradict each other. Justifications of why the conclusion of one over the other is preferred have to be made.

In this regard it is necessary to judge the two different parts of the analysis on their own premises. The advantage of the quantitative analysis is that it can very easily measure to which degree the AMOC correlates with a possible driver - keeping all the assumptions made beforehand in mind. The limits of it, however, concern the fact that the causality is not explicitly examined and as such cannot be determined. This type of analysis can reject causality but never show it. The qualitative analysis on the other hand has the ability to examine in depth causality and explain by which mechanisms the AMOC reacts to a certain change, but it does not - at least as it is presented here - give an actual measure of the reaction. In this sense using both types of analysis provides a thorough overall examination of the hypotheses stated in section 4, and combined they should thus give a more thorough answer to the question of why the AMOC shows the behavior it does. In general, it is also worth mentioning the advantage of the quantitative analysis in setting the frame of the qualitative analysis

In this particular situation, the explanation that the northward transport through the eastern part of the subpolar gyre contributed in setting the meridional density difference seemed more plausible than vice versa. The fact that the hypothesis of the MDD being the driver is not based on the equations of motion also plays a role in this conclusion.

When analyzing the behavior in the second regime, all years concerning the start, peak and end of the oscillations have been extracted manually. It must be stressed that this has not been done in order to favour the examination of some oscillations over others. Other peaks in XBLT, AMOC and BSF could have been used to produce the figures 39 and 40 though and this might have given a different result. But the events highlighted in the figures 37 and 38 nonetheless clearly shows that the timing of the XBLT peaks, precede those of the AMOC, whereas this is not nearly as clear with the BSF. An algorithm used to determine which peaks to examine could have been used, but the threshold values set in such an algorithm would also have included some kind of arbitrariness, although this method would have had a more rigorous nature. It is still believed that the results of this analysis would *not* have changed had such a method been used.

The validity of the analysis in itself as it is - disregarding its flaws in the way the hypothesized drivers have been represented and what other factors may be missing - is sound, however. The influence of the hypothesized drives - in the way they are represented - have been examined thoroughly. Of course, this brings the way in which the drivers are represented into question.

7.2 Discussion of the hypothesized drivers and the AMOC

In order to address the validity of the results, a critical assessment of the way in which the hypothesized drivers are defined and evaluated, and to which degree they are representative of the processes, they are meant to represent, is necessary. This will be provided by the

following paragraph. A brief comparison with recent results and suggestions for further analysis will also be provided

7.2.1 Discussion of the deep water formation

As already emphasized the deep water formation in the northern Atlantic is seen to play a major role in setting the strength of the AMOC. Especially the deep water formed in the Denmark Strait and the Labrador Sea in coexistence with the transport of the subpolar gyre have been explicitly stated as being the most influential processes on the AMOC. It is still important to note, though, that in the periods of time, where the AMOC transport is low - roughly in the years 150 – 300 of the simulation - the deep water formation is largest in the northeastern Atlantic, why it is not unreasonable to assume that in this period of time, this also plays a large role in setting the AMOC, although it has not been thoroughly investigated.

The analysis of the deep water formation is first of all based on the geographically static definitions of the deep water formation regions, however, and this is not necessarily the most representative way of the actual formation of deep water. These regions were defined as those grid points at which the XBLT at any timestep displays an overall maximum in the northern Atlantic (except for a very few grid points off the coast of Scotland and in the Norwegian Sea). The fact that the XBLT experiences a maximum in these regions *is* a good indicator of deep water formation, but it does not necessarily imply that deep water is not formed elsewhere. Furthermore, if the AMOC is believed to be driven by the deep water formation, the actual amount of deep water formed must be the key metric to evaluate. The XBLT is thus not necessarily a bad proxy, but a computation of the actual amount of deep water formed, would have been preferable. Since the sinking in the North Atlantic is itself a branch of the overturning circulation, the amount of deep water formed is naturally believed to be directly correlated with the AMOC, and to correlate the AMOC with the XBLT implicitly assumes a proportionality between the XBLT and the amount of deep water formed, and *this* may (or may not) be misrepresentative. Given both the quantitative and qualitative analysis, though, the deep water formation must be concluded to play a major role in setting the AMOC, and the XBLT must be concluded to be a good indicator for this.

Pickart and Spall (2007) also have a valid point, in this manner, arguing that a distinction between mixing and actual water mass transformation needs to be made. In order for the deep water formation to cause a northward transport, there needs to be a net downward removal of water from the upper ocean, if the water is not just to vertically recirculate. An estimate of this net removal is still lacking in this study, and must be a key element if the deep water formation is to drive the AMOC.

In general, it also seems problematic that a phenomena, which takes place on a timescale in the order of days (Kuhlbrodt et al., 2007), are represented by a variable which is evaluated once per year as is the case with the XBLT. One must wonder to which degree the actual physical process of water mass transformation is captured. Perhaps this is also a cause of the volatile behavior of the XBLT. But although a finer temporal resolution should improve the representation of deep water formation by boundary layer depth, one must still consider whether a calculation of the actual amount of deep water formed is not the right way to investigate the causal relation between the deep water formation and the AMOC strength. And not the least by which mechanisms this formation takes place. Of course, a measure

of the actual amount of deep water formed should therefore be correlated with AMOC, but a computation of this amount would also better allow for an investigation of the processes, which are important for it. The volatile behavior of the XBLT (especially as evaluated in the Labrador Sea region) would most likely also have been less pronounced had mean values of the XBLT been used instead of maximum values. Perhaps this would have better depicted the actual deep water formation, but since the deep water formation occur as convective plumes over a very short time span (Kuhlbrodt et al., 2007), it could also be argued that the maximum values are a good representation.

The fact that deep water formation occurs in regions, which are subject to a net fresh water flux from the atmosphere toward the ocean (i.e. more precipitation than evaporation) also has a great influence on the so-called convective feedback. A vigorous convection acts to vertically equalize density differences, which itself acts to decrease the energy input needed for convection to take place. Since the fresh water flux is positive toward the ocean as compared to the atmosphere, a salinity flux is needed in order to keep the density high. If this does not occur for consecutive years, the surface density can reach a salinity so low, that the energy input needed for convection is too large (Rahmstorf, 2002; Kuhlbrodt et al., 2007). If the XBLT is taken as a good proxy for the deep water formation, this feedback is clearly visible in the deep water formation in the Labrador Sea in this study. Figure 16 clearly shows that the deep water formation is basically absent in the Labrador Sea roughly in the years 100 – 350 whereafter it displays an almost instant increase reaching a local maximum in year 378. As indicated by the qualitative analysis in section 6 this is mainly due to an increase in upper ocean salinity fluxes, and this corresponds extremely well with the convection feedback addressed by Rahmstorf (2002) and Kuhlbrodt et al. (2007).

As also mentioned in Rahmstorf (2002) and Kuhlbrodt et al. (2007) this positive convective feedback implies a bistability of the AMOC transport, where transitions between states can take place due to a shutdown in the convective feedback and due to a shift between deep water formation sites. This highlights the importance not only of the deep water formation itself, but also of the regions in which the deep water formation occurs. In this regard, this study clearly shows how a complex AMOC behavior (and thus all that comes with it) can be explained via a changing deep water formation. Given the influence of the AMOC on the climate state of the planet (McManus et al., 2004) a further analysis of the entire climatic state in this study could elucidate the possible influence of shifts in deep water formation on the global climate.

7.2.2 Discussion of the meridional density difference

The correlation analysis pointed to the meridional density difference evaluated in interval 1 as having the highest correlation coefficient in the first regime while still leading the AMOC. As mentioned previously correlation does not imply causality, though, and it must be stressed, that the situation in which the upper north is heavy and the upper south (or equatorial region) light, can never alone *cause* a northward transport in the upper ocean. The qualitative analysis subsequently showed how the density first increased in the eastern part of the basin and later the northern. The fact that this density anomaly follow the path of the subpolar gyre points to a larger degree to the conclusion that the meridional density difference should therefore be a product of the transport rather than a cause of it. In terms of the theoretical basis deduced in section 3 this seems to indicate, that the arguments based on the fundamental equations of motion used by Luyten et al. (1985) prevails over that of Stommel (1961). When a discrepancy between the conclusions of the quantitative and

qualitative analysis takes place, a justification of why one is preferred rather than the other, should always be provided though. In this particular case, an explanation of why the MDD should be leading the AMOC is still lacking though. In spite of the results of the qualitative analysis, the MDD *is* after all evaluated to be leading the AMOC. In an investigation of the cause of this lead, the most important aspect to consider is whether the changes in MDD is due to changes in the northern or equatorial region, and where the AMOC is evaluated. The first part was actually investigated, and it was clearly showed in figure 25 that changes in the upper ocean MDD occurs due to changes in the northern region. A maximum correlation at a lag of 1 year at the 87th latitude index thus remains an unresolved issue, and it must be underlined that the qualitative analysis was simply deemed more credible. In order for this conclusion to not be seen as drawn on a whim, it must be stressed, that this kind of differentiation between methods of analysis is quite rational. As mentioned, the strength of the correlation analysis is not to find a causal relation.

The meridional density was defined in accordance with the work by Stommel (1961), de Boer et al. (2010) and the spatial structure of the circulation in the study itself. In regards to Stommel there are however a few comments to be made. The two depth intervals inspired by Stommel (1961) was that of the upper 100 meters (interval 1) and that between 1670 and 2555 meters depth (interval 4). These intervals were chosen as to represent the so-called overflow and capillary in the two vessel experiment in Stommel (1961), but since the two containers in Stommel's setup have a uniform density, the vertical interval in which to compute the density difference would not matter. It is important to notice, however, that the flow in Stommel (1961) is *defined* to be from high to low pressure in *the capillary tube in the bottom*. Basically this means that on the basis of the setup a transport from high to low density in the top is rejected. Here the flow *must* be from low to high density.

The consequence of this should be, that although the density difference in the upper ocean does not drive the flow, this can easily be a good indicator of the total transport. In this manner, it could just as well have been a heavier northern deep ocean and a lighter southern deep ocean *causing* the southward flow in the deep ocean, and thereby setting the overturning. This could have been investigated more thoroughly. But as a direct driver, in the meaning that it causes the flow from one region to another, the meridional density difference in the upper ocean should have been anticorrelated with the AMOC, since the flow is from south (or equatorial) to north in the upper ocean. The hypothesis that the meridional density difference drives the AMOC should therefore be rejected.

The force by which the density affect the transport is the pressure gradient. This is however also heavily influenced by the sea surface height, a meridional difference in which could cause a transport from high to low density regions though. Sea surface height was not a part of the data, and have thus not been analyzed, yet it could of course have been calculated as a function of temperature and thermal expansion, although I dare to claim, that this would be embedded with large uncertainties in this particular study because of uncertainties in thermal expansion coefficient and spatial resolution.

7.2.3 Discussion of the role and representation of the subpolar gyre

Both the quantitative and the qualitative analysis showed a large correlation between the subpolar gyre transport and the AMOC. This included a very high correlation coefficient (especially in the first regime) and clear picture of how the subpolar gyre feeds the deep water formation sites with saline water.

As mentioned, however, there is a mathematical bias in the quantitative analysis of the correlation between the AMOC and the BSF, since the BSF is mathematically defined via the meridional transport as

$$U = -\frac{\partial\psi}{\partial y}$$

$$V = \frac{\partial\psi}{\partial x}$$

where U and V are the total vertically integrated zonal and meridional transport, respectively. The correlation coefficient is therefore naturally very high, and it is naturally so a lag of 0 years. So only in regions where the zonal derivative of the BSF is nonexistent is there no bias. A measure of only the zonal velocity integrated meridionally over a certain domain, would eliminate the mathematical bias. However, this only highlights the quantitative bias between the AMOC and the BSF. The actual mechanism by which the subpolar gyre influences the AMOC is also elucidated in section 6. Here it is shown that the northward transport in the eastern part of the basin is paramount for bringing saline water to the deep water formation sites. An alternative measure for this physical process, with which the AMOC can be correlated, must be possible to construct. But since the northward flow then affects the AMOC, the nonlinearity of the problem suddenly arises again. The flow is determined by the flow itself. In this view it is important to notice that the barotropic streamfunction treats the ocean as consisting of a single layer. Therefore it is of course not a direct representation of the northward transport at 500 meters depth in the eastern Atlantic, and a timeseries of this transport may well lead that of both the deepwater formation and the AMOC in the years of the rapid increase.

The representation of the subpolar gyre as the barotropic streamfunction (or in the correlation analysis as the absolute maximum of the barotropic streamfunction) in the northern Atlantic is thus associated with quantitative bias toward the correlation with the AMOC transport. However, there is also a qualitative discrepancy since the barotropic streamfunction treats the ocean as consisting of a single layer, and at every point the BSF is thus a measure of the total vertically integrated transport. Nevertheless the qualitative analysis highlights the transport of saline water in the eastern part of the basin toward the deep water formation sites in the northern Atlantic, and this exact transport *is* attributed to the subpolar gyre, and it is only a small fraction of the AMOC transport at this latitude. Thereby the data clearly points to the subpolar gyre playing a major role in driving the AMOC.

According to Luyten et al. (1985) the meridional transport in the subpolar region is determined by the vertical density differences and the zonally sloping isopycnals. This was also investigated briefly in this study. In figure 43 is therefore shown the potential density and meridional velocity is shown in the same cross section of the Atlantic as used in figure 30

Here the connection between the sloping isopycnals and the meridional velocity is not very clear. Both at the years 280, 320 and 360 it seems as if the largest northward transport is located just at the onset of an upwards sloping isopycnal. The largest southward transport does not seem to mirror any sloping isopycnals whatsoever.

The meridional transport derived by Luyten et al. (1985) in the three layer model is also

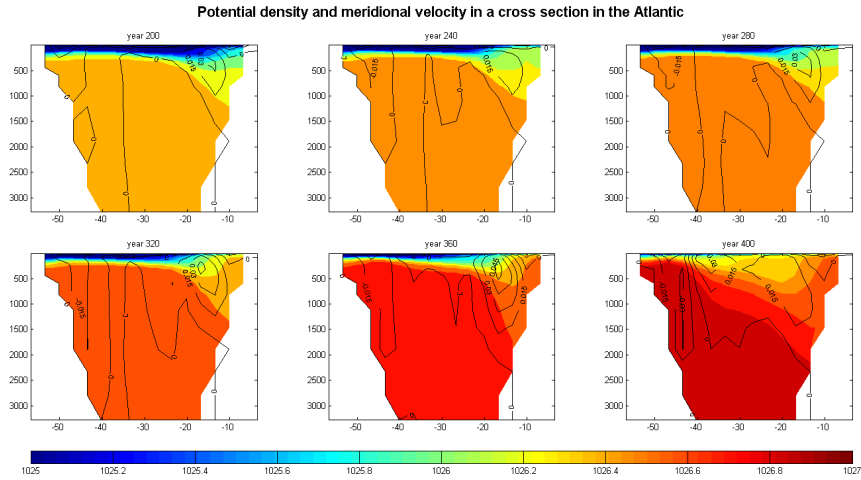


Figure 43: Potential density in filled contours overlaid with meridional velocities in a north Atlantic cross section

dependent on the layer thickness and vertical density differences. In the region of maximum northward transport, these two metrics could perhaps be in better correlation with the meridional velocity. However, the focus in the study was kept on the flow itself, and not the diagnostics of it, why neither the zonal and vertical density difference nor the height between layers of equal density was examined further. Another metric to quantify the effect of the subpolar gyre would simply be northward salinity flux in the eastern Atlantic.

Recent research (Delworth and Zeng, 2016; Kleppin et al., 2015) also highlights the contribution by the subpolar gyre to setting the AMOC strength, and in this context - at least partially - attributes the subpolar gyre strength to the North Atlantic Oscillation (NAO). Although not explicitly stated as a cause, sea surface salinity in the Labrador Sea are linked to increased mixed layer depths and AMOC transport in a NAO perturbation experiment by Delworth and Zeng (2016). Whereas these studies - and this one - focus on the positive salinity-advection feedback (larger northward salinity fluxes by a larger northward transport increases deep water formation, which in turn increases the overturning) the study by Lohmann et al. (2009) finds the subpolar gyre to respond with a weakening subsequent to a positive NAO phase due to a northward transport of warm water by the AMOC. This again highlight the internal feedbacks in the system, this time in a selfregulatory one, if the subpolar gyre is considered causally linked to the AMOC.

Since the salinity anomaly, which is found to serve to increase upper ocean density, originates in the midlatitudes at the boundary between the subpolar and subtropical gyre, a feature such as the cross-gyre boundary salinity flux in the midlatitude could seem an interesting topic for further research. The effect of an increasing upper ocean northward salinity flux in the midlatitudes (or even in the western midlatitude Atlantic) on deep water formation in the north Atlantic could prove illuminating.

Because of the fact that the deep water formation and the subpolar gyre circulation is so closely linked through both vertical velocity and the spatial density gradient, it is only natural that their respective influences on the AMOC are difficult to separate. In this manner, it is important to stress, that a correlation analysis never illuminates causality.

An aspect not covered extensively is the removal of the deep water formed in the subpolar Atlantic. Böning et al. (2006) address the role of the subpolar gyre in transporting water southward in the return flow of the so-called deep western boundary current. This has also only been investigated briefly by this study. Besides illuminating the role of the subpolar gyre, this also highlights the importance of where to evaluate the AMOC both in terms of depth and latitude. Figure 30 does, however, show a strong southward transport extending down to more than 2000 meters. This increase in southward transport could have been examined in terms of density differences. Even though both Böning et al. (1996), Zou and Lozier (2016) and Pickart and Spall (2007) argue for a minimum impact of the deep water formed in the Labrador Sea on the southward return flow the timing and correlation in this study suggests otherwise. The strength of the deep western boundary current was computed as the volume integral of the velocity across 57°N in the western part of the north Atlantic down to the depth of the maximum XBLT in the Labrador Sea. This is shown along with the XBLT in the Labrador Sea in figure 44.

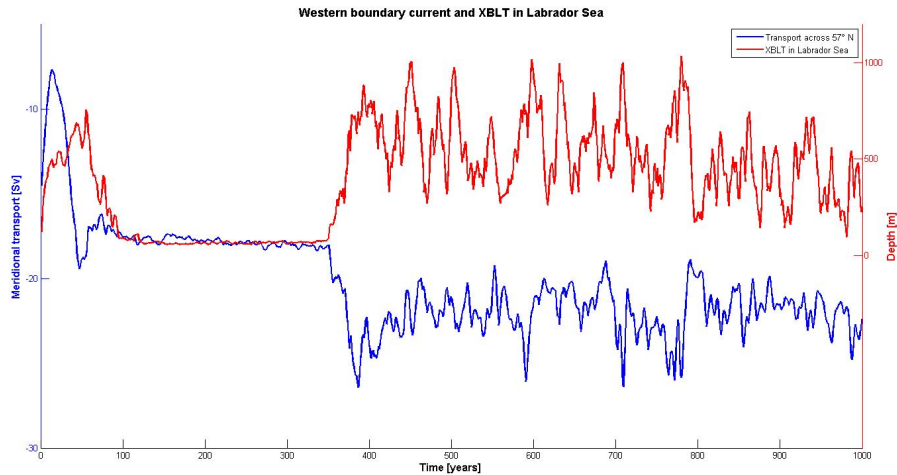


Figure 44: Meridional transport across 57°N in western Atlantic (blue) and maximum XBLT in the Labrador Sea (red)

Here relation between the western boundary current and the Labrador Sea - at least until \sim year 380 is very apparent, since both starts a rapid increase almost instantaneously. The timing of the starts of these increases are of course of interest because they should imply the causal reaction. These two increases start at the same year of the simulation, however, and the causal reaction have not been determined. An interconnection seems obvious nonetheless. The deep western boundary current is an intrinsic component of the subpolar gyre, and the fact the transport here is completely stable for a long period in the simulation, whereafter it displays a sudden "switch on" is interesting. Both because it is distinctly different from the behavior of the subpolar gyre strength as measured as the BSF minimum, and because it enables the possibility of a trigger mechanism and a tipping point of some sort. The same can be said about the deep water formation in the Labrador Sea. According to Luyten et al. (1985) the subpolar gyre transport is set up by the sloping isopycnals, but these do not seem to explain the sudden increase in the deep western boundary current neither, as they do not show nearly the same "switch on"-behavior. These discrepancies could point in the direction of an increase in deep water formation in the Labrador Sea forcing the deep western boundary current, however a conclusion drawn on the method of elimination should be sufficient. The possibility that an increased southward deep

flow causes increased deep water formation in the Labrador Sea must also be considered, and in the end the sudden intensification of the western boundary current remains unresolved and a topic for further investigation.

All in all, the increase in subpolar gyre strength is - at least partially - attributed to the salt-advection feedback. An increase in salinity in the eastern part of the basin increases the zonal density differences, which further increase the meridional flow. An overall more elaborating analysis on the flow as a function of depth would improve the rigorousness of the study, without neglecting the importance of the subpolar gyre as a single physical component of the general Atlantic circulation.

The fact that the flow and velocity themselves *have* been addressed without referring to the subpolar gyre as single entity improve the validity of the results. An increased northward transport in the eastern Atlantic *is showed*. The region in which the flow is distinctly northward *is showed* to shift westward, bringing about a larger recircling close to the deep water formation site and therefore imposing a natural limit to the increase in deep water formation. The fact that these two processes are *then* attributed to the subpolar gyre highlights its importance as a single entity. The cause of an increased western boundary current can be further examined, as can its effect on the total meridional overturning.

7.2.4 Evaluation of the AMOC

As mentioned the AMOC is a geographically defined as contrast to being defined by its drivers. This definition brings with it a large influence of the latitude and depth of evaluation when examining the role of a possible driver. It can not be understated that the meridional transport can have different local drivers at different locations, which can alter the transport in some degree. Correlating the deep water formation in the northern Atlantic with the meridional flow in the equatorial region - where the meridional flow is largest - can contain qualitative discrepancies both because a local driver can exert a strong impact and because a signal can get diluted when travelling large distances. In this view the correlation coefficient, which is given as a function of both lag years and the latitude at which the AMOC is evaluated, can easily be lowered because of a distortion of the signal and because of the effect of a local driver in a certain region. Therefore the necessity of a qualitative analysis must be underlined. The same considerations needs to be taken into account when analyzing the oscillatory behavior in the second regime. Here the AMOC must be evaluated at a latitude as close to the hypothesized driver as possible. The western boundary current in the midlatitudes, i.e. the Gulf Stream, is the best example of this. If the AMOC were to be evaluated here and subsequently compared to the deep water formation, the causality could prove difficult to determine because the signal from the Gulf Stream also would be diluted going northward as would the signal from the deep water formation going southward. This does not necessarily imply that the deep water formation, and the mechanisms by which it is controlled, is not the most important driver of the general flow of the AMOC.

Regarding the AMOC behavior in the second regime, a comparison of the oscillations at different latitudes could also provide insight to the causality between the driver and reactor, since the signals of a possible driver should be possible to trace either southward or northward. In this sense a comparison of the AMOC transport with itself at a different latitude with an emphasis on the timing of signals could elucidate the origin of a driving mechanism or event. If a large increase in the AMOC in the upper ocean is registered at first in the north and subsequently in the south, it must mean that the driving mechanism is

located in the north, since the transport in the upper ocean is northward. Had an increase in the upper ocean been registered first in the south and later the north, this would imply a driving mechanism in the south. The inverse argument can be made of changes in AMOC strength in the deeper ocean, since here the transport is southward.

What could also improve the rigorousness of the study would be an inclusion of an analysis of the AMOC strength in the deep ocean, i.e. an analysis of the southward return flow. At all depths the AMOC is defined as a zonally and vertically integrated transport down to the depth in question. This running sum means that the AMOC strength at the ocean floor should be zero, and only at depths where the cumulative transport is southward should it be negative. In order to calculate the southward return flow at a certain depth, one has to consider the vertical difference in AMOC strength. Especially the role of the deep water formation in the Labrador Sea on this southward return flow seems to be of interest.

7.3 Secondary variables, factors and mechanisms

In a system as complex as the Atlantic it is naïve to believe that a single - even four - variables can control every aspect of the flow. Several other factors than the four hypothesized drivers have been under investigation, and they are here presented; first with a brief theoretical argument as to why the factor in question should be taken into consideration when trying to explain the AMOC flow, second with a comment on its influence on the AMOC based on the model data output.

7.3.1 Sea Ice

Sea ice plays the key role in perhaps the most important feedback of the entire climate system - the sea ice-albedo feedback. As a positive feedback it is associated with behavior which enhances itself. When investigating systems, which displays rapid temperature increases, it is therefore natural to look at the behavior of sea ice. This is of course commonly applied to the theory of glacial cycles as claimed by Milankovitch theory, but Jochum et al. (2012) also reported the sea ice-albedo feedback as the only necessary feedback to glacial inception processes on the basis of CCSM4 data. Besides the sea-ice albedo feedback, a direct effect of sea ice on ocean circulation is that of the insolation - regions covered by sea ice have no interaction between the ocean and the atmosphere. As mentioned in section 3 deep water formation is strongly influenced by the winds, since they provide an energy input which mixes the upper ocean and therefore act to vertically equalize density differences. A high sea ice coverage prevents this effect, and thus acts to inhibit deep water formation. On the other hand, however, a removal of sea ice is associated with a positive fresh water flux to the upper ocean, which would also act to inhibit deep water formation, whereas the formation of sea ice implicates a positive salinity flux to the upper ocean due to salt rejection. Overall, the influence of sea ice on deep water formation and ocean circulation in general is therefore complex.

In the model the sea ice is defined on the atmospheric grid both as monthly and annual averages, and it is given as number between 0 and 1 indicating the fraction of surface area of the grid point in question covered by sea ice. Because of the fact that it is defined on the atmospheric grid, grid points situated over land take the value 0 in the sea ice data output.

With an emphasis on determining its influence on the AMOC initially in the first regime

the sea ice data was analyzed. On the basis of the monthly averages (and not the yearly) figure 45 show three main results hereof - namely the annual maximum of the spatially meaned sea ice coverage north of 80°N , and sea ice as a filled contour plot in the years 325 and 396, which are representative of a maximum (in the first regime) and minimum in the timeseries respectively. The latitude value of 80°N was chosen so as to eliminate as many grid points located over land as possible (since these take the value of 0 and therefore greatly influences the mean). In practice this means that only the two northern most latitude indices have been used for computing the spatial average. These indices have the latitudes 83.48°N and 87.16°N . Only very little land area is situated north of 83°N , why the average should encompass almost no grid points representing land, and therefore not be misrepresentative in this manner. In this regard it must also be stated, that since the analysis of the sea ice was performed with an emphasis on the first regime, these latitude were almost also the only ones where sea ice were present.

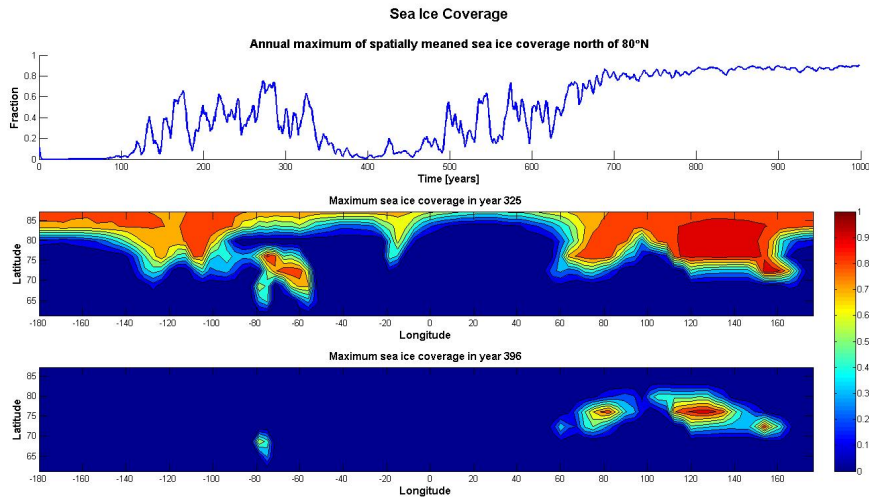


Figure 45: The annual maximum of the spatially meaned sea ice coverage north of 80°N (**upper panel**), annual maximum sea ice coverage in the year of 325 (**center panel**), annual maximum sea ice coverage in the year of 396 (**lower panel**).

The figure shows that, in the period of time where the AMOC and the deep water formation experiences a rapid increase, the sea ice coverage does the opposite. This corresponds well with the knowledge that a strong AMOC brings more heat northward. The portion of sea ice in the center panel centered around $[70^{\circ}\text{W};75^{\circ}\text{N}]$ and almost separated from the large circumfering part is sea ice in the Baffin Bay. This is the region in which large fraction of sea ice extends to the most southern latitude in the model data. Since this region has a short passage to the deep water formation site in the Labrador Sea, it is reasonable to assume, that this is the region in which sea ice can exert the most influence on deep water formation in the model. That being said, the ocean transport itself, between the region covered by sea ice and the deep water formation, of course also plays a role, when the influence of sea ice on deep water formation is evaluated.

However, the sea ice fraction was also evaluated in this region, more specifically at the two most southern grid points at which the sea ice exceeded a value of 0.3. These two points were situated at $[56^{\circ}\text{W};69^{\circ}\text{N}]$ and $[56^{\circ}\text{W};65^{\circ}\text{N}]$, which is in the Baffin Bay and the Davis Strait. The timeseries of the annual maximum of the monthly values of sea ice at these grid points are shown in figure 46.

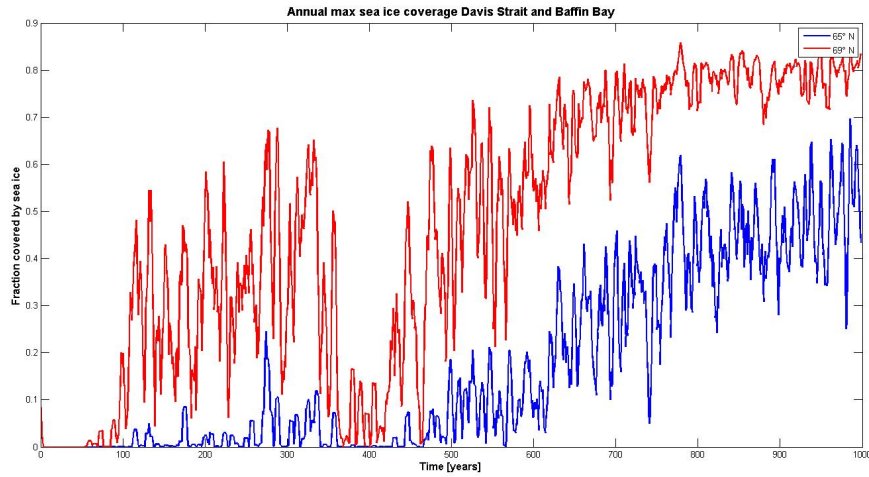


Figure 46: Annual maximum of sea ice at $[56^{\circ}\text{W};69^{\circ}\text{N}]$ and $[56^{\circ}\text{W};65^{\circ}\text{N}]$ (Baffin Bay and Davis Strait).

This figure shows that the sea ice in the Baffin Bay does not cover a very large fraction of the sea surface - at least not until very late in the simulation. Further south in the Davis sea ice is basically absent in the first regime and rarely present until late in the simulation.

In order to give an estimate of the influence of sea ice on deep water formation its latitudinal extent in the Baffin Bay/Davis Strait and in the Nordic Seas was examined as a function of time. Figure 47 thus shows the most southern latitude at which the sea ice covers at least a fraction of 0.1 of the sea surface area in the Baffin Bay/Davis Strait (red) and in the Nordic Seas (green) in any month during each year as a function of time.

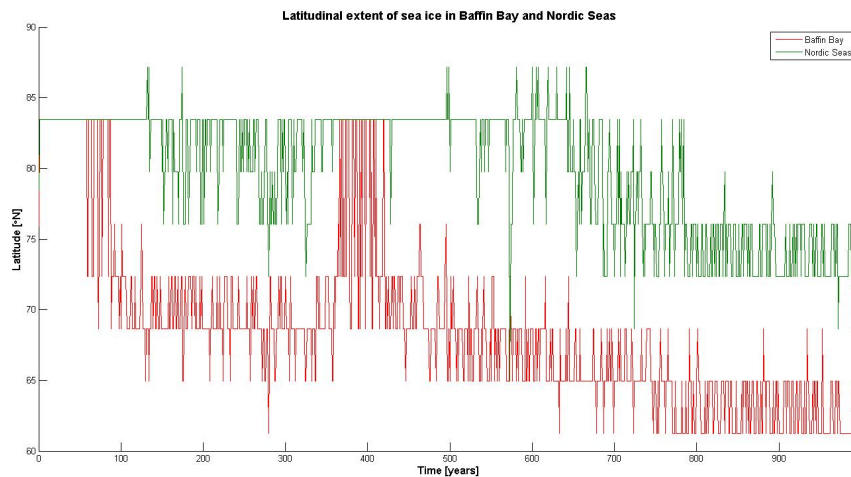


Figure 47: Latitudinal extent of sea ice in the Baffin Bay/Davis Strait (red) and the Nordic Seas (green).

The rather square jumps made by both timeseries is due to the coarseness of the grid,

on which the sea ice is defined. The importance in this figures lies in the fact that very rarely does the sea ice extend farther south than 69°N in the Baffin Bay and basically never farther south than 75°N in the Nordic Seas in the first regime. In comparison, the most northern of the three deep water formation regions analyzed in section 5 and 6 is that in the Labrador Sea, which has its most northern grid point at 61°N.

The aforementioned mechanisms, through which the sea ice can directly influence deep water formation, (i.e. by insolation from atmosphere, fresh water and salinity fluxes) were therefore deemed irrelevant when analyzing the behavior in the first regime. No further analysis of the influence of sea ice were thus made.

However, it is important to notice, that the salinity and fresh water fluxes in the upper ocean caused by sea ice formation/melt could have had an effect on the deep water formation were they advected to the deep water formation site. This was not investigated though. In this regard it is furthermore important to stress that the basis on which the deep water formation regions were defined might not have been optimal. They were defined by which specific grid points experienced a annual maximum of the XBLT in the entire northern Atlantic. This does not mean that deep water is not formed elsewhere.

The overall influence of sea ice was thus deemed irrelevant, but was it to be completely disregarded as having any influence whatsoever some factors, such as the salinity and fresh water fluxes and its influence on temperature, require a more thorough investigation. It must be underlined also that figure 35 does not show any sign of the temperature increase in the Baffin Bay, associated with the depletion of sea ice, being advected to the Labrador Sea. As for the influence of sea ice in the Nordic Seas, it must be underlined that it is first of all very limited even before the increase of the AMOC. Figure 35 does show a cooling in the Denmark Strait from year 240 to 280, where sea ice coverage is increasing southward. This southward spreading of sea ice could thus have been contributing to a lower temperature in the Nordic Seas. This temperature anomaly could have been advected to the Denmark Strait and potentially have contributing to an increase in deep water formation. But this is very speculative, and the overall effect seems nonetheless to be minimal.

7.3.2 The Denmark Strait Overflow Water

In addition to the uncertainties over the deep water formation is also the contribution of the overflow waters from the Nordic Seas. These enter the Atlantic Ocean over sills in the ocean floor between Greenland and Iceland - this is the Denmark Strait Overflow Water, or DSOW, over the Greenland-Iceland ridge - and between Iceland and Scotland - which is dubbed the Faroe Bank channel overflow (Jochumsen et al., 2015; Olsen et al., 2008).

The regions in which deep water formation occurs were in this thesis defined geographically static, and only in these regions were the deep water formation directly analyzed. Since the XBLT was used as a metric for the deep water formation, the mechanism through which the overflow waters influence the deep water formation is not directly addressed.

Olsen et al. (2008) estimated a total overflow over the Greenland-Scotland ridge close to 6 Sv of which close to 2 Sv were Faroe Bank Channel overflow in 2005, whereas Harden et al. (2016) estimates a Denmark Strait overflow of 3.54 Sv. All in all these are not irrelevant amounts of water in terms of deep water formation. In this regard the problem in this study is still the way in which the deep water formation has been analyzed, since it does not properly allow for a distinction between waters entering the from the Nordic Seas, and

waters transported from the midlatitudes by the subpolar gyre which is then transformed to deep water, when reaching the regions in question.

A brief estimate of the influence of the Denmark Strait Overflow was made however. Figure 48 shows the surface velocity in the northern Atlantic and Nordic Seas at 6 different timesteps leading up to year 400. In these chosen years the overall surface velocity is seen to attain a maximum at year 320 and remain somewhat stable from year 360 to 400.

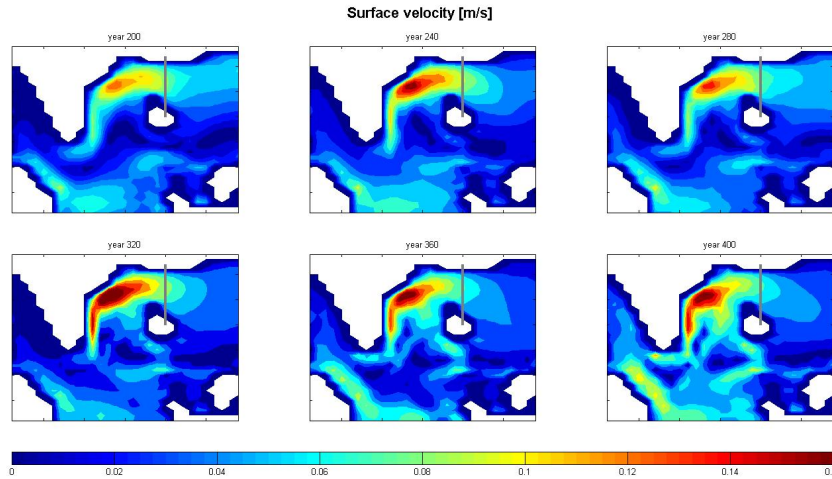


Figure 48: Surface velocity in the northern Atlantic and part of the Nordix Seas. Grey meridional line indicat cross section over which to compute the Denmark Strait Overflow.

As previously mentioned the irregularity of the grid causes a distortion of the zonal and meridional directions as compared to actual long- and latitudes. Therefore the flow across the Denmark Strait can be investigated via the strictly zonal flow across the cross section marked by the grey line in figure 48. This line begins at the long- and latitude coordinates $[17.7^{\circ}\text{W};65.3^{\circ}\text{N}]$ and ends at $[18.3^{\circ}\text{W};65.7^{\circ}\text{N}]$. So even though the line lies in the northwest/southeast plane, the skewness of the grid allows for the transport across to only consists of a zonal component. For the same years of the simulation as in fig 48, the velocity across is shown in figure 49 as a function of depth and latitude.

Here the dashed black line mark the depth and latitude at which the velocity is zero. It is shown that the water flowing towards the Atlantic is situated in the northwestern part of the strait, whereas in the southeastern part water flow into the Nordic Seas. Neither the shape of the zonally positive or that of the zonally negative flowing cell changes particularly over time. The fact that the transport across the Denmark Strait show water flowing both into the Nordic Seas and into Atlantic is at least partially attributed to the circulation of the subpolar gyre. Some of water flowing into the Atlantic will thus be a recirculation of the water flowing into the Nordic Seas, although a transport of water from a more northern region of the Nordic Seas can also be inferred from the velocity arrows in figure 28. The regions from which the overflow waters originates remains an unexplored aspect of this study, despite the heavy emphasis on the deep water formation.

In regards of the AMOC, however, the most important aspect of the Denmark Strait overflow, is the amount of water, which enters the Atlantic. This net transport across the above shown cross section as a function of time is shown in figure 50, where the vertical grey

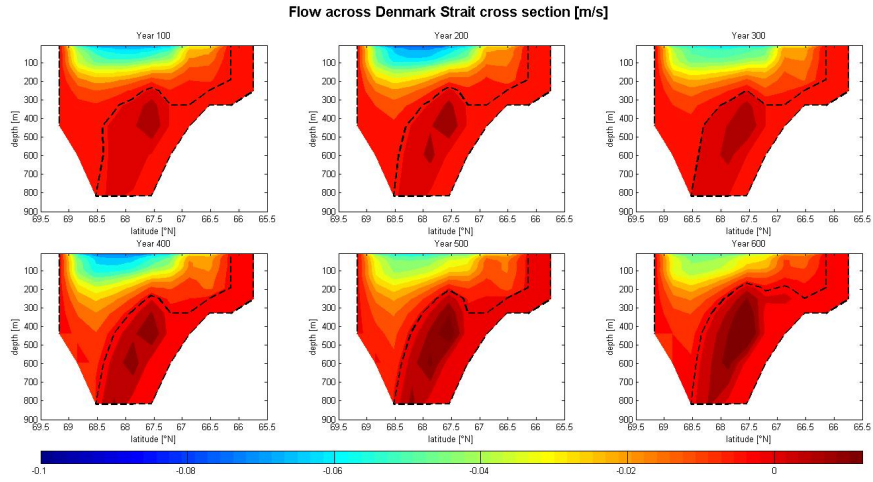


Figure 49: Velocity across the Denmark Strait cross section

line indicate the time at which the XBLT in the Denmark Strait reaches a maximum. The timeseries shown are the absolute values of a net negative transport, i.e. water entering the Atlantic.

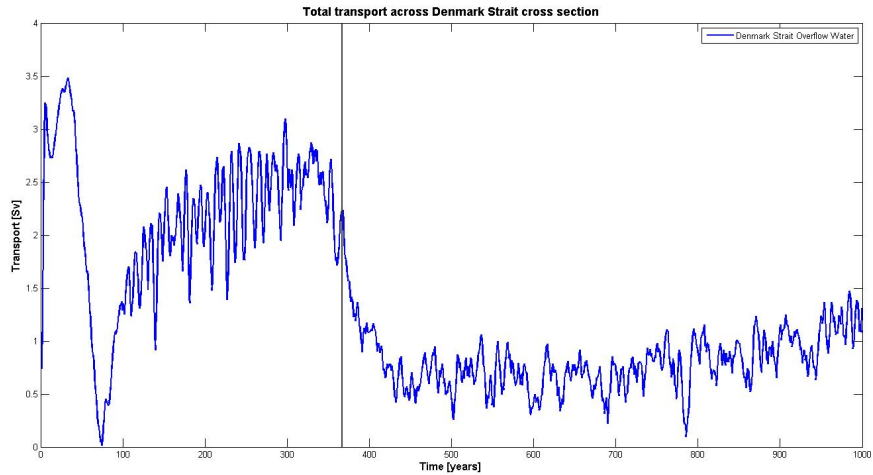


Figure 50: Absolute overflow across the Denmark Strait cross section as a function of time

The fact that more water is seen entering the Atlantic from the Nordic Seas in periods of time, where the deep water formation is low, is somewhat counterintuitive, should the DSOW contribute to a strong deep water formation. The apparent implication of this should be that the DSOW does not contribute very much to the deep water formation, but the possibility that the deep water formation itself has not been properly diagnosed cannot be ruled out. Since the maximum of the XBLT in the Denmark Strait is reached at a time, where the DSOW has just begun to decrease, also does not at all rule out the possibility that the DSOW has an impact on the XBLT in the Denmark Strait.

Overall, a more rigorous analysis of the deep water formation, the DSOW, their mutual dependence and influence on the AMOC could improve the robustness of the study, since the deep water formation is found to have such a high influence on the AMOC. For instance could the determination of the origin of the overflow waters and their density illuminate their influence on the deep water formation and hence the AMOC. Furthermore, a comparison of an actual estimate of the amount of deep water formed in the Denmark Strait and Labrador Sea with the net amount of water entering the Atlantic from the Nordic Seas also could improve the understanding of their respective influence on the AMOC. A feature of their mutual independence and influence of the AMOC is also the aspect of entrainment, the effects of which are still not yet fully understood (Macrander, 2005). This remains for further analysis.

7.3.3 Heat fluxes between ocean and atmosphere

As mentioned previously deep water formation occurs in short lived convection events (Kuhlbrodt et al., 2007), where heat loss to the atmosphere. Therefore wind strength plays a large role in setting the conditions, which enables this convection. Since deep water formation in the Denmark Strait and Labrador Sea has been showed to have a major influence of the AMOC, the wind strength over these areas was also evaluated. This was done as a spatial mean over the areas, from which XBLT values were used, and thus only as a function of time. The result is shown in figure 51.

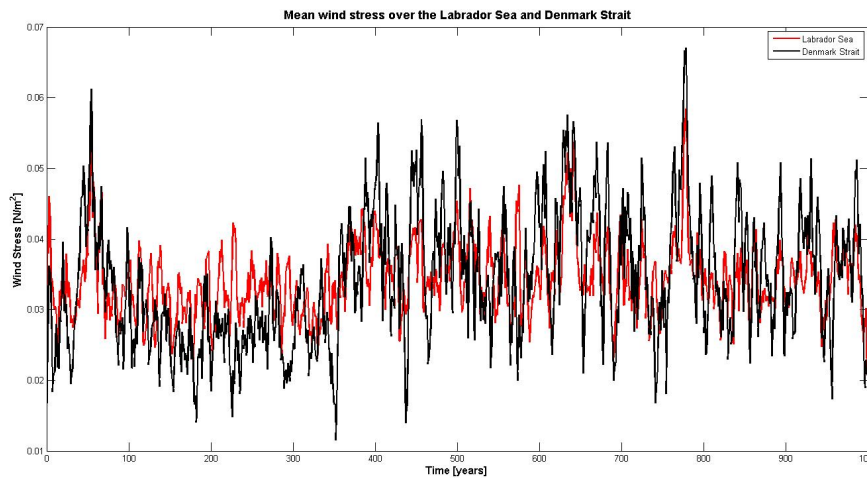


Figure 51: Average wind over the Labrador Sea (red) and the Denmark Strait (black) as a function of time

Overall the winds show a very volatile behavior and not really any behavior similar to that of the deep water formation. The impact of winds on deep water formation was thus deemed irrelevant.

7.3.4 Overall assessment of the influence of secondary variables

All in all, secondary variables which could have been thought to play a role - however indirect this may be - on the AMOC strength have all been deemed not nearly as important as neither the subpolar gyre or the deep water formation in the north Atlantic. It cannot be ruled out on the basis of this analysis that the Denmark Strait overflow and the southward extent of sea ice have had a small effect on the deep water formation in the Denmark Strait though. In order to give a more thorough estimate of this effect, the first thing to include should most likely be the density difference between the waters entering and leaving the Nordic Seas through the Denmark Strait. Since the actual amount of these waters are small, the density of the water into the Atlantic needs to be higher than that flowing into the Nordic Seas.

7.4 Suggestions for further analysis and research

Although the validity of the results have already been critically assessed and deemed robust, there are of course shortcomings in the way in which the analysis have been performed. Since the subpolar gyre plays a large role in feeding the deep water formation regions with saline water, and thereby setting the AMOC, a larger focus could have been on the mechanisms which sets the subpolar gyre circulation. According to Luyten et al. (1985) the zonally sloping isopycnals to a large degree sets the meridional flow. These have only been addressed briefly, and a more in-depth analysis here would have given a more comprehensive understanding of the influence of the subpolar gyre.

A better understanding of the subpolar gyre would most likely also give a better understanding of the removal of deep water. The western boundary current off of Canada is showed to very suddenly intensify, and the reason for this remains unresolved. Unfortunately, the analysis of the southward return flow could in general have been more thorough. The quantitative analysis pointed to the XBLT in the Labrador Sea as having the highest correlation coefficient with the AMOC in the second regime while still leading it, and figure 44 shows a simultaneously increase in the XBLT here and the western boundary current. One wonders therefore what exact influence these two have on each other. It seems appropriate to assume that an increased western boundary current removes more deep water from the Labrador Sea and thereby increase downwelling, but to what degree the deep water formation in the Labrador Sea can affect the western boundary current is also worth a closer look. It is not unrealistic to think the the deep water formation here alter the vertical density, and therefore pressure gradients, which affect the flow.

Performing the study with no direct forcing of the model natural sets a limit to what conclusions of driving mechanisms can be drawn. In order to further address the issue of a driving mechanism of the AMOC perturbation experiments could be made. Since the upper ocean salinity in the Denmark Strait and the Labrador Sea are evaluated to have such a large influence on the AMOC, it seems natural to impose a forcing, which would alter the deep water formation here. This could be done with a flux of water from the northern Labrador Sea or the Nordic Seas, respectively, which would have either lower or higher salinity. A response in the deep water formation should hopefully be mirrored in the AMOC.

Because of the role played by saline water being transported from the midlatitudes to the deepwater formation sites by the North Atlantic current and subsequently the subpolar gyre, the northward flux of salinity in the North Atlantic current or rather boundary between

the subtropical and subpolar gyre could also be investigated. The cross-gyre boundary flux of salinity could thus be important for the deep water formation in the northern Atlantic, and this process is not yet fully understood (Marzocchi et al., 2015). It could be possible however, that such an investigation would need a finer spatial resolution.

7.5 Summary of the discussion

The critical assessment of the results and the analysis leading to the results have focused on mainly two things; the way in which the hypothesized drivers have been defined in the analysis, and the lack of examination of certain features argued to be important for the hypothesized drivers in the theory (section 3).

The first include the fact that the barotropic streamfunction treats the ocean as a single layer, and that there is a mathematical bias toward a high correlation between the BSF and the AMOC, because of the inclusion of the meridional transport in the BSF. Since the BSF treats the ocean as a single layer it fails to capture the depth specific transport associated with the subpolar gyre. However, this was addressed by the qualitative analysis, where the role of the subpolar gyre was highlighted.

The way in which the deep water formation has been defined rests on the assumption, that the XBLT is proportional to the actual amount of deep water formed. Since the three regions investigated were defined on the basis of the grid points which experiences an XBLT maximum in the entire north Atlantic, the separate analysis of these three regions also assumes that deep water is formed only in these static regions. This is not necessarily the case. A different estimate could have been the actual amount of deep water formed. However it should underlined, that the representation of distinct processes via simplified measures is rather normal, and that this kind of representation has intrinsic value.

Not illuminated adequately is the role of the zonal density differences or sloping isopycnals in setting the strength of the subpolar gyre. According to the theory presented in section 3 this should be a key factor, and it has only been evaluated briefly. It has been showed, though, that the subpolar gyre does play a major role in transporting heavy water to the deep water formation sites, and that a shift in the flow of the subpolar gyre cause an arrest in the increasing salinities in the north Atlantic. The specific details of this flow could however have been closer investigated. The same goes for the cause of the sudden intensification of the western boundary current, which play a huge role in the overturning. In this regard, the role of the deep water formed in the Labrador Sea should be examined, since it shows very similar behavior.

Despite possible shortcomings accompanied by the representation of both the deep water formation and the subpolar gyre, the qualitative analysis highlights the key roles of the salt-advection feedback and the convection feedback processes. The fact that both AMOC transport, BSF, and XBLT display such rapid increases up to year 400 of the simulation is indicative of the importance of a (or more than one) positive internal feedback. The arrest of this increase - and thus a state transition of the AMOC - is attributed to two factors: first, the natural limit on salinity brought about by the salinity of the midlatitudes. Second, a shift in subpolar gyre flow, which brings about a larger recircling in the upper ocean, as compared to a further increased northward salinity flux, imposing an even stricter limit on sea surface salinity. The cause of this shift in subpolar gyre recircling could be illuminated further though.

Also investigated were the roles of the Denmark Strait overflow and sea ice in the Baffin Bay and Nordic Seas. Regarding the first, it seemed counterintuitive that the XBLT in the Denmark Strait and the AMOC displayed very low values when the DSOW was high. However, the fact that the XBLT in the Denmark Strait experienced a maximum just after the DSOW had started a large decrease, could point to the conclusion that it does have an effect on the deep water formation. The density of the overflow needs to be examined if this effect is to be evaluated though. Since the sea ice does not reach anywhere near the deep water formation sites (such as they were defined at least), the possible impact of a "lid" effect and the salinity increase/decrease associated with the formation/depletion of sea ice were deemed unimportant. However, a possible effect associated with the temperature changes due to the sea ice albedo effect could have been investigated more thoroughly, but on the basis of the temperature timeseries of the Denmark Strait, this was also deemed unimportant.

A further examination of the data should thereby primarily have focused on the specific details of the flow of the subpolar gyre and the representation of the deep water formation. Were forcing or perturbation experiments to be performed, the response of the AMOC to either a salinity/fresh water flux in the Nordic Seas or northern Labrador Sea, or an increased cross-gyre boundary salinity flux in the midlatitudes, could prove enlightening.

8 Conclusion

In this study data from a the CCSM 3.5 run with initial conditions of very high ocean temperatures and very uniform salinity (details of these are provided in section 2) have been analyzed with the objective of determining the driver of the Atlantic Meridional Overturning Circulation (AMOC).

Given the onset of this study as described in section 4 the results point to the conclusion that the driver of the AMOC is first of all the deep water formation in the northern Atlantic, while a large role is also played by the subpolar gyre transport. The distinctly different behavior of the AMOC before and after roughly year 400 of the simulation lead to the analysis being split into two temporal regimes. This proved fruitful. Both regimes were analyzed both quantitatively by a correlation analysis and qualitatively by the flow and deep water formation in the north Atlantic. In this manner the quantitative analysis also worked as a framework of the qualitative analysis.

The fact that the correlation analysis shows the lowest correlation coefficient between the AMOC and the deep water formation as compared to the other (or at least two out of the other three) hypothesized drivers of course points in a different direction. It is still important to notice that the maximum correlation coefficient between these two always occur when the AMOC lags the XBLT, which ameliorates the slightly lower value. Furthermore the mathematical inclusion of the meridional transport in the BSF leads to a natural bias in the correlation coefficient between this and the AMOC, which should undermine the importance of this particular value. The qualitative analysis supports the conclusion that the meridional density difference is a consequence rather than a cause of the AMOC.

This is based on the transport by subpolar gyre. In the qualitative analysis it was shown that an increase in the northward flux of saline waters in the eastern midlatitude Atlantic brings a large amount of heavy water to the deep water formation sites first in the Denmark Strait and subsequently the Labrador Sea via the subpolar gyre. In the first

regime this is manifested in a salt-advection feedback. An increase in northward salinity flux increases the upper ocean density in the deep water formation sites. This decrease in vertical density difference associated with this further enables deep water formation, which in turn increases the overturning. This behavior highlights the nonlinearity of the flow - an increase in northward transport in the end cause a further increase in northward transport. To arrest this feedback a westward shift in the northward transport by the subpolar gyre is touted as the main cause. Not long after year 360 of the simulation this cell of northward flowing water shifts westward to a region with lower salinity, and waters being transport to the deep wter formation sites are less saline and thus lighter, causing an arrest of the increas in the deep water formation first in the Denmark Strait and thereafter the in the Labrador Sea.

The effect of temperature on the potential for deep water formation was showed to be unimportant as compared to the effect of salinity. This conclusion was drawn on the basis of both upper and middepth temperatures. Here it was inferred that waters being transported to the deep water formation sites in times of high convection were cooled less on its way, than waters being transported in the times of low convection. This lesser cooling should act to lighten the upper ocean water and therefore increase stratification and inhibit deep water formation.

In the second regime it was showed that the oscillatory behavior of the AMOC were mirrored quite precisely only preceeded by a few years by the XBLT in the Labrador Sea. It is also worth mentioning that the overall decrease of the AMOC is also mirrored by the XBLT in the Labrador Sea. Therefore this was concluded to be the driver of the AMOC in the second regime.

An overall emphasis must be put on the internal feedbacks in the system being responsible for the rather extreme AMOC behavior. This include the socalled salt-advection feedback described above and a convective feedback. Since deep water formation acts to equalize vertical density differences an ongoing deep water formation acts to enable itself. And because of the fact that the deep water formation takes place in a region with the fresh water flux from the atmosphere to the ocean a continuing freshening of the upper ocean takes place. This lightens the sea surface waters, and if deep water formation does not take place for consecutive years the cumulative effect of this lightening would further inhibit deep water formation.

Since these feedbacks are both initiated and brought to end by small perturbations, they greatly illuminate the ability of the Atlantic Ocean to act as an amplifier of climate signals (this was first adressed by Rahmstorf (1996)). The nonlinearity of the response of both the AMOC, BSF and XBLT in this study underlines the effect of these feedbacks. As such the AMOC reaches a maximum of close 45Sv and therefore more than doubles in about 50 years.

In the end the main factor which most directly drives this transport is thus determined to be the deepwater formation in the Denmark Strait and the Labrador Sea, with the northward transport associated with the subpolar gyre playing a major role by transporting very saline water to these regions.

List of Figures

1	Setup used by Stommel (1961)	4
2	Schematic illustration of how divergence and convergence of Ekman transport induce a vertical velocity below the Ekman layer	7
3	The AMOC evaluated at 4 different latitudes all at the depth of maximum transport at every timestep. The AMOC exhibits the largest transport at 34°N while the transport at the remaining four latitudes a similar in strength. After the spin-up phase the transport can be characterized by first a steady then a rapid increase until year ~ 400 , after which a somewhat linear decrease with oscillatory behavior is seen	18
4	Transect of the AMOC at six different years of the simulation. The maximum strength is at all times found at the 75 th latitudinal index and close to 1000 m depth. While the spatial structure remains somewhat constant throughout the simulation the strength varies substantially with an increase of more than 20 Sv from year 300 to year 400.	19
5	a Shows the MDD in the four vertical intervals. The largest meridional density differences is seen in interval 1 (top 100 meters) and the MDD decreases with depth. Interval 1 clearly exhibits a behavior similar to the AMOC until year ~ 400 after which an opposite behavior is seen. b A zoom in on the three deepest vertical intervals in order to see their behavior more clearly. It can be seen that interval 4 (1670 – 2555m) exhibits a behavior similar to the AMOC, whereas the intervals 2 and 3 (0 – 1280m and 500 – 1690m) shows a behavior similar to interval 1.	20
6	a Shows the correlation coefficient between the AMOC and the MDD in four vertical intervals as a function of lag years negative (positive) indicating a lag of the AMOC (MDD) to the MDD (AMOC) over the entire simulation. b A zoom in on the lagtime of maximum correlation.	21
7	a shows the correlation between the MDD and the AMOC in the 1 st temporal regime. This is highest when the MDD is evaluated in the top of the ocean with a maximum value of 0.8694. In all 4 vertical intervals the correlation is highest at 0 years lag, which makes it impossible to determine the direction of causality using this method. Figure b shows a zoom in on the years around maximum correlation.	22
8	a shows the correlation between the AMOC and the MDD in the 2 nd temporal regime. Whereas a positive correlation exists in the bottom part of the ocean, an anti-correlation exists in the other 3 intervals. In figure b the absolute values are shown for all 4 correlation coefficients for the sake of comparison. It can be seen that the correlation is highest for the lowest part of the ocean. In all cases the maximum correlation occurs at 0 years lag.	23
9	Average wind stress in the Southern Ocean latitude bands as defined by a northern boundary at 64°S and a southern boundary at 53°S.	24

10	Zonally integrated meridional Ekman transport in the Southern Ocean latitude bands as defined by a northern boundary at $64^{\circ}S$ and a southern boundary at $53^{\circ}S$	25
11	Total upwelling in the Southern Ocean caused by the divergence Ekman transport	25
12	Shows the XBLT in the North Atlantic region, from which XBLT values were used, at year 500. The colorbar indicates XBLT in meters, white color indicate land, and the region shows Greenland in the north, Canada in the west, UK and Scandinavia in the southeast and Iceland in the northeast, and thus both the Labrador Sea and Denmark Strait are included.	26
13	Timeseries of the maximum XBLT (green) in the north Atlantic and the AMOC transport (blue) at 95^{th} latitudinal index. A correlation between the two is clear, with the same rapid increase until year ~ 400 and same oscillatory behavior in the late part of the simulation. The decreasing trend in the late part of the simulation of the AMOC is, however, not as pronounced in the XBLT. The XBLT values are the result of a 5-year running mean.	27
14	Correlation coefficients as a function of lag years between the AMOC and and the XBLT. Left panel shows values for the full simulation, center panel for the 1^{st} regime, and right panel for the 2^{nd} regime.	28
15	2-d histogram of where the maximum XBLT occurs. Values are logarithmic; dark blue indicates places where XBLT not even at a single timestep obtains the maximum value, red indicates places where XBLT often obtains maximum value throughout the entire simulation. From this three distinct regions where deep water formation occurs can be extracted; the Labrador Sea, the Denmark Strait and the northeast Atlantic.	29
16	Timeseries of the AMOC transport (left side y-axis) and the XBLT maximum (right side y-axis) in three regions in the north Atlantic where deep water formation takes place. It can be seen that deep water formation occurs mainly in the northeastern Atlantic in the first 350 years of the simulation, whereafter it is shifted further northward to the Denmark Strait. Whereas the deep water formation in the northeastern Atlantic and the Denmark Strait remain somewhat steady from year 400 that of the Labrador Sea displays large oscillations and a decreasing trend similar to the AMOC transport. Vertical grey lines mark the regime separation years	29
17	Correlation coefficient between the AMOC transport and the XBLT in three subpolar regions in 1^{st} and 2^{nd} regime. Left panel shows the 1^{st} and right panel the 2^{nd} regime.	30
18	Values of the barotropic streamfunction in the subpolar north Atlantic in year 500. The counter clockwise motion of the subpolar gyre is clearly visible with a minimum located south-southeast off of Cape Farewell reaching 35 Sv. The heavy black line is the 0^{th} contour line indicating the transition between clockwise and counter clockwise motion.	31

19	Timeseries of the maximum BSF in the north Atlantic and the AMOC transport at 95 th latitudinal index. A correlation between the two is clear, with the same rapid increase until year ~ 400 and same decreasing trend in the last part of the simulation. The BSF values are the result of a 5-year running mean.	32
20	Correlation between the BSF and the AMOC in the full simulation (left panel), first regime (center panel) and second regime (right panel). The highest correlation occurs when only considering the first regime - reaching a maximum of 0.9406 at 0 years lag - while only considering the second gives the lowest correlation. In all matters the maximum correlation occurs at a lag of 0 years.	33
21	Correlation coefficient between the AMOC and the MDD as a function of lag years (horizontal axis) and the latitude at which the AMOC is evaluated (vertical axis). Upper panel shows the correlation coefficient for the full simulation, lower left panel the 1 st regime, and lower right panel the 2 nd regime. In each regime the depth interval which showed the highest correlation is plotted. White dashed lines indicate the region in which the deep water formation occurs, and the white marker shows the maximum correlation.	34
22	Correlation coefficient between the AMOC and the XBLT as a function of lag years (horizontal axis) and the latitude at which the AMOC is evaluated (vertical axis). Upper panel shows the correlation coefficient for the full simulation, lower left panel the 1 st regime, and lower right panel the 2 nd regime. White dashed lines indicate the region in which the deep water formation occurs, and the white marker shows the maximum correlation.	34
23	Correlation coefficient between the AMOC and the BSF as a function of lag years (horizontal axis) and the latitude at which the AMOC is evaluated (vertical axis). Upper panel shows the correlation coefficient for the full simulation, lower left panel the 1 st regime, and lower right panel the 2 nd regime. White dashed lines indicate the region in which the deep water formation occurs, and the white marker shows the maximum correlation.	35
24	Correlation coefficient between the AMOC and the XBLT in three regions in the first (upper panel) and second regime (lower panel). Left column shows correlation from the Labrador Sea, center column the Denmark Strait and right column the northeast Atlantic.	37
25	Depth averaged density in depth interval 1 (0 – 100m depth) in the northern and equatorial region. The northern region displays a distinct increase in density similar to that of the AMOC, whereas the density in the equatorial region remains steady in the same period of time.	40
26	Timeseries of the depth averaged salinity and temperature in depth interval 1 (0 – 100m depth) in the northern region	40

27	Filled coloured contour plot of the sea surface salinity overlaid by black contour lines of constant barotropic streamfunction values at 6 different years seperated each by 40 years leading up to the arrest of the rapid increase of the AMOC. Salinity values are indicated by the colorbar. The heavy black line is where the barotropic streamfunction is zero indicating a change between clockwise and counterclockwise transport	41
28	Filled coloured contour plot of the sea surface salinity shown along with velocity arrows at 6 different years seperated by 40 years. Sea surface salinity values are indicated by the colorbar.	42
29	Salinity and meridional velocity in a cross section of the Atlantic at 6 different years seperated by 04 years. The latitude of western boundary is 61°N while the latitude in the eastern boundary is 67°N. This is due to the skewness of the grid. The horizontal axis is degrees of west and the vertical axis is the depth index. Salinity is showed as filled coloured contours and values are indicated by the colorbar. The meridional velocity is showed as black contour lines. The heavy black contour line shows the line of 0 meridional velocity. . .	43
30	Same as figure 29 but shown with the actual depth on the vertical axis. Only the upper most 22 layers are displayed,	44
31	Salinity and velocity in the layer of maximum northward velocity in north Atlantic	45
32	Vertical potential density difference between the 1 st and 16 th layer (corresponding to a difference between depths of 4 and 815 meters) in the Atlantic. White patches indicate land or sea bed.	46
33	Vertical potential density difference in the three deep water formation sites only as a function of time.	46
34	Potential density in the three deep water formation regions in 1 st (upper panel) and 16 th layer (lower panel).	47
35	Sea surface temperature in north Atlantic	48
36	Temperature in the 13 th layer in north Atlantic	48
37	Maximum AMOC transport at the 89 th latitude index (or 55°N) and XBLT in the Labrador Sea in the second regime. Vertical black lines indicate the timing of 6 oscillation events in AMOC transport, which are all preceeded by similar behavior in the XBLT.	50
38	Maximum AMOC transport at the 89 th latitude index (or 55°N) and absolute maximum of the BSF in the north Atlantic. Vertical black lines indicate indicate the timing of 6 oscillation events in AMOC transport. . . .	50
39	Potential density in uppermost layer before, at the peak of and after the first three oscillations in the second regime.	51
40	Potential density in uppermost layer before, at the peak of and after the last three oscillations in the second regime.	52

41	Sea surface salinity in uppermost layer before, at the peak of and after the first three oscillations in the second regime.	52
42	Sea surface salinity in uppermost layer before, at the peak of and after the last three oscillations in the second regime.	53
43	Potential density in filled contours overlaid with meridional velocities in a north Atlantic cross section	60
44	Meridional transport across 57°N in western Atlantic (blue) and maximum XBLT in the Labrador Sea (red)	61
45	The annual maximum of the spatially meaned sea ice coverage north of 80°N (upper panel), annual maximum sea ice coverage in the year of 325 (center panel), annual maximum sea ice coverage in the year of 396 (lower panel).	64
46	Annual maximum of sea ice at [56°W;69°N] and [56°W;65°N] (Baffin Bay and Davis Strait).	65
47	Latitudinal extent of sea ice in the Baffin Bay/Davis Strait (red) and the Nordic Seas (green).	65
48	Surface velocity in the northern Atlantic and part of the Nordix Seas. Grey meridional line indicat cross section over which to compute the Denmark Strait Overflow.	67
49	Velocity across the Denmark Strait cross section	68
50	Absolute overflow across the Denmark Strait cross section as a function of time	68
51	Average wind over the Labrador Sea (red) and the Denmark Strait (black) as a function of time	69

List of Tables

1	Correlation between the AMOC, MDD, XBLT and BSF. For the correlation between the AMOC and XBLT and BSF the AMOC was here evaluated at the 95 th latitude index in both full simulation, 1 st , and 2 nd regime. For the correlation between the AMOC and the MDD the AMOC was evaluated at the 75 th latitude index. The correlation values for MDD have been obtained using the depth interval which gave the highest correlation	35
2	Correlation between the AMOC evaluated at the 75 th latitude index (roughly 33°N) and the MDD in specific depth intervals and in the two temporal regimes	36
3	Maximum correlation coefficients between AMOC at 95 th latitude index and XBLT in specific regions and temporal regimes. The two right most columns indicate at how many lag years the maximum correlation occurred.	36
4	Results of correlation analysis between the AMOC and the MDD, XBLT, and BSF as a function of lag years and latitude of evaluation of the AMOC. The values for the correlation with the MDD have been obtained using the depth interval which showed the highest correlation. For the full simulation and the first regime this is from 0 – 100 meters, while for the second regime it is the interval spanning 1650 – 2555 meters.	36
5	Years at which AMOC and possible drivers stops rapid increase prior to year 400 and at which the overall maximum is reached.	39

References

- Böning, C. W., Bryan, F. O., Holland, W. R., and Döscher, R. (1996). Deep-Water Formation and Meridional Overturning in a High-Resolution Model of the North Atlantic. *Journal of Physical Oceanography*, 26(7):1142–1164.
- Böning, C. W., Scheinert, M., Dengg, J., Biastoch, A., and Funk, A. (2006). Decadal variability of subpolar gyre transport and its reverberation in the North Atlantic overturning. *Geophysical Research Letters*, 33(21).
- Collins, M., Krutti, R., Arblaster, J., Dufresne, J.-L., Fichefet, T., Friedlingstein, P., Gao, X., Gutowski, W., Johns, T., Krinner, G., Shongwe, M., Tebaldi, C., Weaver, A., and Wehner, M. (2014). Long-term Climate Change: Projections, Commitments and Irreversibility. In: Climate Change 2013: The Physical Science Basis. Contribution of Working Group I to the Fifth Assessment Report of the Intergovernmental Panel on Climate Change [Stocker, T.F., D. Qin, G.-K. Plattner, M. Tignor, S.K. Allen, J. Boschung, A. Nauels, Y. Xia, V. Bex and P.M. Midgley (eds.)]. In *Climate Change 2013 - The Physical Science Basis*. Cambridge University Press, Cambridge.
- de Boer, A. M., Gnanadesikan, A., Edwards, N. R., and Watson, A. J. (2010). Meridional Density Gradients Do Not Control the Atlantic Overturning Circulation. *Journal of Physical Oceanography*, 40(2):368–380.
- Delworth, T. L. and Zeng, F. (2016). The Impact of the North Atlantic Oscillation on Climate through Its Influence on the Atlantic Meridional Overturning Circulation. *Journal of Climate*, 29(3):941–962.
- Ganachaud, A. and Wunsch, C. (2000). Improved estimates of global ocean circulation, heat transport and mixing from hydrographic data. *Nature*, 408(6811):453–457.
- Harden, B., Pickart, R., Valdimarsson, H., Våge, K., de Steur, L., Richards, C., Bahr, F., Torres, D., Børve, E., Jónsson, S., Macrander, A., Østerhus, S., Håvik, L., and Hattermann, T. (2016). Upstream sources of the Denmark Strait Overflow: Observations from a high-resolution mooring array. *Deep Sea Research Part I: Oceanographic Research Papers*, 112:94–112.
- Hatun, H. (2005). Influence of the Atlantic Subpolar Gyre on the Thermohaline Circulation. *Science*, 309(5742):1841–1844.
- Holdsworth, A. M. and Myers, P. G. (2015). The Influence of High-Frequency Atmospheric Forcing on the Circulation and Deep Convection of the Labrador Sea. *Journal of Climate*, 28(12):4980–4996.
- Jochum, M. and Eden, C. (2015). The Connection between Southern Ocean Winds, the Atlantic Meridional Overturning Circulation, and Indo-Pacific Upwelling. *Journal of Climate*, 28(23):9250–9257.
- Jochum, M., Jahn, A., Peacock, S., Bailey, D. A., Fasullo, J. T., Kay, J., Levis, S., and Otto-Bliesner, B. (2012). True to Milankovitch: Glacial Inception in the New Community Climate System Model. *Journal of Climate*, 25(7):2226–2239.
- Jochumsen, K., Köllner, M., Quadfasel, D., Dye, S., Rudels, B., and Valdimarsson, H. (2015). On the origin and propagation of Denmark Strait overflow water anomalies in the Irminger Basin. *Journal of Geophysical Research: Oceans*, 120(3):1841–1855.

- Kirtman, B., Power, S., Adedoyin, J., Boer, G., Bojariu, R., Camilloni, I., Doblas-Reyes, F., Fiore, A., Kimoto, M., Meehl, G., Prather, M., Sarr, A., Schär, C., Sutton, R., van Oldenborgh, G., Vecchi, G., and Wang, H. (2014). Near-term Climate Change: Projections and Predictability. In: *Climate Change 2013: The Physical Science Basis. Contribution of Working Group I to the Fifth Assessment Report of the Intergovernmental Panel on Climate Change* [Stocker, T.F., D. Qin, G.-K. Plattner, M. Tignor, S.K. Allen, J. Boschung, A. Nauels, Y. Xia, V. Bex and P.M. Midgley (eds.)]. In *Climate Change 2013 - The Physical Science Basis*, pages 741–866. Cambridge University Press, Cambridge.
- Kleppin, H., Jochum, M., Otto-Bliesner, B., Shields, C. A., and Yeager, S. (2015). Stochastic Atmospheric Forcing as a Cause of Greenland Climate Transitions. *Journal of Climate*, 28(19):7741–7763.
- Kuhlbrodt, T., Griesel, A., Montoya, M., Levermann, A., Hofmann, M., and Rahmstorf, S. (2007). On the driving processes of the Atlantic meridional overturning circulation. *Reviews of Geophysics*, 45(2).
- Lohmann, K., Drange, H., and Bentsen, M. (2009). Response of the North Atlantic subpolar gyre to persistent North Atlantic oscillation like forcing. *Climate Dynamics*, 32(2-3):273–285.
- Lohmann, K., Jungclauss, J. H., Matei, D., Mignot, J., Menary, M., Langehaug, H. R., Ba, J., Gao, Y., Otterå, O. H., Park, W., and Lorenz, S. (2014). The role of subpolar deep water formation and Nordic Seas overflows in simulated multidecadal variability of the Atlantic meridional overturning circulation. *Ocean Science*, 10(2):227–241.
- Luyten, J., Stommel, H., and Wunsch, C. (1985). A Diagnostic Study of the Northern Atlantic Subpolar Gyre. *Journal of Physical Oceanography*, 15(10):1344–1348.
- Macrander, A. (2005). Interannual changes in the overflow from the Nordic Seas into the Atlantic Ocean through Denmark Strait. *Geophysical Research Letters*, 32(6).
- Manabe, S. and Stouffer, R. J. (1988). Two Stable Equilibria of a Coupled Ocean-Atmosphere Model. *Journal of Climate*, 1(9):841–866.
- Marzocchi, A., Hirschi, J. J.-M., Holliday, N. P., Cunningham, S. A., Blaker, A. T., and Coward, A. C. (2015). The North Atlantic subpolar circulation in an eddy-resolving global ocean model. *Journal of Marine Systems*, 142:126–143.
- McCartney, M. S. and Talley, L. D. (1984). Warm-to-Cold Water Conversion in the Northern North Atlantic Ocean. *Journal of Physical Oceanography*, 14(5):922–935.
- McManus, J. F., Francois, R., Gherardi, J.-M., Keigwin, L. D., and Brown-Leger, S. (2004). Collapse and rapid resumption of Atlantic meridional circulation linked to deglacial climate changes. *Nature*, 428(6985):834–837.
- Munk, W. H. (1966). Abyssal recipes. *Deep Sea Research and Oceanographic Abstracts*, 13(4):707–730.
- Olsen, S. M., Hansen, B., Quadfasel, D., and Østerhus, S. (2008). Observed and modelled stability of overflow across the Greenland–Scotland ridge. *Nature*, 455(7212):519–522.
- Pedlosky, J. (1998). *Ocean Circulation Theory*. Springer Verlag Berlin Heidelberg, 2nd edition.

- Pickart, R. S. and Spall, M. A. (2007). Impact of Labrador Sea Convection on the North Atlantic Meridional Overturning Circulation. *Journal of Physical Oceanography*, 37(9):2207–2227.
- Rahmstorf, S. (1996). On the freshwater forcing and transport of the Atlantic thermohaline circulation:. *Climate Dynamics*, 12(12):799–811.
- Rahmstorf, S. (2002). Ocean circulation and climate during the past 120,000 years. *Nature*, 419(6903):207.
- Rhein, M., Kieke, D., Hüttl-Kabus, S., Roessler, A., Mertens, C., Meissner, R., Klein, B., Böning, C. W., and Yashayaev, I. (2011). Deep water formation, the subpolar gyre, and the meridional overturning circulation in the subpolar North Atlantic. *Deep Sea Research Part II: Topical Studies in Oceanography*, 58(17-18):1819–1832.
- Stommel, H. (1961). Thermohaline Convection with Two Stable Regimes of Flow. *Tellus*, 13(2):224–230.
- Stommel, H. and Arons, A. (1959). On the abyssal circulation of the world ocean—I. Stationary planetary flow patterns on a sphere. *Deep Sea Research (1953)*, 6:140–154.
- Toggweiler, J. and Samuels, B. (1995). Effect of drake passage on the global thermohaline circulation. *Deep Sea Research Part I: Oceanographic Research Papers*, 42(4):477–500.
- Zou, S. and Lozier, M. S. (2016). Breaking the Linkage Between Labrador Sea Water Production and Its Advective Export to the Subtropical Gyre. *Journal of Physical Oceanography*, 46(7):2169–2182.